LBL-12228

Lawrence Berkeley Laboratory
UNIVERSITY OF CALIFORNIA

Materials & Molecular
Research Division

THE SYNTHESIS AND CHARACTERIZATION OF GRAPHITE-METAL FLUORIDE INTERCALATION COMPOUNDS

Barry William McQuillan
(Ph.D. thesis)

April 1981

TWO-WEEK LOAN COPY

This is a Library Circulating Copy
which may be borrowed for two weeks.
For a personal retention copy, call
Tech. Info. Division, Ext. 6782

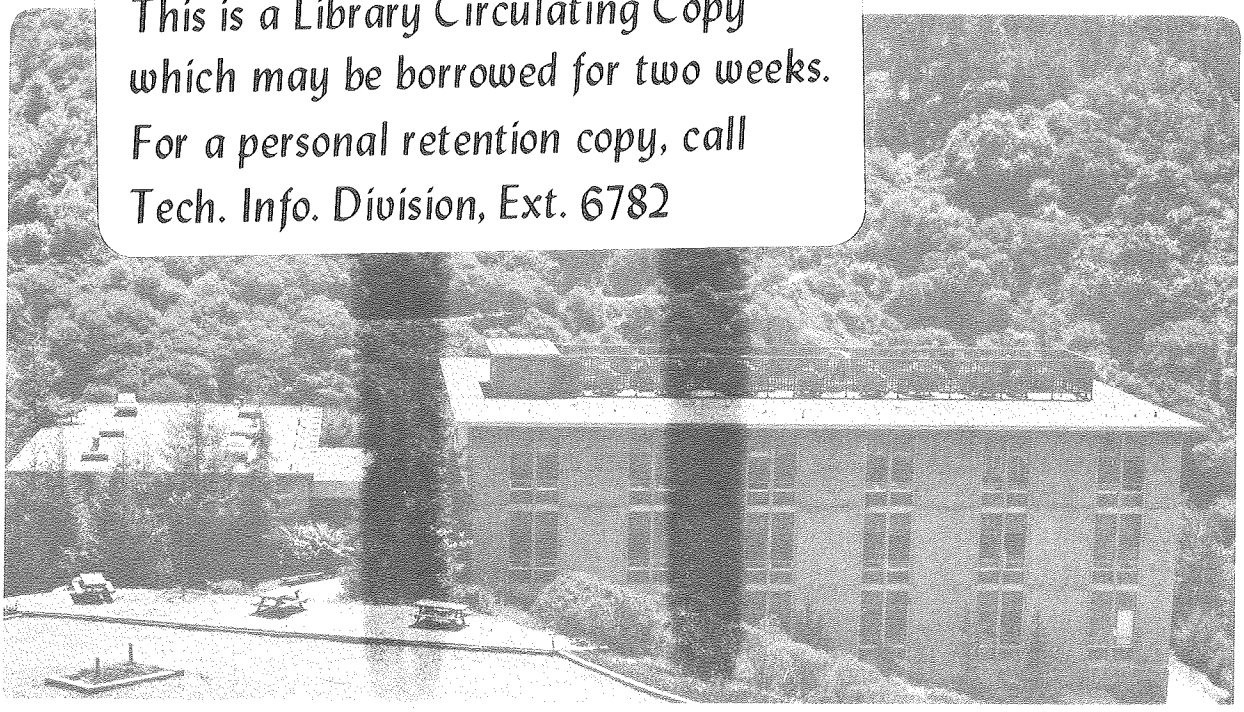

Prepared for the U.S. Department of Energy under Contract W-7405-ENG-48

LBL-12228

DISCLAIMER

This document was prepared as an account of work sponsored by the United States Government. While this document is believed to contain correct information, neither the United States Government nor any agency thereof, nor the Regents of the University of California, nor any of their employees, makes any warranty, express or implied, or assumes any legal responsibility for the accuracy, completeness, or usefulness of any information, apparatus, product, or process disclosed, or represents that its use would not infringe privately owned rights. Reference herein to any specific commercial product, process, or service by its trade name, trademark, manufacturer, or otherwise, does not necessarily constitute or imply its endorsement, recommendation, or favoring by the United States Government or any agency thereof, or the Regents of the University of California. The views and opinions of authors expressed herein do not necessarily state or reflect those of the United States Government or any agency thereof or the Regents of the University of California.

LBL-12228

The Synthesis and Characterization of Graphite-Metal Fluoride Intercalation Compounds

Barry William McQuillan

Department of Chemistry
Materials and Molecular Research Division
Lawrence Berkeley Laboratory
University of California
Berkeley, California 94720

Abstract

The compound "C_xAsF_5" was prepared and characterized by X-ray diffraction and X-ray absorption. The X-ray absorption studies show the presence of As(III) and As(V), and the As-F bond distances are consistent with AsF_3 and AsF_6^-, and not with gaseous AsF_5. These findings are consistent with the known oxidation half-reaction:

$$3AsF_5 + 2e \longrightarrow 2AsF_6^- + AsF_3$$

The equilibrium lies toward the right, although in a fully saturated compound "C_8AsF_5", the reaction may not go to completion as $C_{24}^{+2}(2AsF_6^-, AsF_3)$, but may contain some neutral AsF_5. A proposed solution to the identity of this "AsF_5" is given.

To corroborate these findings, $C_8^+AsF_6^-$ and $C_8^+OsF_6^-$ were synthesized. The C_xAsF_6 and numerous standard arsenic-fluorine compounds were studied by x-ray absorption. Magnetic susceptibility of $C_8^+OsF_6^-$ confirms the high degree of oxidation in this compound.

X-ray absorption studies were begun to determine the species present within the graphite when BrF_3 or $GeF_4 + F_2$ are added. In the BrF_3 case, Br_2 is evolved and only Br(III) is present in the graphite. This result is consistent with the oxidation reaction:

$$4BrF_3 + 3e \longrightarrow 3BrF_4^- + \frac{1}{2} Br_2$$

In the germanium case, all germanium is Ge(IV), and is probably GeF_5^- or GeF_6^{-2}.

An impressive correlation of some fifty reactions of various halides with graphite with their gas phase oxidation strengths is given. These oxidation strengths are calculated using a Born-Haber cycle and Kapustinskii's equation for lattice energies. Only those halides which have an oxidation strength greater than approximately 110 Kcal react with graphite at room temperature to form intercalation compounds. This correlation supports the model that formal oxidation or reduction of the graphite is required to form the intercalation compound.

The binary phase diagram XeF_2:$Xe_5^+AsF_6^-$ was investigated by melting point determination and Raman spectroscopy. This mixture near 1.3:1 forms a kinetically stable glass at room temperature and is molten at 50°C. Several new species or phases are observed in the Raman spectra. These species have been assigned tentative structures based on comparison with known phases and their appearance in the phase diagram.

Table of Contents

CHAPTER 1

The Reactions of WF_6 and OsF_6 with Graphite

Salts of graphite in which stable anions are intercalated in the galleries of the graphite have long been known. However, the characterization of the intercalated species, except for chemical analysis, has rarely been performed. The series of transition metal hexafluorides W to Pt provide a unique system for studies of the reactions with graphite. There is a monotonic increase in the oxidizing ability of the hexafluoride to make the anion. The changes in magnetic properties of the neutral and anionic species are well established. The magnetic properties of the intercalated species can be used to characterize the degree of oxidation of the graphite by the identification of the intercalated species. The similar size of the species eliminates size differences from being a significant factor in the properties which differ among the hexafluorides. In this chapter, the reactions of WF_6 and OsF_6 are reported, as well as magnetic and X-ray crystallographic results.

The Reaction of WF_6 with Graphite

Pure WF_6 (from Matheson) was distilled at -22°C, and found to contain no infrared active impurities. The WF_6 was condensed onto graphite and kept at room temperature for 8-48 hours. The graphite (density 2.25 g/cc) floated on top of the WF_6 (density 3.44 g/cc) and did not react. The graphite recovered after removal of the WF_6 was grey and the powder pattern was identical to the pattern of the initial graphite. The failure of WF_6 to react is consistent with

its relatively low oxidation strength (80 kcal/mole) compared with the other third row transition metal hexafluorides. These results are confirmed by French workers.[2]

The Reaction of OsF_6 with Graphite

The reaction of OsF_6 with graphite was performed because OsF_6 is a stronger oxidant than WF_6. OsF_6 was prepared by fluorinating the metal powder (99.9 percent, Orion, Huntington Beach, CA) in a prefluorinated monel bomb for two days at 250°C, removing all volatiles at -78°C, and then distilling at room temperature into a prefluorinated monel can. The OsF_6 was pure by its infrared spectrum and showed no $OsOF_5$.

The powdered graphite was heated at 100°C overnight at dynamic vacuum, and then heated under dynamic vacuum with a torch until the quartz tube was glowing red. This final heating was continued until the graphite failed to jump about and the pressure failed to rise above 50 microns. The yellow OsF_6 was condensed onto KF or CsF to remove any trace HF, and then condensed onto the graphite. Sufficient OsF_6 was condensed so that a solid was present at all times. The OsF_6 was removed after five to twenty-four hours, the entire container and contents were weighed, and the samples were removed to the Drilab.

In Table 1-1 are given the results for several preparations. The elemental analysis for carbon, hydrogen, and nitrogen was performed by the analytical services within the department. The carbon analysis gives a more consistent stoichiometry near C_8OsF_6 than does the

gravimetry. However, a problem arose in the C, H, and N analysis because a sizable amount of nitrogen was seen. As much as one "N_2" was seen for each OsF_6 present. For a C_8OsF_6 stoichiometry, there is not sufficient room within the galleries to contain any nitrogen. The initial graphite contained no nitrogen. In order to test the analysis, a sample of $SF_3^+OsF_6^-$ — which had been handled in the nitrogen atmosphere of the Drilab — was analysed and showed no nitrogen. A mixture of graphite and $SF_3^+OsF_6^-$ was then analysed and nitrogen appeared. Apparently in the analysis, "nitrogen" is analysed at the end of a long train by gas chromatography. The final signal has been calibrated for nitrogen and is always presumed to be nitrogen. In the combustion of the graphite compound, carbon fluorides are formed which pass through the train and are detected as nitrogen. There was no way to correct for this lost carbon, although estimates showed that it was small relative to the percent carbon analysis (24 percent carbon as compared to about 1 percent carbon being in the "6 percent nitrogen"). Because carbon fluorides have a larger heat capacity than N_2, the gas chromatograph would detect more "N_2" than was present as CF_4. Because the percent carbon in CF_4 is less than that in the intercalation compound, the percent carbon given here is an upper limit on the amount of carbon. This upper limit is established by taking the percent nitrogen and multiplying by the weight percent carbon in CF_4. Within the errors of the carbon analysis, these samples are all C_8OsF_6.

The stability of these compounds to heating provides a qualitative test for the degree of oxidation. The sample $C_{8.55}OsF_6$ was heated to 150 and 200°C while being pumped intermittantly under vacuum to see if any OsF_6 could be driven off. There was no significant weight loss over the ten hours of the experiment. This experiment supports the contention that no neutral OsF_6 is within the graphite. OsF_6 cannot be removed from the graphite upon pumping.

The Reaction of OsF_6 with Graphite in WF_6

Earlier work had used WF_6 as a solvent for the OsF_6 reaction. The reasoning was that WF_6 does not intercalate, so that only OsF_6 ought to intercalate. WF_6 was condensed onto graphite at -196°C, and then OsF_6 was added. The mixture was allowed to warm to room temperature. Within one hour, the graphite which had been floating on top of the solution had sunk to the bottom. The samples were left for seven to thirty-six hours, and then all the volatiles were removed at room temperature. Table 1-1 gives the gravimetric stoichiometry assuming only OsF_6 was the intercalated species. One other sample was run in Teflon-FEP tubing rather than in quartz. This sample indicated an unreasonable weight gain, which was later shown to be WF_6 soaking into the FEP wall.

While the assumed stoichiometries give little indication about the amount of WF_6 which might be present, two important features arise from this work. First, the samples sank within about one hour. McCarron later showed that the MF_6^- ions which are present within the graphite stage as $C_{12n}MF_6$. WF_6 has a density of 3.44, and

carbon has a density of 2.25. A $C_{12}OsF_6$ would have a density of 2.93 g/cc based on a carbon-carbon interplanar distance of 8.04 A. C_8OsF_6 would have a density of 3.94 g/cc. Since WF_6 has nearly the same molecular weight as OsF_6, these densities are within two percent of the "C_xWF_6" hypothetical compounds also. The impressive point is that on these powdered samples, the material reached beyond a first stage $C_{12}MF_6$ composition within the hour. The intercalates would sink near a composition $C_{10}MF_6$. The hexafluorides enter the graphite rapidly.

The second significant point from this work comes from the determination of the degree of oxidation in these intercalates. This determination can be made by comparing the magnetic susceptibility of the C_8OsF_6 compounds made from OsF_6 alone with the C_xMF_6 compounds made in WF_6. Figure 1-1 compares the magnetic susceptibility of C_8OsF_6 with $SF_3^+OsF_6^-$. Clearly, from the parallel slopes of the lines, the magnetic moments of the compounds are virtually identical. Two different samples of C_8OsF_6 gave moments of 3.49 and 3.50 Bohr magnetons compared to the 3.44 and 3.46 Bohr magnetons of $SF_3^+OsF_6^-$.[3] The intercalation compound can be characterized as $C_8^+OsF_6^-$.

The antiferromagnetic tail observed in the graphite compound below 16 K is of some interest. While the close packing of OsF_6^- within a gallery may provide for some magnetic exchange, an alternative mechanism called the RKKY (Ruderman, Kittel, Kasuya, and Yosida) interaction is possible.[4] In this mechanism, one magnetic moment polarizes the conduction electrons nearby. This polarization of electrons leads to an oscillatory polarization of the conduction electrons as one moves

away from the first ion. A second ion feels the polarization in its neighborhood. Depending on the distance from the first ion, the second ion will sense either a ferromagnetic or antiferromagnetic interaction with the conduction electron polarization. By the mechanism of the conduction electrons' polarization, one magnetic ion is coupled to another ion either ferromagnetically or antiferromagnetically. While the distance between osmium sites is 4.92 Å within a plane, the distance from an osmium to the graphite π electrons if 4.0 Å or less. The closer approach of the osmium to the graphite may support the contention that the osmium exchanges with the conduction electrons rather than directly with neighboring ions. The $SF_3^+OsF_6^-$ shows no such magnetic coupling, which is consistent with its lack of conduction electrons. Studies of other magnetic ions within graphite, and with different spacings between the ions within a gallery, might show whether this RKKY mechanism is the source of the magnetic exchange. The graphite system provides a unique opportunity to look at isolated molecular ion magnetic moments in an an isotropic conduction electron media.

The degree of oxidation in the C_xMF_6 compounds can now be determined. The compound "$C_{11}OsF_6$" was made from a mixture of WF_6 and OsF_6. There was insufficient WF_6 to form a visible liquid during the reaction. The composition quoted above comes from a carbon analysis done three months after the synthesis, and the magnetic susceptibility was done four months after synthesis. Thus, some WF_6 may have come out of the sample, and one can presume that not much more WF_6 came out within the month's time. The moment observed was 3.16 Bohr magnetons,

which indicates about 80 percent OsF_6^- and 20 percent WF_6. The compound is C_{55}^{+4} $(4OsF_6^-, WF_6)$, and thus, has a C_{14}^+ degree of oxidation. A second sample "$C_{8.55}OsF_6$" was made in liquid WF_6. It had a moment of 2.42 BM and is thus only 50 percent OsF_6^-. This implies a C_{18}^+ degree of oxidation. Lastly, a third sample of "$C_{10}OsF_6$" gave 50-66 percent OsF_6^-, and thus has a degree of oxidation of C_{15}^+ to C_{20}^+. It is interesting that all three samples given here end up with degrees of oxidation C_{14}^+ to C_{20}^+. Perhaps insufficient OsF_6 was added to go beyond this degree of oxidation in these samples. It may well be that the compounds formed are the kinetically stable forms when WF_6 is present to occupy the space. The activity of OsF_6 may be less when it is diluted in WF_6. For whichever of the three reasons, the presence of WF_6 in the compounds has been clearly shown. It is also noteworthy that in these compounds, no magnetic exchange was evident at low temperatures. Apparently the WF_6 molecules separate the OsF_6^- sufficiently so that no exchange occurs. This evidence supports the argument that the coupling of OsF_6^- moments in the saturated compounds $C_8^-OsF_6^+$ is a direct ion-ion interaction and is not coupled through the conduction electrons. However, if disorder of the ions is present, then the conduction electron mechanism would not appear either.

X-Ray Diffraction Results of $C_x^+OsF_6^-$

To further confirm the structure $C_8^+OsF_6^-$, X-ray diffraction experiments were performed. Powder patterns were gathered from pyrolytic graphite samples listed earlier. Precession photos were taken using monochromator graphite (Union Carbide) or graphite single crystals

isolated from marble found in the Santa Lucia mountains near Carmel, California. The chips of graphite from the monochromator graphite were made by cleaving them with a razor blade. The monochromator chips were reacted in quartz vessels for several hours, and then loaded into quartz capillaries in the Drilab. The crystals were mounted in quartz capillaries between pieces of quartz wool. A piece of Teflon FEP tubing was molded around the capillary neck and helium leak tested. The FEP was then attached to the vacuum line with Swagelock. OsF_6 was added to the crystals for three to 24 hours. This time was presumed adequate since, in WF_6, a composition $C_{10}MF_6$ was reached within an hour. Table 1-2 gives a summary of the X-ray results.

Due to the disorder of the graphite from one plane to another, the pyrolytic graphite and monochromator graphite showed no ab plane order. Precession photos showed rings in the ab plane. The only prominent lines in the powder patterns or precession photos were the (00L) lines. In all cases, the strong lines are for L=1,2,4, and 6. This pattern is consistent with a structure factor analysis placing the Os on the mid-plane between the graphite, and the fluorines at ±3/8. (For fluorines with a radius of 1.33 Å, the center of the fluorines must be 3.0 Å from the carbon layer.) For cases where WF_6 was present, all the data show c to be 8.02(7) Å. In the cases C_xOsF_6 where $x > 8.2$, c=8.06(3) Å. For the single case where x=8.00, the c value drops to 7.80 Å. In the monochromator work, the c axis angular distribution was sizable, due either to the graphite itself or to mechanical bending of the piece upon cleaving. These spots were larger in breadth and thickness, and

therefore would be more susceptible to errors in measurement. Another source of error was from misalignment of the chip, because the ab plane gave no orientation criteria. However, all measurements showed 8.05(5) Å.

The single crystal work was the most definitive. The crystals were exposed to the OsF_6 for three or more hours, and the crystal was pumped briefly and sealed in the capillary. The ab plane showed distinct spots rather than rings. The photographic spots were smaller and had less angular spread than the monochromator chips.

The c axis in both crystals showed 7.75(5) Å, with L=1,2,4, and 6 being the priminent reflections. No intermediate spots, indicating a c of 15.50 Å were seen on (00L) or (H0L) reflections. Apparently the graphite planes lie directly above one another. This is a significant structural development. If the graphite planes were oriented to fit tightly with the three neighboring fluorines of the MF_6, then one layer would be slipped relative to another as in graphite. This slipping would double the observed c, but was not observed. That the graphite planes lie directly over one another implies the graphite layer does not organize with respect to the fluorines. The c axis contraction from 8.05 to 7.75 Å as one approaches a C_8OsF_6 composition has also been observed in the C_8AsF_6 situation. The contraction of the spacing must be due to the enhanced coulomb attraction of the positive carbon for the negative ion.

The (HK0) photographs showed a clear hexagonal set of spots with a=4.92 Å, which is twice the graphite a. This spacing is seen only if the reaction is stopped after three to six hours and the photographs

are taken immediately. At room temperature, the hexagonal array of spots at (100) broaden and eventually form a diffuse ring within 24 hours. The spots at (200), which are the (100) of graphite, always remain sharp due to the graphite lattice although they grow much weaker in intensity (Fig. 1-2). The best photographs were attained by reacting a crystal for three hours, and then immediately cooling the sealed evacuated capillary to -40 C. Photographs were taken over a week while keeping the capillary cold (-40 C) with a stream of cold nitrogen. Rather than disordering within 24 hours, the crystal remained ordered for over a week. Upon warming, the crystal disordered quickly and irrereversibly. Only by cooling can the $\underline{a}$=4.92 Å spacing be seen, which corresponds to a C_8OsF_6 unit cell.

This disordering explains why the powder patterns only showed OOL lines. This behavior is consistent with the graphite planes not registering with the ions because the graphite cannot locally distort to fit with the disordered ions. This disorder of the ions may explain why the graphite planes lie above one another. This disorder may well be more common in the graphite intercalation compounds. There are several reports in the literature where a "single crystal" study shows an $\underline{a}$=2.46 Å, and yet the unit cell volume cannot hold the molecular unit. This error could be explained by a disorder of the molecular species, which left diffraction spots from the graphite planes. A similar disordering was observed in the C_8AsF_6 crystals.

References for Chapter I

1. N. Bartlett, Angew. Chem. Internat. Ed., 7(6), 433, 1968; Canterford and Colton, Halides of the Second and Third Row Transition Metals, Wiley Interscience, 1968.
2. A. Hamwi, P. Touzain, L. Bonnetain, Mat. Sci. Eng., 31, 95, 1977.
3. N. K. Jha, Ph.D. Thesis, University of British Columbia, 104, 1965.
4. M. A. Ruderman and C. Kittel, Phys. Rev. 96(1), 99, 1954; T. Kasuya, Prog. Theoret. Phys., 16, 45, 1956; K. Yosida, Phys. Rev. 106(5), 893, 1957; P. G. deGennes, Journal de Physique et le Radium, 23, 510, 1962.

Table 1-1. Compositions of $C_x^+OsF_6^-$.

Gravimetric Composition	Composition from Analysis C	H	N	Stoichiometry	Magnetic Moment (Bohr magnetons)
"C_8OsF_6"	24.0	0	0		
"$C_{7.8}OsF_6$"	23.0	0.1	6.72	$C_{8.24}OsF_6$	3.49 (after heating)
	$C_{8.55}OsF_6N_{2.08}$				3.54 (before heating)
"$C_{8.64}OsF_6$"	23.2	.16	4.41	$C_{7.95}OsF_6$	3.50
	$C_{8.13}OsF_6N_{1.32}$				
"$C_{12.3}OsF_6$"	23.5	0.1	6.48	$C_{8.19}OsF_6$	3.40 (sample was not strong antiferro-magnetic)
	$C_{8.51}OsF_6N_{2.0}$				
"$C_{10.4}OsF_6$"	no analysis done				none
Compositions of C_xMF_6 from $OsFO_6$ in WF_6					
"$C_{9.35}OsF_6$"	28.3	.16	6.78	$C_{53}^{+4}(4OsF_6\ WF_6)$	3.16
	$C_{11.0}OsF_6N_{2.26}$				
"$C_{12.7}OsF_6$"	24.8	.23	1.79	$C_{17}^+OsF_6^-\ WF_6$	2.42
	$C_{8.55}OsF_6N_{0.53}$				
"$C_{10.25}OsF_6$"	no analysis sample had sunk			$C_{103}^{+7}7OsF_6^-\ 3WF_6$	2.94
"$C_{7.2}OsF_6$"	no analysis done				none

Table 1-2. X-Ray Diffraction Results

Composition	c-spacing (angstroms)	00L L=	
Powder Pattern Results			
Samples from WF_6			
$C_{53}^{+4}(4OsF_6^- \cdot WF_6)$			
$C_{17}OsF_6^- \cdot WF_6$	8.00	1,2	
"$C_{10.25}OsF_6$"	7.98	1,2	
"$C_{7.2}OsF_6$"	8.1	1,2,4,6	
Samples from OsF_6 alone			
$C_{8.24}OsF_6$	8.08	1,2,4	
$C_{7.95}OsF_6$	7.80	1,2,4,6	
$C_{8.19}OsF_6$	8.05	1,2,4	
"$C_{10.4}OsF_6$"	8.06	1,2,4	
Precession Photographs			
Monochromator chips			
"$C_{10.4}OsF_6$"	8.10	1,2,4,6	
Chip "I" 25 C (made from WF_6)	7.98	2,4,6	(001) is hidden by the beam stop.
-100 C	7.93	1,2,4,6	
Chip 25 C	8.04	1,2,4,6	
-100 C	8.00	1,2,4,6	

(continued)

Table 1-2 (continued)

Single Crystals		c-spacing	OOL	a spacing
Crystal R		7.75	2,4,6	5.0 Spots are very broad
Crystal "5"	Polaroid	7.75	1,2,4	4.97 (5)
(kept at -40 C for one week)	X-ray film	7.75	1,2,4,6	4.95(3)

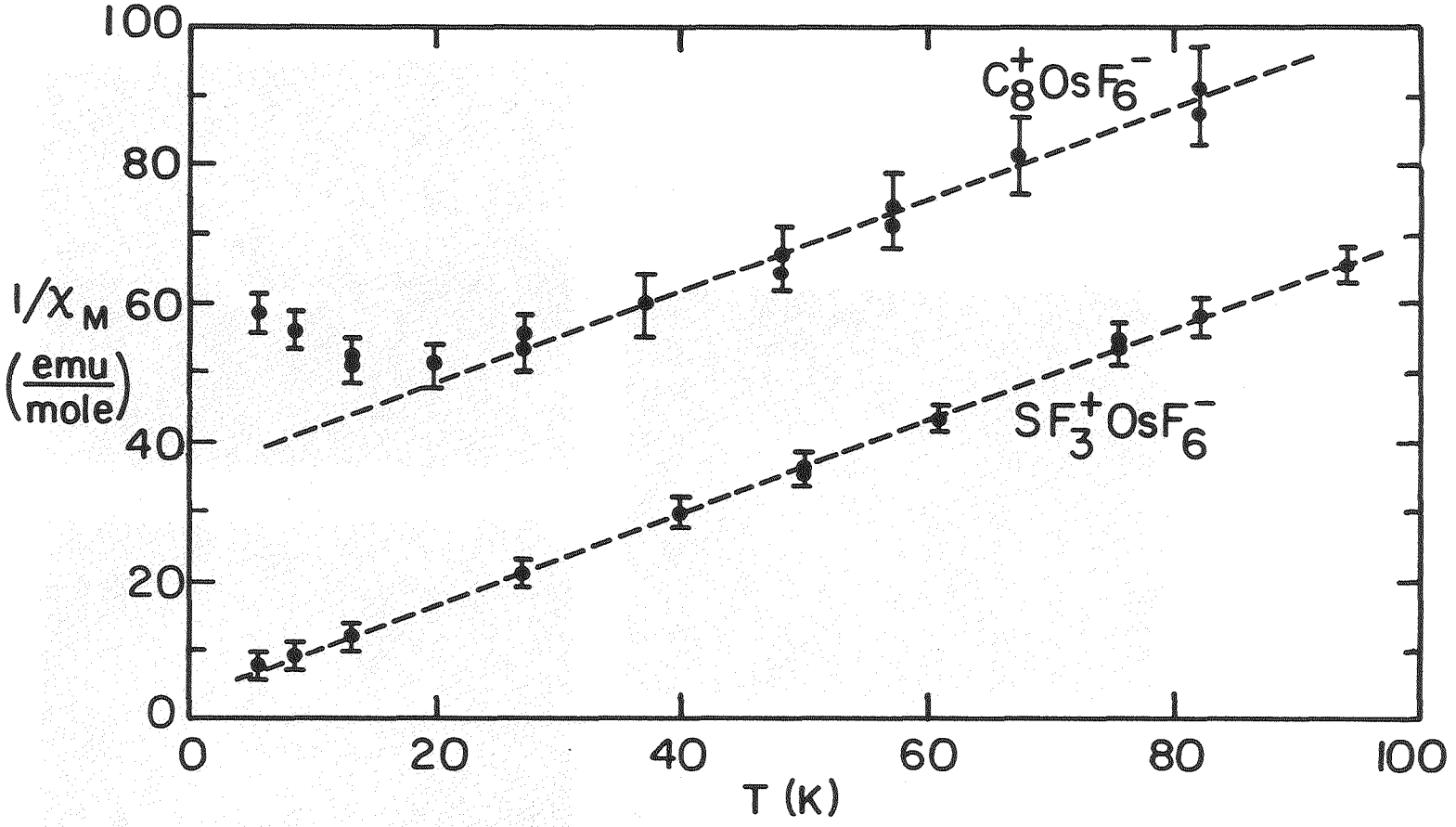

Figure 1-1

Magnetic Susceptibility of $C_8^+OsF_6^-$

Figure 1-2

Loss of HK0 Order Over 24 Hours of $C_8^+OsF_6^-$

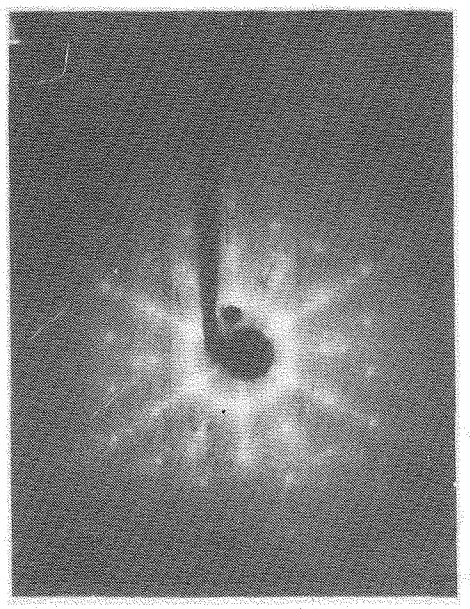

One hour
after reaction

8 hours
after reaction

24 hours
after reaction

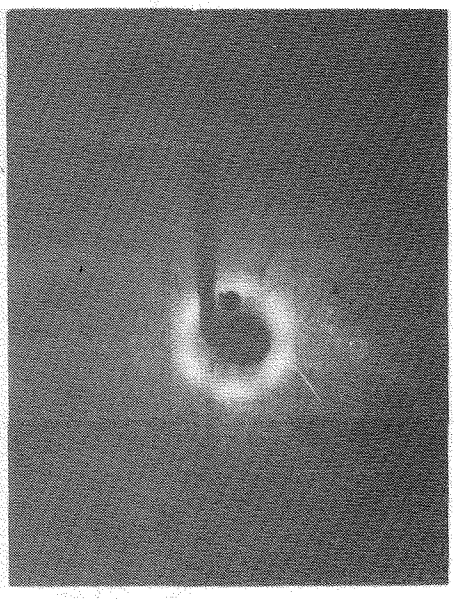

XBB 801-13922

CHAPTER 2

$C_x^+AsF_6^-$ Synthesis and Characterization

Introduction

The most significant portion of this research was based on the synthesis and identification of the intercalated species in "C_xAsF_5". Selig and coworkers first prepared a "$C_{10}AsF_5$" by reaction of AsF_5 gas with graphite.[1] They presumed that the neutral AsF_5 molecule was present within the gallery. An entire theory had grown which supported the presence of neutral molecules (Lewis acids) within the graphite galleries.[2] When the group at the University of Pennsylvania claimed in 1976 that the conductivity of C_xAsF_5 was as high as copper, a great interest was taken in this compound.[3] How could neutral molecules lead to such a dramatic increase in conductivity? A wealth of experimental techniques were employed to determine the electronic properties of this compound.[4] The Lewis acid theory so dominated the thinking that no one looked at the chemical identity of the species present within the graphite. The graphite literature has only a few simple cases where the chemical species present within the graphite was conclusively identified. Most researchers perform elemental analysis, and see the stoichiometry is nearly identical to the starting species. For instance, in "C_nAsF_5," the As:F ratio is 1:5. This identity has lead researchers to assume that the intercalated species is the initial reagent.[5] This assumption can be flawed, and work in this lab has shown conclusively[6] that the oxidation reaction:

$$3AsF_5 + 2e^- \longrightarrow 2AsF_6^- + AsF_3$$

occurs in the reaction of graphite with AsF_5. This proposed reaction would oxidize the graphite and place the AsF_6^- (and AsF_3) within the graphite. Holes created in the valence band would be the principle charge carriers for the enhanced conductivity. This half-reaction would still allow for an arsenic:fluorine ratio of 1:5. Earlier antimony Mossbauer work of graphite with SbF_5 showed Sb(V) and Sb(III),[7] presumably made in an analogous oxidation reaction. This proposed reaction has stirred a vigorous discussion of the chemical and electronic characterization of the graphite-AsF_5 compound.

In the next two chapters, the synthesis and characterization of "C_xAsF_5" and $C_x^+AsF_6^-$ will be discussed. The synthesis of C_xAsF_6 from $O_2^+AsF_6^-$ provides a parallel compound to the C_xAsF_5 compound. Both compounds are expected to have AsF_6^- ions present, and a direct comparison can be made. In a following chapter, the utility of X-ray absorption spectroscopy in identifying the species within the graphite is described.

Synthesis of $C_x^+AsF_6^-$

The synthesis of C_xAsF_6 was performed in the following routine. The graphite powder was prepared and heat treated as described in the C_8OsF_6 case. The salt $O_2^+AsF_6^-$ was synthesized by photolysis of a stoichiometric mixture of O_2, F_2, and AsF_5 in a five liter pyrex bulb. The salt was added to the graphite in the Drilab, and the solvent

SO_2ClF (Ozark Mahoning) was condensed into the tube. The sample was kept at -63 to -78°C for one to three days. The tube was then warmed and the solvent was removed. The entire assembly was weighed in order to determine the weight uptake of AsF_6^- and taken into the Drilab. Table 2-1 gives a summary of the experimental conditions and results. The composition was determined by weight uptake and by carbon analysis, which presumed the remaining weight percent was AsF_6^-.

Several synthetic details arose during these reactions. First, the elemental analysis frequently showed 1.5 percent nitrogen, even when the sample was handled under a helium atmosphere. As in the OsF_6 case, this "nitrogen" is apparently volatile carbon fluorides which are detected as nitrogen. Less "nitrogen" was seen in C_xAsF_6 than was seen in C_xOsF_6, so that a small correction was necessary. Second, in the OsF_6 case, WF_6 appeared to cointercalate. In these cases with SO_2ClF, an insignificant amount of sulfur (0.19 percent) was detected in the $C_{8.17}AsF_6$ sample. However, a sizable percent chlorine (2.79 percent) was detected. This "chlorine" is presumably a product from the fluorine given off in combustion. The inability of SO_2ClF to cointercalate is apparently due to the slightly larger size of the chlorine compared to the fluorine. One might have expected the pseudo-tetrahedral SO_2F_2 to be the same thickness as a hexafluoride, and therefore it would cointercalate. The SO_2ClF would be slightly larger than SO_2F_2, and probably is too large. Only if the S-Cl bond were parallel with the a-axis would SO_2ClF present a minimum thickness, but the constrained orientation may not allow the molecule sufficient motional freedom to diffuse

through the galleries. The greater thickness of SO_2ClF compared to AsF_6^- prevents the cointercalation of SO_2ClF.

The third factor in the synthesis is the reaction of the solvent SO_2ClF with the $O_2^+AsF_6^-$. There was an unidentified impurity in the solvent which formed a very deep purple color at low temperature (-63°C) when the salt was present. This impurity could be removed by reaction of the solvent with the salt at room temperature. The clean solvent could then be distilled after removal of other volatiles such as SO_2F_2. Roughly half of the reactions listed in Table 2-1 used the purified SO_2ClF. The production of SO_2F_2 and other volatiles comes from the reaction of $O_2^+AsF_6^-$ with SO_2ClF near room temperature. No reaction was observed by Biagioni and Bartlett below -63°C. By warming the solution near room temperature, one could remove excess salt by reaction with the solvent. In all cases here, the synthesis of the graphite salt was performed at -63°C or below. However, the carbon:AsF_6 ratio of the graphite salts are always greater than the initial ratio of carbon:$O_2^+AsF_6^-$. One could only reach C_8AsF_6 by having an excess of $O_2^+AsF_6^-$. By following the evolution of oxygen, one could see that a C_8AsF_6 composition was reach. Only by destroying any excess O_2AsF_6 by warming the solution could a C_8AsF_6 composition be isolated. No $O_2^+AsF_6^-$ remained in the powder patterns of the graphite samples. The discrepancy between the final carbon:AsF_6^- ratio and the initial reagent ratio must be due to some small amount of solvent reaction at these low temperatures, and to errors in the carbon analysis due to formation of volatile carbon fluorides.

X-Ray Diffraction Results

The X-ray diffraction data for samples of $C_x^+AsF_6^-$ are given in Table 2-2. All powder diffraction showed the c-spacing to be 7.80 Å to be indicative of a first stage compound. No hint of a second stage composition, nor a hint of a c-axis superlattice was seen. In all samples, the d-spacing 2.13 Å (100 of graphite a=2.46) was seen. In two samples, $C_{12.5}AsF_6$ and $C_{11.05}AsF_6$, a line at 4.26 Å was seen which indicates 100 of a hexagonal a=4.92 Å. No other hk0 lines were ever observed in the powder data.

These parameters presented a puzzle. First, one rarely saw any a-axis lines except lines which can be attributed to the graphite planes. The failure to see a larger unit cell must be due to disorder of the intercalated ions. Second, it is curious that in the two samples which showed an a=2.46 Å, (which is indicative of a C_8MF_6 unit), their compositions were near $C_{12}AsF_6$. No lines were ever seen for an a-axis distance of 6.02 Å, which would be the hexagonal unit for $C_{12}AsF_6$. Third, the thickness of a rigid octahedral AsF_6^- is expected to be 2(1.33 + 1.7/ 3)=4.65 Å. When the graphite sheet thickness 3.35 Å is added on, the c-spacing is predicted to be 8.00 Å. The experimental c value is approximately 0.20 Å shorter than predicted.

To further determine the unit cell, X-ray precession photos were used. Two pieces of monochromator graphite were reacted with $O_2^+AsF_6^-$, mounted in quartz capillaries, and sealed. Because this graphite is "well ordered" pyrolytic graphite, the ab plane is disordered, and rings are seen in the hk0 plane. In cleaving the chip, some distortion of the

graphite occurred, which appeared as a distribution of c-axis angles. This disorder and distortion makes orientation of an ac plane photo more difficult. Both samples may be slightly aligned, so that the c-spacing can be in error by ±0.05 Å. In chip C, it is apparent that one has a mixture of second and third stage. It is also noteworthy that this mixture would predict a first stage thickness of 8.00 Å, rather than the 7.80 Å. No HOL spots were observed. The monochromator work gave no significantly new information from that of the powders.

More information was garnered from the single crystal graphite work on the precession camera. The crystals were reacted in quartz tubes with an excess of $O_2^+AsF_6^-$ in SO_2ClF. The crystal was removed in the Drilab, mounted in a quartz capillary, and sealed. All crystals showed a distinct array of "graphite" hkO diffraction spots indicative of a=2.46 Å. However, two crystals showed larger spots at 4.26 Å indicative of an a=4.92 Å. These spots are weak, against a strong diffuse ring. As in the OsF_6 case, these spots become more broad and diffuse while the photos are being taken. One possible interpretation of this loss of ab plane order is that the crystals are not at the limiting C_8AsF_6 composition. At a lower composition of AsF_6^-, there are voids in the ab plane which are disordered. This disorder destroys the long range ordered array of AsF_6^- which one expects in C_8AsF_6. To test this idea, a crystal (Z) which was disordered after the first reaction, was reacted again with $O_2^+AsF_6^-$. One could expect that the crystal, after the second reaction, would be $C_8^+AsF_6^-$. The diffuse ring remained after the second additional reaction. This experiment shows that the C_8AsF_6 is

disordered just as the C_8OsF_6 is disordered. This disorder problem prevents one from ascribing the unit cell parameters $\underline{a}$=4.92 and $\underline{c}$=7.86 Å as the unit cell of the final product.

References for Chapter 2

1. Lin, Chun-Hsu, H. Selig, M. Rabinovitz, I. Agranat, and S. Sarig, Inorg. Nucl. Chem. Lett., 11(9), 601, 1975.

2. A. Herold, Mat. Sci. Engineering, 31, 1, 1977; W. Rudorff, Adv. Inorg. Chem. Radiochem. 1, 223, 1959; G. R. Hennig, Prog. Inorg. Chem., 1, 125, 1959.

3. G.M.T. Foley, C. Zeller, E R. Falardeau, and F. L. Vogel, Solid State Comm. 24, 371, 1977; E. R. Falardeau, G.M.T. Foley, C. Zeller, and F. L. Vogel, JCS Chem. Comm., 389, 1977.

4. J. E. Fischer and T. Thompson, Physics Today, 36, July 1978; L. R. Hanlon, E. R. Falardeau, and J. E. Fischer, Solid State Comm., 24, 377, 1977; B. R. Weinberger, J. Kaufer, A. J. Heeger, E. R. Falardeau, and J. E. Fischer, 27, 163, 1978.

5. J. E. Fischer, "Electronic Properties of Graphite Intercalation Compounds," Physics and Chemistry of Materials with Layered Structures, Vol. 6, D. Reidel, 520, 525, 1979; J. E. Fischer, JCS Chem. Comm., 544, 1978; J. S. Kasper, L. V. Interrante, and R. S. Markiewicz, 2nd International Conference on Intercalation Compounds of Graphite, Provincetown, MA, May 1980 (to be published in Synthetic Metals).

6. N. Bartlett, R. N. Biagioni, B W. McQuillan, A. S. Robertson, and A. C. Thompson, JCS. Chem. Comm., 200, 1978; N. Bartlett, B. McQuillan, and A. S. Robertson, Mat. Res. Bull. 13, 1259, 1978.

7. J. G. Ballard and T. Birchall, JCS Dalton, 18, 1859, 1976.

Table 2-1. Summary of Synthesis of C_xAsF_6

X of C_xAsF_6 from Gravimetry	C,H,N analysis	mmoles of carbon	mmoles of $O_2^+AsF_6^-$	mmoles of $C:O_2^+AsF_6^-$	Conditions of Synthesis
10.9	none	8.73	0.860	10.15	-78°C, 2 days
5.33	7.84 based on amount of O_2 evolved	9.89	1.72	5.75	-78°C, 3 days
64.7	11.05 9.57 is based on O_2 evolved	8.975	1.13	7.94	-78°C, 2 days
15.4	11.5	7.28	0.927	7.85	-63°C, 1 day
11.1	7.78 based on C,H,N. 8.17 based on C,H,N, S,Cl	6.125	2.26	2.70	-63°C, 2 days SO_2ClF was warmed for 10 hours, and more fresh solvent was added.
15.0	none	3.81	0.658	5.79	-78°C, 1 day
14.8	12.5	20.37	3.196	6.37	-63°C, 2-1/2 days used for EXAFS
13.6	11.93	10.09	1.357	7.43	-63°C, 3 days, used for EXAFS

10.8 (made from $C_{10.8}AsF_5 + F_2$). The weight uptake of F_2 implied the sample may be $C_{10.8}AsF_6 \cdot 1/4F_2$. This sample was sent for EXAFS.

Table 2-2. X-Ray Results of C_xAsF_6

Composition	c-spacing	00L reflections L=	
	Powder Pattern Results		
"$C_{10.9}AsF_6$"	7.82	1,2,3,4	
$C_{7.84}AsF_6$	7.76	1,2,3,4	
$C_{11.05}AsF_6$	7.76	2,3	
$C_{11.5}AsF_6$	none collected		
$C_{8.17}AsF_6$	none collected		
"$C_{15}AsF_6$"	none collected		
$C_{12.5}AsF_6$	7.75	1,2,3,4	
$C_{11.93}AsF_6$	8.04	2,3,4	
	7.80	1,2,3, 5	
	Monochromater Chips		
Chip E	7.82	2,3,4,5,6	(001 is blocked, (005 is very weak.)
Chip C 2nd Stage	11.32	4,6,7	
3rd Stage	14.67	4,8	

(continued)

Table 2-2 (continued)

	Single Crystal Data		
	c-spacing	L =	a-spacing
Crystal N (5-6 hours at -63°C)	7.96(5)	1,2,3,4,6	4.92 (100 spots are faint against background)
Crystal V (3 days at -63°C)	8.01	1,2,3,4,5,6,8 (005 and 008 are weak)	4.92 (100 spots are faint against background)
Crystal Z (3 days at -63°C)	7.86	2,3,4,6	Only a bright ring near a=4.92. The addition of more $O_2^+AsF_6^-$ left the same ring.

CHAPTER 3

The Synthesis and Characterization of "C_xAsF_5"

Synthesis of "C_xAsF_5"

The synthesis of "C_xAsF_5" was performed in the following routine. AsF_5 was purchased from Ozark Mahoning and purified by pumping on the solid at -196°C to remove any fluorine, followed by distillation at -86°C to remove AsF_5 from any AsF_3. No infrared active impurities were observed. The graphite was prepared and heat treated as described in the OsF_6 case. A pressure of AsF_5 was let into the vacuum line, and then expanded into the quartz tube. On one occasion, the AsF_5 was was condensed into the quartz tube above the graphite, and allowed to expand up to the pressure gauge. The reaction was generally run for 1-2 days, and then the AsF_5 was removed by brief (~30 second) pumping of the sample at room temperature. The samples were then taken into the Drilab. A summary of the experimental conditions is given in Table 3-1.

One apparent synthetic characteristic is that, if the final pressure of AsF_5 is below one atmosphere, then the limiting composition C_8AsF_5 is not reached.[1] At a pressure of 150 torr of AsF_5 and a molar ratio C/AsF_5 of 16/1, $C_{16}AsF_5$ is found. Carbon, hydrogen, and nitrogen analysis always gave a higher percent carbon than did the gravimetry. Because the small sample was at vacuum or over N_2/Ar for several hours, some intercalant could diffuse out. Therefore, the gravimetry is a more accurate measure of composition at the time of preparation. The molecules AsF_6^- and AsF_3 are in equilibrium with AsF_5 and the AsF_5

content must be greater at "C_8AsF_5" than at "$C_{16}AsF_5$". The removal of AsF_5 under vacuum may well represent this neutral AsF_5.

The x-ray diffraction data for these compounds is given in Table 3-2. The apparent c-spacing of the powder patterns is 8.05 Å. For second and third stage C_xAsF_6, subtraction of 3.35 Å and 6.7 Å respectively from the c-spacing yields a value of approximately 8.0 Å for the gallery height to be associated with a $C_{12}AsF_6$ occupancy. This spacing (8.05 Å) is greater than the C_8AsF_6 gallery spacing (7.9 Å) but one anticipates that the more highly charged carbon $C_8^+AsF_6^-$ will result in a shorter c-spacing than in $C_{12}AsF_6$. In any case, this spacing is consistent with AsF_6^- being the species which determines the gallery height. We can allow that neutral AsF_5 could pack as truncated octahedra into AsF_6^-. This truncation represents a considerable distortion from the ground state D_{3h} trigonal bipyramidal geometry of gaseous AsF_5 to a C_{4v} square pyramidal species. Fluorine NMR data for AsF_5 liquid shows that intramolecular rearrangement is facile.[2] Such rearrangements probably involve a square pyramidal AsF_5 as an intermediate.

X-Ray Diffraction Results

The most informative X-ray structural data was the single crystal diffraction data. Several graphite single crystals were mounted inside quartz capillaries, attached to FEP as in the OsF_6 reactions, and reacted with AsF_5. Table 3-2 gives the pertinent data. On all crystals where the AsF_5 was pumped off briefly before sealing, the crystal

showed a mixture of first and second stage. In order to maintain a first stage compound, an excess pressure of AsF_5 had to be maintained over the crystal. The crystal was reacted with 1500 torr AsF_5. The crystal was then cooled to -63°C, in order to slow any removal of intercalant while the AsF_5 pressure was reduced. A small amount of AsF_5 was condensed into the bottom of the capillary, and the capillary was sealed. The amount of AsF_5 remaining in the capillary was estimated to create about 3 atmospheres pressure at room temperature. Both crystals prepared in this manner appeared similar. Because one crystal had sharper diffraction spots in precession photos, further Weissenberg diffraction photos were taken.

The precession photographs indicated that two pseudo-hexagonal phases were present. In the HOL photos, one sees "1OL" spots for a phase $\underline{a}$=4.92 Å and $\underline{c}$=16.05 Å and the second phase has $\underline{a}$=5.38 Å and $\underline{c}$=16.05 (Figure 3-1). In the hkO plane, there appears to be a two-fold axis based on the intensity of the hexagonally arranged spots. This discussion will ignore this possible monoclinic cell, and will describe the "4.92 Å" phase and the "5.38 Å" phases in terms of hexagonal units cells. Weissenberg photos were also taken of this crystal, based on an orthohexagonal unit cell.

For the "4.92 Å" phase, the HKO precession photo shows extinctions. These extinctions indicate a hexagonal unit cell with $\underline{a}$ larger than 4.92 Å is the more appropriate one for conventional space groups. Because the proposed half reaction

$$3AsF_5 + 2e \longrightarrow 2AsF_6^- + AsF_3$$

involves three molecules, the plausible cell would have $\underline{a} = 4.92\sqrt{3}$ Å=8.52 Å. Figure 3-1 shows the plausible idealized arrangement of ions within the ab plane. The AsF_3 is located at (H,K)=(0,0), while the AsF_6^- are located at (1/3,2/3) and (2/3,1/3). The fluorines of the AsF_3 must be disordered in order to satisfy this unit cell. This arrangement places the arsenics in the same positions and at the same distance as in the cell based on 4.92 Å.

Table 3-3 gives the diffraction spots visable on the HK0 precession photo and the HK1 spots visable on the Weissenberg photos. The spots are indexed based on the orthorhexagonal unit cell, the hexagonal $\underline{a}$=4.92 Å unit cell, and the hexagonal $\underline{a}$=8.52 Å unit cell. For all cells, $\underline{c}$=16.05 Å. The orthohexagonal indexing shows the expected pattern H+K=2n for a C-centered orthohombic cell based on a hexagonal cell. Looking at the "8.52 Å" cell, one can see why the 100 and 200 spots are rigorously extinct, while 110, 220, and 600 are present. The arrangement of arsenic species allows only H-K=3n to be seen in the L=0 level. The spots 300 and 410 are not seen in the L=0 level, but are seen in the L=odd levels. A simple structure factor analysis shows that the arsenics and carbons do not contribute to the 300 and 410. Since the packing of the fluorines is very similar to the carbons, they would be expected to be, at best, very weak. The pattern with 411 and 301 being present when L is odd does not fit known extinction patterns. By expanding $\underline{c}$ to a four gallery height of 32.10 Å, one

has all visible spots obeying (H-K=3n, L=2n). In order to have a four gallery c-spacing, each of the four galleries must be shifted relative to one another. This four gallery stacking is known in the C_8K compound. This phase thus becomes a=8.52 Å and c=32.10 Å, and the unit cell is $C^+_{96}(8AsF^-_6, 4AsF_3)$.

The second phase "5.38 Å" is more difficult to define. Weissenberg photos showed that this phase was probably twinned, which helps to distinguish it from the first phase, but complicates its interpretation. Weissenberg photos confirmed precession photos that 11L, 20L, and 00L have even L, while 10L and 21L have odd L. There is no apparent extinction pattern visable here, although if a is expanded by $\sqrt{3}$ to 9.32 Å, and c is doubled to 32.1 Å, one has a different extinction pattern from the previous "4.92 Å" phase. The graphite lattice has no 5.38 Å distance, although a distance from one carbon to a distant center of a carbon hexagon is 9.32 Å. Due to the paucity of spots available, it is futile to try to state a unit cell dimension.

This lattice spacing (5.38 Å) is puzzling. The graphite network does not have a carbon-carbon distance of 5.38 Å. This 5.38 Å distance must be related to the As-As distance, and is most likely the As-As distance. If two AsF^-_6 did not close pack, but have two triangular faces juxtaposed, the As-As distance would be 5.38 Å apart.* An a-spacing of 5.38 Å would contain 9.56 carbons, rather than the eight carbons of an a=4.92 Å. Whether the neighboring molecular species to an AsF^-_6

---

*This distance is based on 2 X (1.7 X sin(54.71) + 1.30) = 5.375 Å.

is a non-close packed AsF_6^-, an AsF_3, or a square pyramidal AsF_5 which is bridging to an AsF_6^- fluorine, cannot be determined. It is notable that this crystral appears to have a mixture of "C_8AsF_5" (which is the dominant phase) and "$C_{9.6}AsF_5$." This crystal cannot have a limiting composition of C_8AsF_5, although it must be near this composition.

References for Chapter 3

1. E. R. Falardeau, L. R. Hanlon, and T. E. Thompson, Inorg. Chem. 17(2), 301, 1978.

2. E. L. Muetterties and W. D. Phillips, JACS 81, 1084, 1959.

Table 3-1. Summary of Synthesis of "C_xAsF_5"

X of C_xAsF_5 Gravimetry	C,H,N	Synthetic Details	Comments
9.49	none	Initial pressure was 600 torr. After about 12 hours the final pressure was 240 torr.	Sent for EXAFS
10.82	none	Initial pressure was greater than 1500 torr. Final pressure was 575 torr. The sample was pumped intermittently over a five minute span.	Sent for EXAFS
7.8	11.5	Initial pressure was 1000 torr. Pressure was raised until no pressure drop was seen at 1000 torr. Reaction time was 36 hours. The C,H,N sample was in a nitrogen atmosphere for two days before analysis.	Sent for EXAFS
16.2	20.55	A stoichiometric amount of 150 torr was the initial pressure. This pressure dropped to zero over nine hours. Pumping time was less than a minute.	Sent for EXAFS
Large chip			
8.7	none	1400 torr was continuously maintained over the sample for two days. The excess AsF_5 was removed at -63°C.	Sent for EXAFS orientation studies.

Table 3-2. "C_xAsF_5" X-Ray Results

Composition	c-spacing (A)	00L L=	Comment
Powder Data			
"$C_{9.49}AsF_5$"	8.08 7.77 11.36	2 2,3 2,3,4	100 and 200 of a=4.92 Å are seen.
"$C_{10.82}AsF_5$"	8.04	1,2,3,4,5,6	Only 1st stage
"$C_{7.8}AsF_5$"	8.05	1,2,3,4, 6	
Single Crystal Precession Photos			
(O)	8.12 11.31	2,3,4,5,6 3,4, 6,7,8,9,11	Crystal was pumped
(T)	11.32	2,3,4, 6,7,8,9	Crystal was sealed with some AsF_5. 100 and 200 of a=4.92 Å are observed.
(U)	8.08	1,2,3,4, 6	Crystal sealed with AsF_5
(X)	8.11 11.35	1,2,3,4, 6 2,3,4,6,7,8,9,11	Crystal was sealed with one atmosphere AsF_5.

(continued)

Table 3-2 (continued)

(1)	"8.03"	1,2,3,4,5,6,8	"a=4.92 Å" was related to this c-spacing in 10L, 20L, 22L.
	"16.05"	1,3,5,7,9	"a=5.38 Å" was related to this c-spacing in 10L and $\bar{1}$1L
	This crystal was also used for Weissenberg photos and the actual unit cells is discussed later.		

Table 3-3. Parameters of "4.92 Å" Phase

Indexing of spots

Orthohexagonal	Hexagonal	Hexagonal
a=4.92 Å	a=4.92 Å	a=8.52 Å
b=8.52 Å		
c=16.05 Å	c=16.05 Å	c=32.10 Å
H K L	H K L	H K L
0 0 2n (n=0-6,8)	0 $\bar{0}$ 2n	0 0 4n
4 0 2n (n=0-6,8)	4 $\bar{2}$ 2n	6 $\bar{0}$ 4n
1 1 2n (n=0-5)	1 0 2n	2 $\bar{1}$ 4n
0 2 2n (n=0-4)	0 1 2n	1 $\bar{1}$ 4n
2 2 2n (n=0-4)	2 0 2n	4 $\bar{2}$ 4n
2 0 2n+1 (n=0-6)	2 $\bar{1}$ 2n+1	3 $\bar{3}$ 4n+2
3 1 2n+1 (n=0-3)	3 $\bar{1}$ 2n+1	4 1 4n+2

Spacing of spots

00L L=	4	8	12	16	20	24	28	32
d A (Weiss)	8.11	4.04	2.67	2.03	1.60	1.34	none	1.003
d A (Pre-cession)	8.01	4.06	2.69	2.016	1.605	1.359		1.001
d A (calculated for c=32.1 Å)	8.025	4.013	2.675	2.016	1.605	1.338		1.003

(continued)

Table 3-3 (continued)

H K O	d(Weissenberg)	d(Precession)	d(calculated for a=8.52 Å)
1 1 0	"4.278" (based on 020 of 4.94 Å ortho-hexagonal cell)	4.20 broad spot	4.26
2 2 0		2.13	2.13
6 0 0	1.23		1.23
4 1 0	1.617 (based on 1.647 of 300 portion of 310 ortho-hexagonal cell)		1.61

Table 3-4. Spacings and Indexing of "5.38 Å" Phase of C_xAsF_5

Precession photo HKL	Weissenberg photo	HKL	a=5.38 Å c=32.1 Å	HKL	a=9.32 Å c=32.1 Å
				100	8.084
	4.77(10)	10 4n+2	4.667	11 4n+2	4.667
				200	4.042
				210	3.056
2.67	2.68	11 4n	2.695	30 4n	2.695
	2.36	20 4n	2.333	22 4n	2.333
				310	2.242
				400	2.021
				320	1.855
1.77		21 4n+2	1.764	41 4n+2	1.764

Figure 3-1
HK0 and H0L Zero Level Precession Photoghraphs
of "C_8AsF_5"

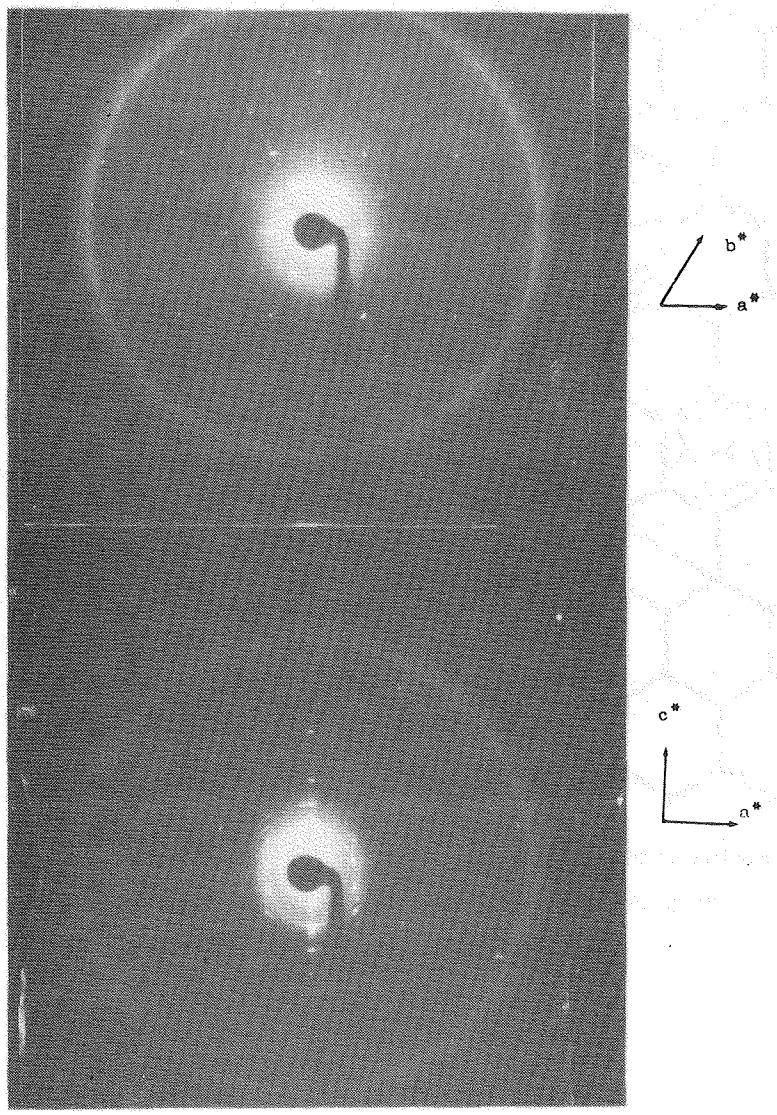

XBB 801-13921

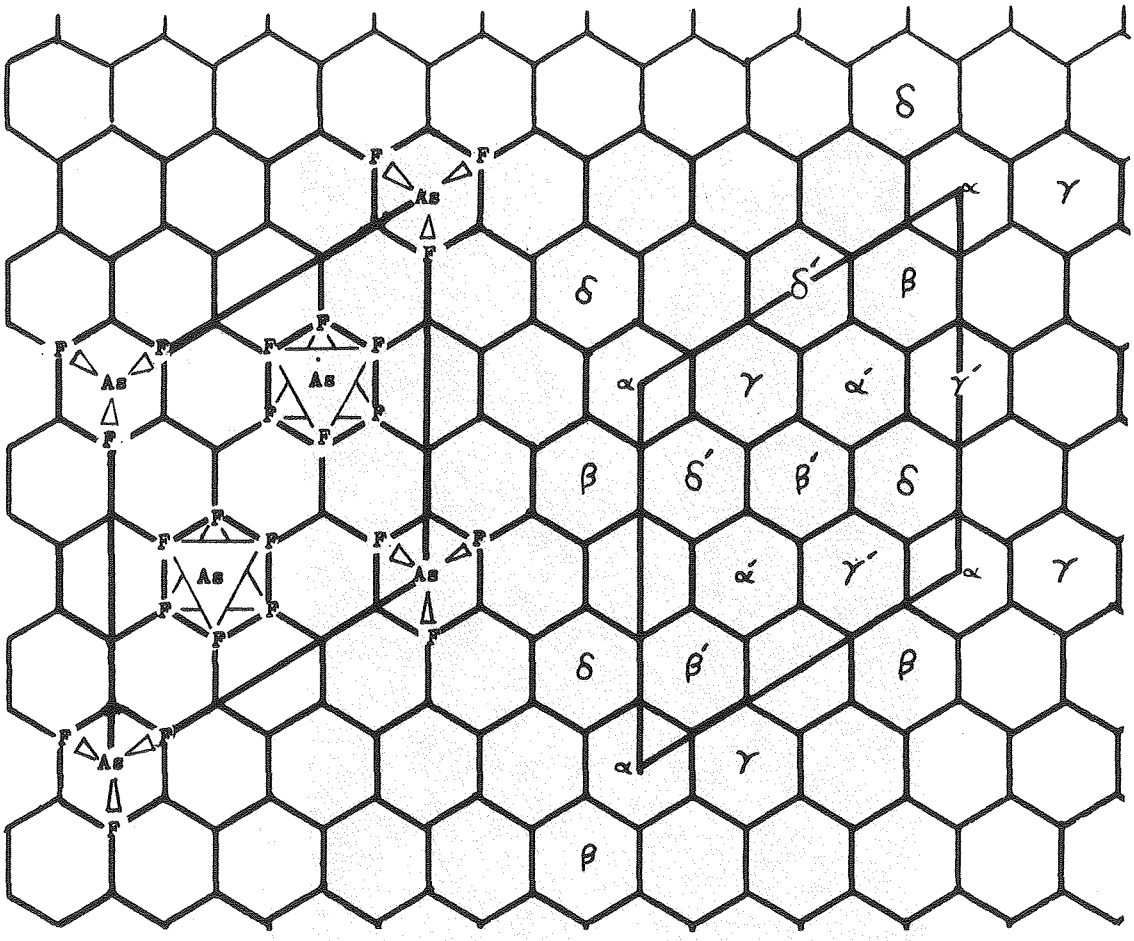

Packing Within a Gallery — Stacking of Four Galleries Along c

Proposed Unit Cell for "C_8AsF_5": a= 8.52 A, c= 32.10 A

XBL 8011-7400A

Figure 3-2

CHAPTER 4

X-Ray Absorption Theory

Due to the recent derivation of the theory of EXAFS,[1] the descriptions of the theory are at several levels of complexity depending on the audience of the author. In this chapter, an attempt wil be made to explain the salient features of the X-ray absorption event and the derivation of the EXAFS equation in qualitative yet physically significant quantum mechanical terms. This approach will attempt to skirt between the two poles of a classical mechanics description (which is easy to visualize) and a rigorous mathematical calculation (which loses all appearance of physical reality). Certain aspects of the quantum mechanical theory will be described by parallel features in other experimental techniques commonly known to chemists.

In any absorption process, whether it be X-ray, UV, infrared, or visual, the absorption coefficient changes as the energy of the exciting radiation changes. For a technique such as IR, a small change in energy leads to a rapid change in the absorption coefficient as a particular vibration mode is excited, and a change in absorption appears as a peak in an infrared spectrum. In X-ray absorption, dramatic changes in the absorption coefficient occur as the energy of the X-ray radiation approachs certain energies characteristic of the particular element. These characteristic energies are called the edges due to the dramatic increase in the value of the coefficient. Two distinct regions appear as one passes in energy through an edge, as shown in Figure 4-1. The 10-40 eV wide region at the rise in the coefficient

is the edge region. The EXAFS (Extended X-ray Absorption Fine Structure) region extends from about 20 to 1500 eV above the absorption rise. These two regions occur from similar, but non-identical processes, and will be discussed separately. Figure 4-2 contains the essential elements for a description of these two regions.

Edge Region

Near an X-ray K-edge, excitations from the 1s orbital of an element to higher levels occur. This excitation can be visualized as a transition of a 1s electron to a higher unoccupied orbital. In the edge region of molecules, these higher orbitals are molecular orbitals.

In quantum mechanics, the probability of a transition is proportional to

$$\left[\int \psi_i \, D\psi_f \, dT\right]^2 \qquad (1)$$

where ψ_i and ψ_f are the initial and final state wave functions, and D is the operator characteristic for the transition. In X-ray absorption, as in IR, D is the dipole moment operator. For a particular transition to have a finite probability, the product group theory representation must have some $A_{(1g)}$ symmetry. For a molecule with a center of symmetry, the initial state 1s has A_{1g} symmetry, D has ungerade symmetry, and thus the final state must also have ungerade symmetry in order to show an absorption. In the literature, this symmetry requirement is stated by having the final state have p character. Figure 4-2 shows such a transition to an atomic 4p state.

In principle, if one knew the molecular orbital symmetry and energies of the neutral molecule up to the continuum level (E=0 in Figure 2), one could assign particular absorption peak energies to particular levels and determine whether E=0 was located on the absorption scan. (This E=0 determination is crucial for the analysis of the EXAFS region, as described below.) In many cases though, the creation of a +1 charge in the 1s orbital upon excitation requires that the outer molecular orbitals change their character-or "relax"- before the electron occupies the molecular orbital. This relaxation would mix the neutral molecule's wave functions and shift their energies so as to lose any identity with the neutral molecule. For instance, the increased core charge would make an AsF_3 molecule's outer orbitals look more like those of an "SeF_3" molecule.* At the present time, there is no sure way to determine whether the particular absorptions seen near the K-edge are characteristic of relaxed or unrelaxed molecular orbitals. The nature of the final states is left ambiguous, no peak assigments can be given with any certainty, and E=0 cannot be given with any certainty.

However, the peak positions for various molecules do <u>generally</u> shift in energy as a function of the oxidation state of the absorbing atom. The higher the oxidation state, the higher the energy of the principle absorption peaks. While the peaks are rigorously determined by the particular molecular orbital arrangement of the individual

---

*Figure 4-3 shows a possible assignment of the AsF_3 edge features using atomic Se(III) state energies.

molecule, this shifting can be thought of as a 1s electron being more tighly bound to the nucleus due to the higher effective nuclear charge. Similar peaks of molecules of the same oxidation state will often group themselves into narrow regions indicative of the oxidation state. By examining several spectra of different oxidation states, one can determine what is the energy span of each oxidation state region.[2] One can then determine the oxidation state of an unknown absorber by observing which region its peak energy occurs.

Along with shifts in energy are shifts in peak intensity as a function of orientation. When the electromagnetic field has a preferred direction or polarization, orientation dependences are seen in single crystal studies using magnetic susceptability or polarization of Raman spectra. Synchrotron radiation is highly polarized in the plane of the electrons' orbit. The electric vector of this polarized beam is parallel with the dipole vector. The initial state 1s is totally symmetric, and thus has no polarization. If the orientation of the final state molecular orbital is spatially orthogonal to the electric vector, no absorption can occur. By rotating the molecule so that the orbital has a component parallel to the electric vector, the transition probability can become finite and the absorption coefficient can grow in intensity.[3] The absorption spectrum can then be described by the equation

$$u(\theta) = u_{\parallel}^2 \cos \theta + u_{\perp}^2 \sin \theta \qquad (2)$$

Here, $u_{\parallel}$ and $u_{\perp}$ are the absorption coefficient scan values over a given energy range, corrected to a unit sample thickness, for θ equal to 0° and 90°. The angle θ is the angle between the electric vector and the molecular orbital.

In summary, the most significant chemical parameter to be determined in the edge region is the oxidation state of the absorbing atom. Changes in absorption intensity using polarized X-rays can aid in making some peak assignments based on symmetry considerations. However, these peak assignments are only tentative and more elaborate molecular orbital calculations which take into consideration core hole relaxation and other secondary excitations would be necessary to confirm such assignments.

EXAFS Region

When the X-ray radiation has sufficient energy to eject the 1s electron from the absorbing atom ($E>E_K$ in Figure 4-2), the EXAFS regions of the spectrum is entered. One can consider this excitation as a transition from the 1s to a final state where a photoelectron is generated and escapes from the atom. For an X-ray energy E, the photo electron will have energy $E'=E-E_K$. Thus, in Figure 4-2 the X-ray of energy $E=E_K+E_1$ generates a photoelectron of energy E_1. For small photoelectron energies, local potential energy variations would perturb the actual energy of the electron and its energy would be directionally dependent. The present status of EXAFS theory cannot deal with this small energy regime due to its complexity. The EXAFS theory has been developed for the higher energy region ($\sim\geq$50-100 eV) where these

perturbations are negligible. In this region, the photoelectron can be considered free, directionally independent of energy, and propagating spherically as described by

$$E = \frac{P^2}{2m_e} = \frac{\hbar^2 k^2}{2m_e} \tag{3}$$

Here, P is the classical momentum of the electron, and is equal to $\hbar k$ where k is a wave number for the free electron. The mass of the electron is m_e. Using this free electron limit, the EXAFS equations for the fractional oscillations $\chi(k)$ of the absorption coefficient $\mu(k)$ develop in the following way:

$$\chi(k) = \frac{\mu(k)-\mu_o(k)}{\mu_o(k)} = \frac{\mu(k)}{\mu_o(k)} - 1 = \frac{\langle \psi_{1s} | D | \psi_{f,s} \rangle^2}{\langle \psi_{1s} | D | \psi_f \rangle^2} =$$

$$\frac{\langle \psi_{1s} | D | \psi_{f,s} \rangle^2}{\langle \psi_{1s} | D | \psi_f \rangle^2} - 1 \tag{4}$$

By making the suitable separation

$$\langle \psi_{1s} | D | \psi_f + \psi_s \rangle^2 = |\langle \psi_{1s} | D | \psi_f \rangle + \langle \psi_{1s} | D | \psi_s \rangle|^2$$

$$= \langle \psi_{1s} | D | \psi_f \rangle^2 + 2\langle \psi_{1s} | D | \psi_f \rangle \langle \psi_{1s} | D | \psi_s \rangle^* + \langle \psi_{1s} | D | \psi_s \rangle^2 \tag{5}$$

and assuming that

$$\langle \psi_{1s} | D | \psi_s \rangle \ll \langle \psi_{1s} | D | \psi_f \rangle$$

then

$$\chi(k) = 1 + \frac{2\langle\psi_{1s}|D|\psi_f \times \psi_{1s}|D|\psi_s\rangle}{\langle\psi_{1s}|D|\psi_f \times \psi_{1s}|D|\psi_f\rangle} - 1 + \begin{bmatrix}\text{small}\\ \text{terms}\end{bmatrix}$$

$$\cong \frac{2\langle\psi_{1s}|D|\psi_f\rangle\langle\psi_{1s}|D|\psi_s\rangle^*}{\langle\psi_{1s}|D|\psi_f\rangle\langle\psi_{1s}|D|\psi_f\rangle} \tag{6}$$

$$= \sum_i \frac{N_i\langle\cos^2\theta\rangle}{R_i^2} \frac{1}{k} A(k)\, e^{-\sigma^2 k^2} \frac{1}{k} \sin(2kR_i + P(k)) \tag{7}$$

The following terms define the parameters used in the previous equations (4) through (7):

$\mu_0(k)$ is the smoothly varying background above the edge of the experimentally measured absorption coefficient $\mu(k)$.

ψ_{1s} is the wave function of the 1s orbital.

ψ_f is the wave function of the outgoing spherical wave and usually has the form $C\sin(kx + P')$.

ψ_s is the wave function of the back scattered portion of the photoelectron.

$\psi_{f,s}$ is the wave function of the "true" final state, and is assumed to be composed of the outgoing and backscattered wave functions in equation (4).

D is the dipole moment operator which governs the X-ray absorption transition probability.

R_i is the distance from the absorbing atom to the scattering atom. N_i is the number of scattering atoms at the distance R_i. A(k) and P(k) are the amplitude and phase functions determining the general shape of the $\chi(k)$ curve for the particular pair of absorbing and scattering atoms.

In the EXAFS equation (7), the chemically significant values to be extracted are N_i, the type of atoms i, the radial distance of those scattering atoms R_i, and a general Debye-Waller term σ_i.

As the photoelectron proceeds out, it will scatter from any potential (Atom B in Figure 4-2) located a distance R_i away from the absorber. Because EXAFS only considers the elastically scattered wave, the backscattered wave has the same energy, and therefore the same wavelength and wave number, as the outgoing wave. The presence of this scattering potential perturbs the wave function of the outgoing photoelectron by giving the "final state" a backscattered wave contribution. Equation (4) shows that the final state scattered wave function $\psi_{f,s}$ is composed of the sum of the outgoing wave and the backscattered wave. If ψ_s were zero, then $\chi(k)$ would be zero.

Equation (5) makes the assumption that $\psi_{f,s}$ is separable into the two component wave functions. Equation (6) makes use of the inequality that the backscattered wave is only a small perturbation on the outgoing wave. This assumption is equivalent to saying that the amplitude of the oscillations of $\chi(k)$ are small compared to the edge jump. Experimentally, the oscillations are 5-10 percent of the edge jump. The transition from equation (6) to (7) involves complex scattering theory and will not be discussed here. However, the various elements of the equation will be explained in terms of the model in Figure 2 and in terms familiar to the chemist.

The most significant part of the EXAFS equation is the $\sin(2kR_i + P(k))/k$ term. This term shows that $\chi(k)$ should oscillate

in sign as the energy is changed, and the peak separation in k-space should be a linear function of the distance R_i. While the sinusoidal oscillation is not apparent, one can qualitatively see this oscillation by comparing the waves at E_1 and E_2 in Figure 2. At E_1, the backscattered wave is in phase with the outgoing wave, so that $\psi_{f,s} = (1 + \delta)\psi_f$. Thus

$$\langle \psi_{1s} | D | \psi_{f,s} \rangle = (1 + \delta) \langle \psi_{1s} | D | \psi_f \rangle$$

$\chi(k)$ in equation (6) should be increased by 2δ. At E_2, the waves are 180 degrees out of phase, and similar argument would show that $\chi(k)$ should be decreased by 2δ. At an intermediate energy, where the backscattered wave is 90 degrees out of phase, δ=0 and the value of $\mu(k)$ at that particular energy should be the same as $\mu_0(k)$. The $2kR_i$ term appears plausible, since the overall wave must travel $2R_i$ to return to the absorbing atom where $\psi_{f,s}$ is defined. Changing R_i by ΔR such that $2k\Delta R=2\pi$ does not alter the interference. Thus, the $2kR_i$ term plays a role analogous to the role of $2(1/\lambda)d$ in the Bragg equation $n\lambda=2d\sin\theta$. If one had a single scatterer at a distance R_i, then one should be able to look at the peak separations in $\chi(k)$ to determine what value of R would give this progression of peaks. A more elegant computational approach would be to Fourier transform $\chi(k)$ into R-space, so that a single peak at $2R_i$ would be seen.

Experimentally, however, the peak separations are not at the correct distance for known compounds. This observation is a result of the phase factor P(k) also present in the sine term. The phase of ψ_f at the point R=0 leaving the absorber is not always zero. Thus, $\psi_f=\sin(kx+P'(k))$. Upon scattering, the backscattered wave also changes phase so as to be $\psi_s=\sin(k(R_i-x)+P''(k))$. The sum of the two waves gives a net phase shift P(k) for the final state wave function. This net phase shift P(k) can be expressed numerically as

$$P(k) = P_0 + P_1k + P_2k^2 + ...$$

$\chi(k)$ then becomes

$$\chi(k) \propto \sin(2kR_i + P_0 + P_1k + P_2k^2 + ...)$$

$$\propto \sin(k(2R_i + P_1) + P_0 + P_2k^2 + ...)$$

Thus, a Fourier transform of $\chi(k)$ will isolate a peak at $(2R_i+P_1)$ rather than at $2R_i$. In order to determine the correct R_i, the terms P_i must be determined either from the empirical phase shifts of standard compounds or from theoretically calculated phase shifts.

The other undetermined parameter in the EXAFS equation is A(k). A(k) is the amplitude function which determines the envelope of the $\chi(k)$ oscillations. A(k) is a function characteristic for each type of backscatterer. For low Z elements (Z<20), A(k) falls off monotonically.

For higher Z elements, A(k) reaches a peak before falling off. Figure 4-2 shows such a case, since the amplitude of the backscattered wave at E_2 is greater than at E_1. In this case, $A(k_1) < A(k_2)$. This peaking of A(k) at particular energies is indicative of increased scattering as the energy of the photoelectron reaches the energies of orbital levels of the scatterer. The drop off of A(k) at high energies can be considered a measure of decreased scattering as the energy of the photoelectron is less perturbed by the scattering potential. An equivalent description would be that the scatterer becomes more transparent to the photoelectron. This peaking of A(k) is diagnostic for the approximate value of Z of the scatterer. Differences in A(k) can also be used to separate scattering due to two scatterers that vary significantly in Z. For curve fitting, the functional form of A(k) must be known either from theory or from empirically determined A(k) of standard compounds.

In real compounds, the vibrations of the scatterer relative to the absorber change the instantaneous distance R_i. This variation in R_i would lead to a summation of $\chi(k)$ for various R_i. This summation would be composed of various waves slightly out of phase with each other. Their sum would be of smaller magnitude than that of an equivalent sum of a single static R_i. This effect can be incorporated in a generalized Debye-Waller term $e^{-\sigma^2 k^2}$. In practice, the Debye-Waller term is of only qualitative value. It is strongly coupled to the amplitude function A(k) in any fitting program. It frequently serves to correct for any errors in the functional form of A(k). As long as σ^2 remains

small and positive — which is physically plausible — this parameter is serving primarily as a Debye-Waller term. However, the value of σ^2 should not be considered accurate until the functional forms of A(k) are known to sufficient accuracy.

The thermal vibrations are also significant in comparing the EXAFS bond distances with known crystal structures. In many crystal structures, each atom is treated as an independent atom vibrating within a given volume. The size of this volume correlates with its Debye-Waller term. The bond length R_i' is defined by the centers of these volumes. However, these centers are not independent of one another. As one atom moves, the other atom is also moved. If the circumstances are appropriate, a riding model correction to this bond distance can be made. This model couples the two atoms. It has the effect of slightly lengthening the bond distance to R_i and of changing the Debye-Waller terms. Physically, the EXAFS experiment already measures the bond distance between two coupled atoms. A comparison of the EXAFS results with a riding model distance is a more appropriate test of the EXAFS accuracy.

The $1/R_i^2$ term for a particular shell is related to the intensity of the outgoing and backscattered wave at a particular distance R_i. The energy density of a propagating spherical wave decays as 1/R. By the time the outgoing wave reaches the scatterer, the initial wave has decayed by $1/R_i$. The backscattered wave, which is some fraction of the outgoing wave, now decays again as 1/R as it passes back to the absorber. For the total trip of the outgoing and backscattered wave, the drop in intensity has fallen as $1/R_i^2$.

References for Chapter 4

1a. D. E. Sayers, Ph.D. Thesis, University of Washington, 1971;

b. D. E. Sayers, F. W. Lytle, and E. A. Stern, Advances in X-ray Analysis, Vol. 13, Plenum Press, New York, 1970;

c. E. A. Stern, Phys. Rev. B., 10, 3027, 1971;

d. B. M. Kincaid, Ph.D. Thesis, Stanford University, 1975 and SSRP Report 75/03.

e. S. P. Cramer and K. O. Hodgeson, "X-ray Absorption Spectroscopy: A New Structural Method and Its Applications to Bioinorganic Chemistry," Prog. Inorg. Chem., 25, 1, 1979.

2. U. C. Srivastava and H. L. Nigam, Coordinating Chemistry Reviews, 9, 275, 1972-3; see 1e also.

3. D. H Templeton and L. K. Templeton, Acta Cryst. A., 36(2), 237, 1980.

4. S. H. Hunter, Ph.D. Thesis, Stanford University, p. 130 and SSRP Report 77/04, 1977.

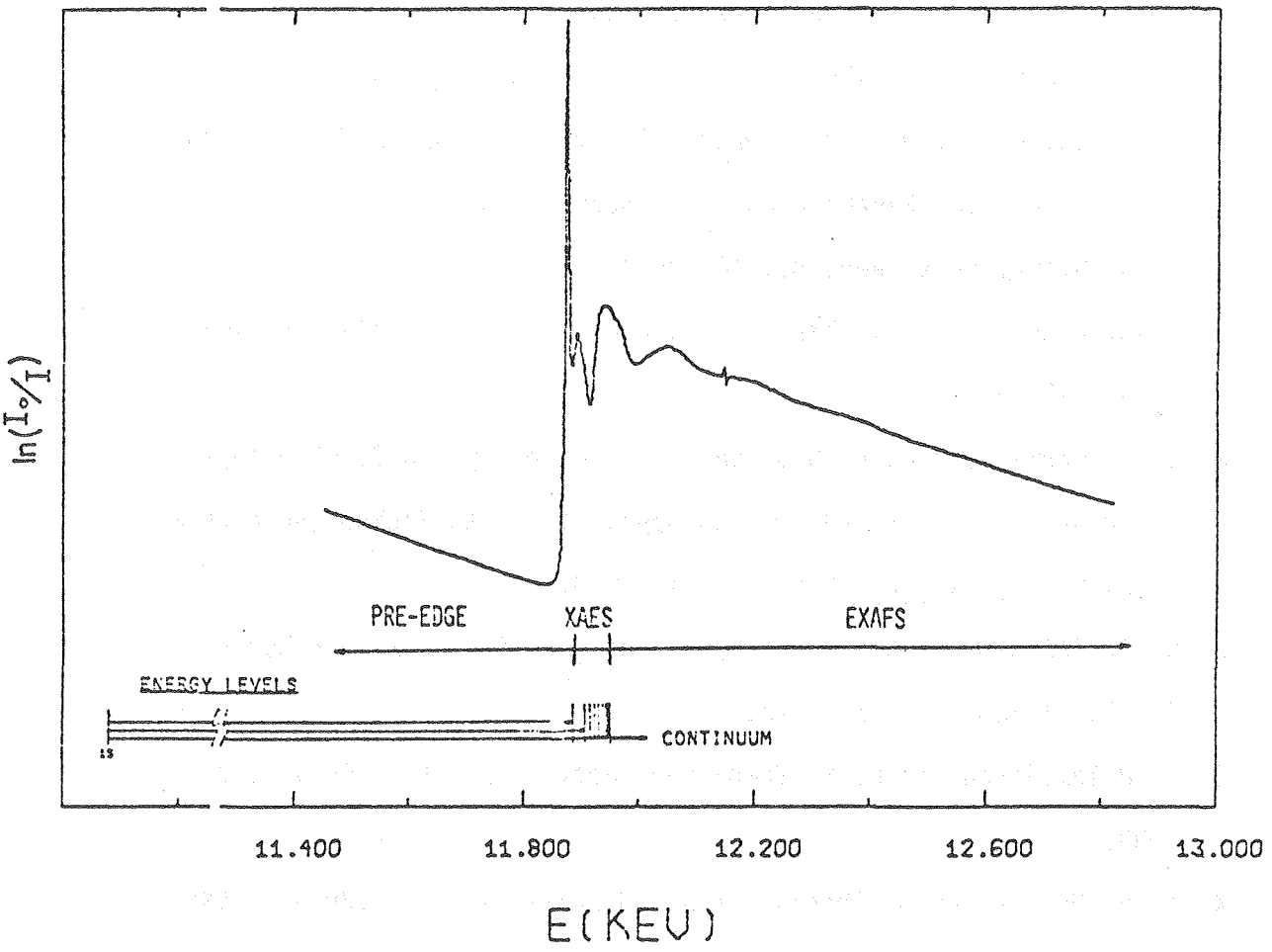

XBL 798-10995A

Figure 4-1

X-ray Absorption Edge Structure (XAES) and Extended X-ray Absorption Fine Structure Regions of $Cs^+AsF_6^-$

Figure 4-2

Depiction of Processes Occurring in X-ray Absorption

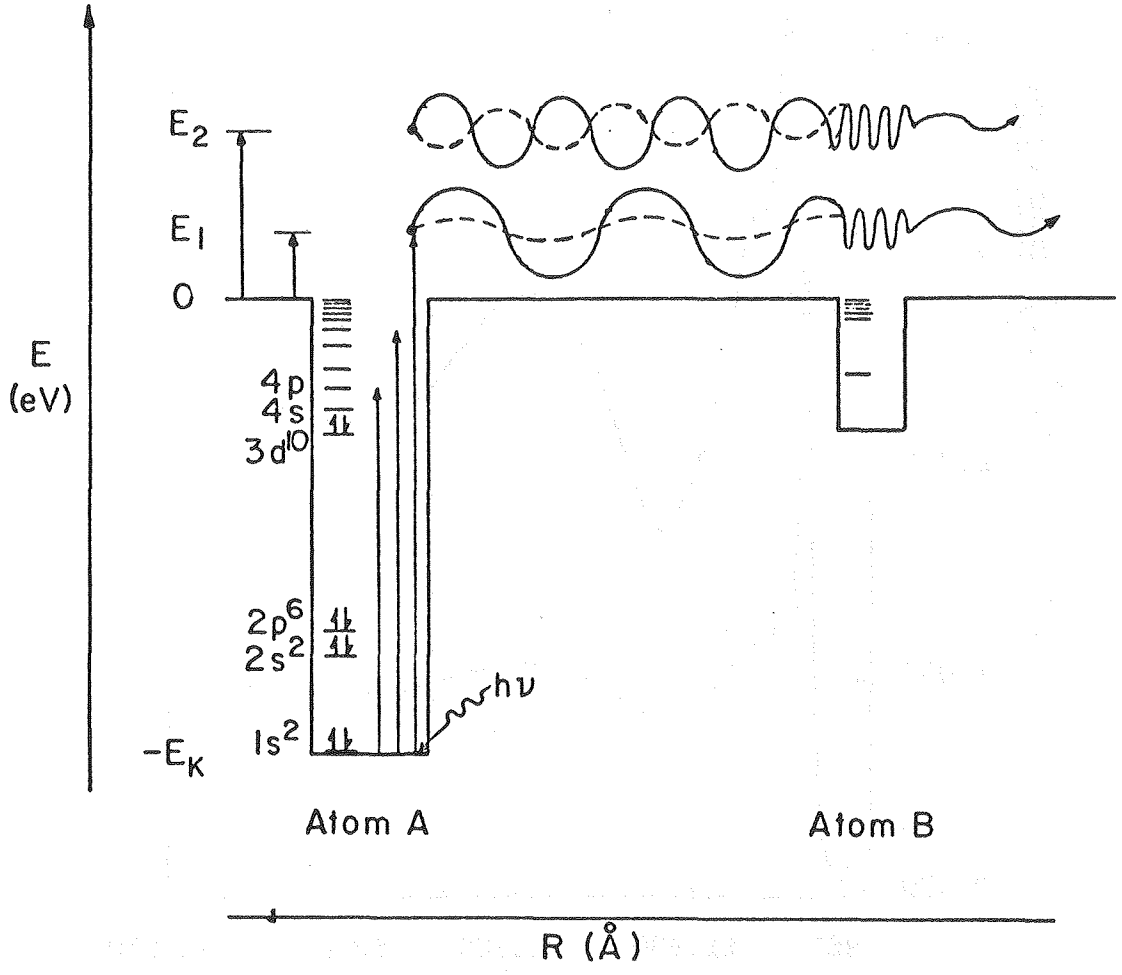

XBL 808-10921A

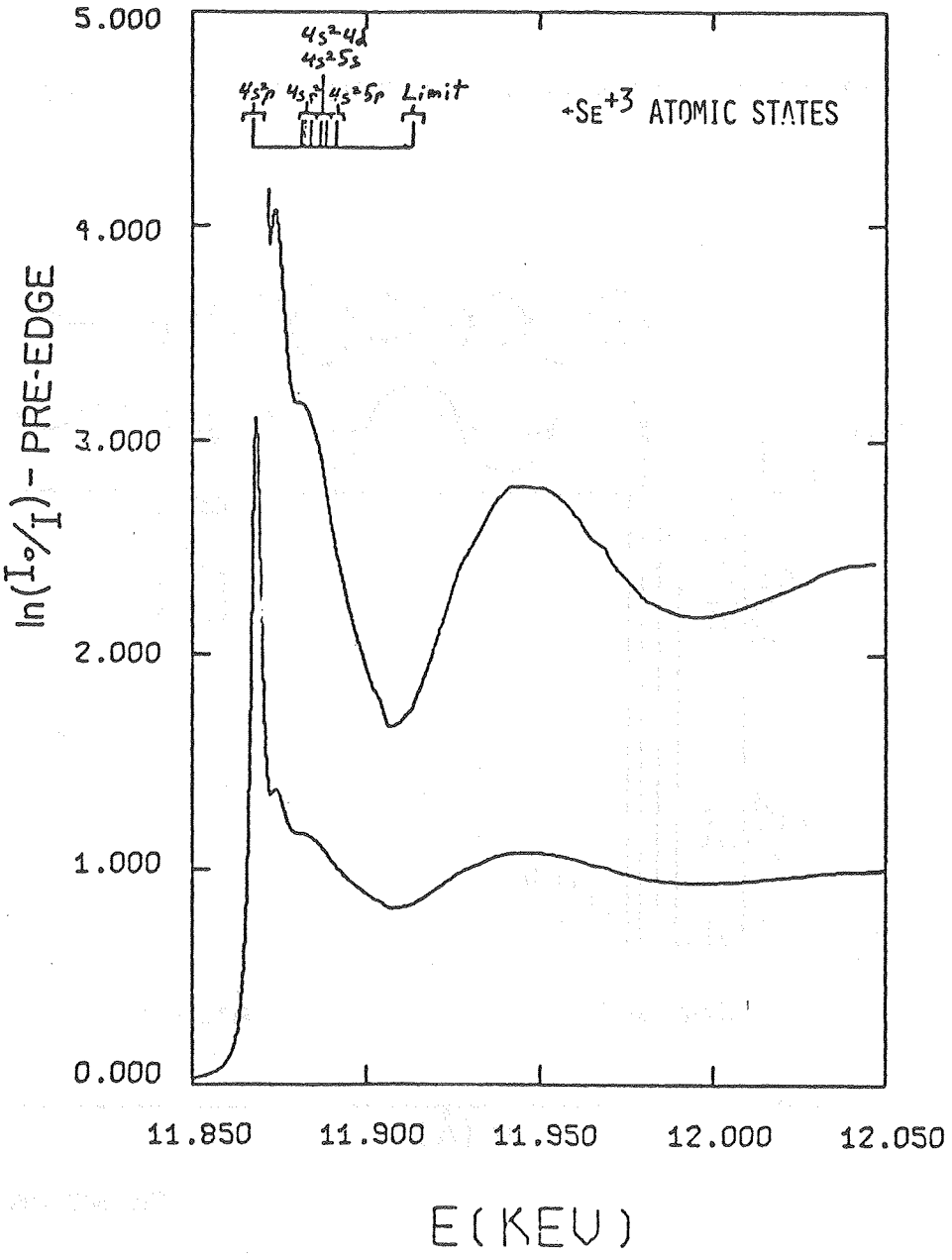

Figure 4-3

Comparison of the Edge Structure of AsF_3 with the Atomic States of Se^{+3}

CHAPTER 5

X-Ray Absorption Studies of Arsenic Standard Compounds

While X-ray absorption edge studies have been performed for decades, the recent development of EXAFS (Extended X-ray Absorption Fine Structure) theory has fostered renewed interest in the structural information X-ray absorption can supply. Particularly valuable is the ability to determine the local radial order around particular atoms when the long range order necessary for an X-ray diffraction analysis is absent.[1] As shown in earlier chapters, the graphite intercalation compounds with AsF_6^- and AsF_5 could not provide single crystal data of sufficient quality for X-ray structural analysis, so the X-ray absorption experiments are appropriate. In the following chapter, the graphite intercalates will be discussed. This study investigates known arsenic fluorides and As_2O_3 using the arsenic K-shell absorption near 11.9 keV. The absorption coefficient μ was measured from 11.4 to 13.1 keV, using the Stanford Synchrotron Radiation Lab's SPEAR storage ring. The edge and EXAFS regions of As_2O_3, $Na^+AsF_6^-$, $Cs^+AsF_6^-$, $XeF^+AsF_6^-$, $Xe_2F_3AsF_6^-$, $O_2^+AsF_6^-$, $C_6F_6^+AsF_6^-$, $C_{10}F_8^+AsF_6^-$, AsF_5 gas and AsF_3 gas have been investigated.

Sample Preparation

All compounds were made using reported literature preparations. The xenon salts were prepared by reaction of XeF_2 with AsF_5 in HF or BrF_5. They were characterized by their characteristic Raman spectra and X-ray powder patterns.[2] $Na^+AsF_6^-$ and $Cs^+AsF_6^-$ were prepared from reagent grade NaF or CsF and AsF_5 in anhydrous HF. The powder pattern of $Na^+AsF_6^-$ matched the unreported $Na^+AsF_6^-$ pattern with only a small impurity of

NaF.[3] The $Cs^+AsF_6^-$ was pure. $O_2^+AsF_6^-$ was made by photolysis of O_2, F_2, and AsF_5.[4] $C_{10}F_8^+AsF_6^-$ or $C_6F_6^+AsF_6^-$ were prepared by reaction of $C_{10}F_8$ or C_6F_6 with $CO_2^+AsF_6^-$ in SO_2ClF.[5] AsF_3 was prepared by fluorinating As to AsF_5, and then adding more As to the AsF_5 to form AsF_3. The sample was cooled to -63°C and was pumped to vacuum to remove any remaining AsF_5. The room temperature infrared spectrum of the vapors remaining showed only $AsF_{3(g)}$, although a small shoulder might indicate a trace of SeF_4.[6] AsF_5 gas was purchased from Ozark Mahoning as 99 percent pure. The gas was condensed at -196°C and was pumped to vacuum to remove any possible fluorine. A room temperature infrared spectrum showed only AsF_5 gas.[6] Reagent grade As_2O_3 was used as purchased from Mallinckrodt.

All solid samples except As_2O_3 were handled in a nitrogen atmosphere Vacuum Atmospheres Drilab with less than 5 ppm O_2 and water. $Na^+AsF_6^-$ was mixed with dry Teflon TFE powder and pressed into a 1-1/4" pellet die. This composite now had more structural integrity and was presumably more uniform. The solid powders or composite were loaded between 10 mil thick Teflon TFE windows, which were placed between aluminum plates with narrow beam slots. The plates were screwed together in order to seal the Teflon windows along a flat edge. This cell was then attached to the bottom of a Dewar along with a thermocouple attachment. The cell was then enclosed within a vacuum tight chamber with Kapton windows. This arrangement placed the solid within two layers of vacuum tight protection within a very dry nitrogen atmosphere. If the sample was to be cooled with liquid nitrogen by filling the dewar, the nitrogen gas

was pumped from the chamber before cooling to prevent frost formation on the Kapton windows. As_2O_3 was also mixed with the Teflon powder to make a pressed composite, and then loaded in a plastic holder.

The room temperature vapor pressure of AsF_3 (160 torr) and 380 torr of AsF_5 were placed in 10 cm long metal IR cells fitted with pre-fluorinated 5-10 mil thick Teflon TFE windows. These cells had been helium leak tested before use to insure no exposure of the gases to air. After adding the gases, pure dry N_2 (99.999% purity) was added to bring the total pressure in the cells to 760 torr, in order to minimize any substantial diffusion of air through the Teflon windows. These cells were then sealed, capped with Swagelock caps to prevent possible air leaks through the valves, and placed within a Plexiglas box fitted with Kapton windows.

Experimental Details

The samples were placed in the X-ray beam between two gas ion chambers. The front chamber (containing a 10% He/90% Ne gas mixture) measured the incident X-ray intensity I_0. The rear chamber I, containing Ar, measured the X-ray intensity after passing through the sample. Dark currents were measured and subtracted from the current measured at each data point. The current produced in the ion chambers was amplified and converted to a voltage which was digitized by a voltage-frequency converter. Control of all data collection was performed using a PDP-11 computer and programs written by Jon Kirby.[7]

The X-ray energy was selected by turning a channel-cut Si(220) or Si(111) crystal for Bragg reflection. I_0 and I were measured as a function of crystal angle, which was later converted to X-ray energy.

An initial energy calibration was made by looking at a pre-edge feature of the copper K edge at 8980.3 eV. The "white peak" of As_2O_3 was then measured. This As_2O_3 peak was used to recalibrate the energy scale every 5-10 samples scans and following beam injections. Energy resolution per point was ~ 0.2 eV in the edge region near 12 keV. Approximately 500 data points were taken over the region 11.4-13.1 keV, with different energy spacings depending on the resolution requirements in particular regions. Generally 15-30 minutes were used to scan the 1.7 keV range, and several scans were taken and later coadded to improve signal to noise. The data were transfered to magnetic tape and analyzed at UC Berkeley - LBL using methods described elsewhere.[8]

Edge Studies

The energy region near the onset of the K-shell absorption, after a pre-edge background removal, is shown in Figures 5-2, and 5-3. Data points were taken at 0.2 eV intervals, except for the xenon, cesium, O_2^+, $C_6F_6^+$ and $C_{10}F_8^+AsF_6^-$ salts which were taken at 0.5 eV intervals.

From Table 5-1, one sees that the initial peaks (the white peak) for the formally As(III) compounds fall at 11968 ± 0.3 eV, the white peaks of the AsF_6^- compounds fall at 11975 ± 0.3 eV, while the AsF_5 white peak fall approximately one volt lower at 11974.2 eV. Thus the energy position of the white peak appears to be a sensitive function of the arsenic oxidation state, and the AsF_5 peak is distinctly different in energy from the AsF_6^- peak.

Two other determinations of the white peak position of As_2O_3 have been reported.[9] Values of 11879.9 (±0.5) and 11876.8 eV are given and energy referenced to nearby tungsten L edges. Our value is substantially lower in absolute energy, and the error in the absolute energy scale may be as large as 5 eV in translating from the copper reference at ~ 9 keV to the arsenic K edge near 12 keV. Our values of the energy shifts relative to As_2O_3 are accurate to ~ 0.3 eV.

The increased absorption in the region above the onset of absorption is due to symmetry allowed transitions from the 1s to molecular orbitals having np character. The large white peak of each sample is presumed to be 1s → empty molecular orbital with 4p character. Above the white peak energy, other transitions are observed which are qualitatively similar, but are shifted in energy and intensity. These differences in intensity cannot be attributed to specific orientation of the molecular orbitals with respect to the polarized X-ray beam because all the samples were randomly oriented. The differences in intensity and energy can be rationalized as transitions to higher empty molecular orbitals. No molecular orbitial calculations for these compounds have yet been published, so further assignments cannot be made.

Because we had no molecular orbital calculations, we looked at gaseous atomic level spectra to ascertain if qualitative assignments might be made to these features.[10] In Figures 5-4 and 5-5, the data for AsF_3 and AsF_5 are shown with the atomic states of Se^{+3} and Se^{+5} respectively. By choosing selenium states, we tacitly assume a relaxed core model. These selenium states have been positioned so as to align

the white peak with the first significant state with p character. While the model is obviously crude, it may allow some qualitative statements.

In both AsF_3 and AsF_5, there appears to be a relationship between the experimental features and the atomic states. In the AsF_5 case, one sees no transition 1s→4s below the white peak near 11961 eV. This transition would be symmetry forbidden. Transitions to pure 4d or 5s are also symmetry forbidden, yet a sizable feature is seen near these levels. Mixture of 4d or 5s with p orbitals rationalizes this result. A more striking limitation arising from this relaxed core approximation is the prediction that the continuum levels are ~ 44 and 67 eV above the lowest empty p state. These empty p states so far below the continuum seem physically unreasonable, especially in the AsF_5 case. The valence shell ionization potential of AsF_3 is reported to be 13.0 eV from photoelectron spectra.[11] The energy difference from white peak to continuum would then be expected to be less than 13 eV for an unrelaxed core model. A corroboration that the atomic states predict an unreasonable continuum level comes from the EXAFS analysis (discussed below). E_0, the energy at the onset of the continuum, is empirically determined in the Bell Lab's model used.[12] E_0 was found to be near 11886 ± 5 eV for all arsenic compounds (see Table 5-3). This E_0 would be ~ 15 eV above the As(V) white peak, and 16-21 eV above the As(III) white peak. These E_0 values seem more reasonable, and the As(III) value is much more consistent with the ionization potential. Thus the relaxed core approximation using atomic states appears to give a fortuitous description of the features. However, this approximation is of dubious utility in finding a physically meaningful continuum level.

EXAFS Analysis

For all samples except AsF_3, AsF_5, and $NaAsF_6$, data points were collected every 3.0 eV from 11915 eV to 13015 eV. For these three samples, data were taken every 2.5 eV from 11888 eV to 12367 eV, and every 5.3 eV from 12367 to 13166 eV.

The data preparation to create $\chi(k)$ for analysis consists of the following three steps:

(1) The pre-edge region is extrapolated over the entire energy region and subtracted. This procedure removes absorption from all lower energy processes other than the K-shell absorption.

(2) A post-edge normalization at 11943 eV is made in order to create a file, μ', with $\mu x = 1.0$ at this energy. This step normalizes the K-edge absorption pump, so that the EXAFS amplitudes of various samples are all normalized to this same μx jump. The amplitudes of the EXAFS oscillations should then all be directly comparable.

(3) To generate χ - the EXAFS oscillations in μx - we start from

$$\chi = \frac{\mu' - \mu's}{\mu_M'} .$$

Here, μ' is the normalized file created in (2). μ_s's is a smoothly varying background composed of free atom absorption, instrumental background, and any background residual from the pre-edge strip. μ_s's is empirically constructed by performing a running average strip across the data to create a smooth file S_1. On this S_1, a second and third running smooths were performed to create a slowly varying background function S_1^3 which does not significantly follow the

EXAFS oscillations. McMaster plots,[13] which were normalized to $\mu x = 1$ at 11943 eV, generate the μ_M' file. An initial EXAFS file is created.

$$\chi_1 = \frac{\mu' - S_1^3}{\mu_M'} .$$

Because many of our later analyses would be with $k^n\chi$, we then do a second triple smooth S_2^3 on $k^n\chi$ ($n = 3$) to generate

$$\chi_2 = k^{-n}[k^n\chi_1 - S_2^3].$$

This second smooth should remove any residual background which is magnified by the k^n weighting. This χ_2 is now used in further analysis.

Fitting Programs

To analyze the $\chi(k)$ data, the procedure of Teo and Lee[12] was used in order to fit the data to

$$\chi(k) = \sum_j A_j \, e^{\sigma_j k^2} \frac{f_j(k)}{k} \sin[2kR_j + \alpha_j(k)].$$

Here $A_j = \frac{N_j}{R_j} 2 (\langle \cos^2\theta_j \rangle)$, where N_j is the number of atoms j at a a distance R_j, and θ_j is the angle between the bond vector to j and the electric vector of the polarized X-ray beam. α_j and f_j are the phase shift and amplitude for the specific absorber/scatterer pair. The theoretically calculated f and α for As, F, and O were used.[12] A_j, R_j, α_j and E_o' remain to be determined.

E_0' is determined in this model by taking $k\chi_2(k)$, generated from a preliminary E_0, and removing $\alpha(k)$. Then the Fourier transform into R space is calculated, and E_0 is varied until the peak of the sine transform matches the peak in the magnitude transform. At this E_0', any cosine component has been removed, and E_0' is the empirically correct continuum level.

$k^3\chi_2(k)$ is now created at the correct E_0' and directly Fourier transformed to R space. The desired R-space peak is windowed and back transformed to k space to generate the $\chi_3(k)$ which contributes to that R space peak. This E' is then used along with the theoretical α and f to fit the file. This $k^n\chi(k)$ is then fit to the function

$$F_1(k) = k^n A e^{\sigma k^2} \sin(2kR)$$

where A, σ, and R are to be determined. A least squares fitting function (FCN) is calculated in order to determine the best fit.

To determine the error in R and E, E_0' is varied by ΔE_0 and R is varied by ΔR, and the best value of the FCN is found. A contour plot of the value of FCN as a function of fixed ΔR and ΔE_0 is constructed. Contours of constant FCN on the R vs E_0 graph are plotted where the FCN value has doubled compared to its best value which is at $(\Delta R, \Delta E_0) = (0,0)$. On these plots (Fig. 5-6), a doubling of the FCN is plotted as "10" on the contour plot. Acrivos[14] pointed out that ΔR and ΔE_0 are coupled variables in this error analysis. An approximate form of the coupling is

$$\Delta \text{ FCN} \approx \frac{4N}{R_i} \sum_E (F_E - D_E)\, e^{\sigma^2 k^2} \cos(2kR_i + \alpha)\left[\frac{\Delta R}{R_i} - \frac{(1 + \frac{\alpha'}{2R})\,\Delta E_o}{2\,(E-E_o)}\right]$$

where the bracketed term shows the coupling of ΔR and ΔE_o. Here, F and D are the fitted and data values of $k^3\,\chi(k)$ at each point k, and the sum is taken over all data points in energy or k-space. This equation does show that when ΔR is zero, the variation of ΔFCN with ΔE_o are uncoupled for any value of ΔE_o. A similar representation holds for ΔR when ΔE_o is zero. Therefore, one can draw horizontal and vertical lines through the center of the ellipses, and the length of these lines is a true measure of the error in ΔR and ΔE_o.

Fitting to the above $F_i(k)$ gives excellent values of A, R, and σ for all compounds. However, the FCN has contributions from the errors in A and σ. By removing the total amplitude from $k^3\chi(k)$, one can fit to

$$F_2(k) = A \sin(2kR)$$

where A should be close to 1.0. With this fit, the error limits on R and E_o decrease substantially. Comparison of the fits to F_1 and F_2 are made in Tables 5-2 and 5-3, and a visual comparison of the fits can be made in Figures 5-7 and 5-8.

All samples except As_2O_3 were analyzed using $k^3\chi(k)$. This k-weighting emphasizes the high k-data, so that the fitting function would perform a balanced fit over the entire data region. While some files extended to k = 18, we have Fourier transformed all compounds

over the same k range to insure comparable results. The initial Fourier transform into R space uses $4.0 < k < 15.0$, and the data are fitted over the region $5.5 < k < 13.5$.

EXAFS Studies

The various $\chi(k)$'s of all samples except As_2O_3 appear quite similar. Figure 5-9 shows an assortment of various files multiplied by k^2. These $k^2\chi(k)$ apparently show only one sine wave frequency, which is indicative of only a single shell contributing to $\chi(k)$. Transforms into R-space of all As-F data sets show only a single peak which corresponds to the As-F distance (Figure 5-10).

As-F Distances

The As-F distances found in the fitting programs are listed in Table 5-2. It is immediately apparent that the value of the best R does not vary significantly when the amplitude is removed from the fit.

A comparison of known As-F distances with those found here is quite impressive. A comparison of AsF_3 and AsF_5 distances with the reported electron diffraction distances shows a startlingly good agreement. We could not distinguish the two different As-F distances in AsF_5 separated by 0.06 Å. The interference beating between these two distances would only become observable much further out in k-space than we could collect data. This experimental limitation, plus vibrational broadening, limits the EXAFS technique to measuring only the average As-F distance. That average, though, is known quite accurately.

In the $Xe_2F_3^+AsF_6^-$ case, the known disorder in the As-F distances[2c] apparently underlies the much larger error limits. The weighted average

of the known bond distances agrees well with the fit F_1 with amplitude present. The value of R of the fit F_2 with ampli- tude removed agrees well with the weighted average of the three shortest distances (1.732 /Å). In the $XeF^+AsF_6^-$ case, the fitted values of R agree very well with the first short distances,[2d] and are barely within the error limits for the weighted average bond distance. In both samples, it appears that the EXAFS is not measuring the longest As-F bond in the sample. This appears most likely in the $XeF^+AsF_6^-$, because the calculated number of scatterers (4.9) also indicates that the EXAFS does not see the most distant atom. The samples are powders and no preferred orientation would be expected to occur. If preferred orientation were to occur so as to eliminate this particular As-F, then another shorter As-F would also have been eliminated, causing an even further lowering in the number of neighbors. A second possibility is that the furthest fluorine has a larger thermal disorder which would dampen its contribution to the EXAFS. However, the crystallographic data for $XeF^+AsF_6^-$ shows the long bonded fluorine (which bridges the As to Xe) to have virtually the same root-mean-square displacements of the thermal ellipsoids as the other fluorines on arsenic. Neither preferred orientation nor thermal dampling appear to explain the results in disordered shells. Eisenberger has reported that the average distance found by EXAFS from distorted shells in Zn can be shorter than the crystallographic average distance.[18] This effect of a non-gaussian pair distribution function gives an additional component in the phase shift which is not accounted for by the theoretical phase shift. We cannot eliminate this possible explanation.

The crystal structures of the remaining AsF_6^- salts are not known, so no comparison with the fitted R can be made. The determined R is comparable with the distorted AsF_6^- compounds, while the smaller error limits imply that the AsF_6^- unit is less distorted than in the xenon salts. The one reported structure of a simple AsF_6^- salt ($K^+AsF_6^-$) gives a bond distance of 1.80 Å,[17] which, in comparison with our results, appears to be too long.

The disorder effect also appears in the values of σ (Table 3). In all cases except one, σ is small and negative (~ 0.001 A^2). The largest value of $|\sigma|$ is seen in the $Xe_2F_3^+AsF_6^-$, with $\sigma = -0.0052$. This large negative value is consistent with the sizable errors in R found for this compound. The smallest $|\sigma|$ (< 0.0010) is found where the error in R, and the error in R measured by other techniques, are smallest. Thus a correlation between ΔR and σ can be seen.

The actual value of σ should not be interpreted too strictly. One might interpret $|\sigma|^{1/2}$ to be the root-mean-square deviation of the bond length. For $Xe_2F_3^+AsF_6^-$, $|\sigma|^{1/2} = 0.072$ Å, while the estimated error in the EXAFS is 0.007 Å and in the X-ray crystal structure is 0.030. For AsF_3, $|\sigma|^{1/2} = 0.018$ Å, while electron diffraction and EXAFS measure 0.002 and 0.005 Å, respectively. This calculated σ must compensate for thermal vibrations and any inaccuracies in the shape of the theoretical amplitude functions. For this reason, the actual value of σ is of limited value in determining the error in R for EXAFS. Increasing disorder does qualitatively correlate with the magnitude of σ.

When the fit with amplitude removed is used, disorder affects the value of A. A ought to be close to 1.000. For the ordered AsF_6^- salts, A lies between 0.996 and 0.999. For $XeF^+AsF_6^-$, which has a fairly small σ, A = 0.995. For the distorted $Xe_2F_3^+AsF_6^-$, A = 0.982. The deviations of A from 1.000 give another qualitative indication of disorder.

The placement of E_o' using the fit to the EXAFS region was mentioned in the edge discussion. There is a general trend that $E_o(AsF_3) < E_o(AsF_5) < E_o(AsF_6^-)$, consistent with the trend in the white peak energies. The actual magnitudes of the shifts are barely significant statistically. E_o must also compensate for other inaccuracies in the model. For instance, the theoretical amplitude and phase were calculated using a compromise between an unrelaxed and totally relaxed core model. E_o would have to shift to fit these model parameters to the physically occurring excitation process. E_o would also have to correct for any different pair distribution functions which may be present in the disordered systems. While all the E_o's fall into a reasonable energy region, the barely significant trend in E_o may only be fortuitous.

The number of nearest fluorine neighbors around the arsenic atoms are found in Table 5-3. The fitting parameter A equals $N/R^2 \langle \cos^2\theta_j \rangle$ for all samples. The equation to calculate the number of neighbors for an unknown N_2 from a standard N_1 is

$$N_2 = N_1 \frac{A_2 R_2^2}{A_1 R_1} \frac{\langle \cos^2\theta_1 \rangle}{\langle \cos^2\theta_2 \rangle} .$$

Because all the present samples are random, $\langle \cos^2\theta \rangle$ equals 1/3 for both standard and unknown. We chose the AsF_3 gas sample as our standard, and calculated N_2 for all other samples.

One sees the expected number of neighbors for AsF_5, the other AsF_3, $Xe_2F_3^+AsF_6^-$, $Cs^+AsF_6^-$, and $C_{10}F_8^+AsF_6^-$. The samples of $O_2^+AsF_6^-$ and $C_6F_6^+AsF_6^-$ were visibly inhomogeneous. For the same edge jump, the EXAFS amplitude is smaller for inhomogeneous samples than for homogeneous samples. This smaller amplitude gives the smaller number of neighbors.[19] The white $Na^+AsF_6^-$ was mixed with white Teflon and pressed to make a pellet. One would not be able to determine visibly if the sample were homogeneous. Apparently the $Na^+AsF_6^-$ was inhomogeneous. The $XeF^+AsF_6^-$ sample gives a curious value of N = 5. One might easily ascribe this low value to inhomogeneity. However, the EXAFS As-F bond distance discussed above is almost exactly the As-F crystallographic distance of <u>five</u> of the six arsenic-fluorine distances. It may be that the EXAFS is truly showing only the five short bonds, and contains no information on the sixth bond located 0.13 Å further away. Perhaps the location of this fluorine on a line between the As and Xe atoms is causing the EXAFS to fail to sense this fluorine.

<u>As_2O_3 Results</u>

The one remaining arsenic compound studied is As_2O_3. Here, the data is no better than the fluoride data, but the analysis involves more parameters for multiple shells. Figure 5-11 clearly shows a beating interference in $\chi(k)$, which is indicative of two shells. The initial Fourier

transform to R-space clearly shows the two shells (Fig. 5-12). The individual shells windowed, back transformed to K-space, and $\chi_i(k)$ of each shell, i, was independently fitted. E_0 was determined from the first shell distance, and initially used for both shells.

A summary of all fitting results, as well as a comparison with the published structure of cubic As_2O_3,[15] are given in Table 5-4. The first shell As-O distance of 1.797(7) agrees well with the reported crystallographic distance. The E_0 of AsF_3 is also found. This result supports the proposition that E_0 does compensate for changes in oxidation state. The σ value of -0.0025 is also reasonable. The fit to F_1 is shown in Figure 5-13.

Fitting to the windowed second shell $\chi_2(k)$ with a single shell As-As scattering gives a distance of 3.23 Å, which agrees well with the crystal structure. However, the fit at low k was very poor (see Figure 5-14). The difference in k from peak to valley at low k was larger than at high k. This behavior implies that a second, shorter distance is present at low k. All of the above work was done fitting $k^3\chi(k)$, in the same manner as all the other compounds. By using $k^3\chi(k)$, the fitting program primarily emphasizes the high k data where As-As scattering predominates. If there were some As-O scattering present, it's amplitude would only be significant at low k. A two scatterer fit to the $k^3\chi(k)$ data fails to find a plausible As-O distance. The initial starting value of As-O (which was close to the crystallographic distance) travels up to fit the As-As distance. The

As-As scattering so dominates the fitting routine for $k^3\chi(k)$ that the program simply folds the additional parameters into the As-As minimum.

To redistribute the regions of emphasis for fitting, a fit to $k^0\chi(k)$ was attempted. This k weighting should give a balanced weighting at low and high k, and the As-O scattering would be more significant in the fit. A single scatterer As-As failed completely to fit the data, as expected. A two scatterer fit, with As-As and As-O scatterers, proved to be very sensitive to the initial starting parameters of As-O. The As-As distance and E_0 always went to nearly the same values as the single shell $k^3\chi(k)$ case, regardless of where the initial starting values were placed. For the As-O case, if the initial E_0 was near 11880 - where the first shell As-O and second shell As-As fits place E_0 - then R for the As-O travels up to the As-As distance near 3.23. This behavior is similar to the behavior for $k^3\chi(k)$. The minimization routine simply has extra parameters to fit the data, and uses those parameters to minimize the fitting function dominated by As-As. If the As-O initial E_0 is placed near 11920 eV (about 50 eV above the white peak), the distance does not travel to 3.23, but gives a smaller value of ~ 3.0-3.1 Å. E_0 also stays near 11930. However, the amplitude of this As-O contribution is negative, which says that the phase shift is incorrect by π. If the initial As-O E_0 is placed near 11945 eV, the As-O converges to a distance R = 3.02 Å, E_0 stays near 11945 (11948 eV), and the amplitude is positive as desired. The As-O and As-As distances now agree very well with the reported second shell crystallographic distances (Table 5-4). The fit is also excellent (Figure 5-15).

The only difficulty with this analysis is the unreasonable E_0 that the As-O scatterer requires. This E_0 is almost ~ 50 eV above the E_0 found for the first shell As-O. A plausible explanation is that the "surface" of the fitting function has many minima. For instance, in the separate program that finds a "best" E_0, the program actually finds several minima where E_0 matches the peak in the R-space sine transform with the magnitude peak of the transform. These minima in E_0 are spaced apart in a manner proportional to 1/R of the R value the program is using. In the main fitting routine, the same repetition is occurring - a relatively good E_0 is found ~ 50 eV above another E_0. The fitting of the As-O component is only sizable over the region k = 5.5-7.5 A^{-1}. An As-O distance of 3.00 Å gives sine wave peak separations in energy of about 50 eV in this small K range. In effect, moving E_0 up by 50 eV simply moves the sine wave by 2π, so that the peaks superimpose again. This idea also explains why a shift of E_0 about 20-40 eV to higher energy would give a fairly good R value, but with a negative amplitude. With this shift, the experimental peaks would line up with the theoretically fitted valley, so the best fit occurs by inverting the theoretically fitted sine wave. For the 50 eV shift, the registry of peak with peak would not be perfect, because $(E-E_0) \propto k^2$. But in our programs, we cannot see the fits to each component - only the sum is seen.

In summary, the X-ray absorption data near the arsenic K-edge provides much useful information. The near edge region provides white peak energy shifts which are self-consistent with the oxidation state of the arsenic absorber. The EXAFS data provides excellent radial distances from the

arsenic to the neighboring atoms. These distances are comparable in accuracy and precision with X-ray diffraction and electron diffraction techniques. The theoretical amplitude and phase parameters calculated by Teo and Lee[12c] worked superbly. The number of neighboring scatterers could be determined to ± 0.4 atoms for well prepared homogeneous samples when scaled to a known homogeneous sample. This study of standard compounds provides confidence that the investigation of graphite intercalation compounds would be profitable.

References for Chapter 5

1. S. P. Cramer and K. O. Hodgeson, Prog. Inorg. Chem., 25, 1, 1979.
2. a) N. Bartlett and F. O. Sladky, JACS, 90, 5316, 1968;
   b) F. O. Sladky, P. A. Bulliner, and N. Bartlett, J. Chem. Soc. A, 2179, 1969;
   c) N. Bartlett, B. G. DeBoer, F. J. Hollander, F. O. Sladky, D. H. Templeton and A. Zalkin, Inorg. Chem. 13, 780, 1974;
   d) A. Zalkin, D. L. Ward, R. N. Biagioni, D. H. Templeton and N. Bartlett, Inorg. Chem., 17, 1318, 1978.
3. A. Levchuk and Bartlett, unpublished.
4. J. Shamir and J. Binenboyin, Inorganic Syntheses, XIV, 39, 1973.
5. N. Bartlett, R. N. Biagioni, G. McCarron, B. McQuillan, and F. Tanzella, Molecular Metals, ed. W. E. Hatfield, Plenum. Pub., 293, 1979; F. Tanzella, Ph.D. Thesis, University of California, Berkeley, LBL 10478, 1980.
6. K. Nakamoto, Infrared and Raman Spectra of Inorganic and Coordination Compounds, 3rd ed., Wiley, 1979.
7. J. A. Kirby, UCID 4017, LLB-LBL, 1978.
8. A. S. Robertson and J. A. Kirby, to be published, A. S. Robertson, Ph.D. Thesis, University of California, Berkeley, 1979, LBL report 9840; J. A. Kirby, Ph.D. Thesis, University of California, Berkeley, 1981.
9. a) V. B. Sapre and C. Mande, J. Phys. C: Solid State Phys. 5, 793, 1972.
   b)B. K. Agarwal and L. P. Verma, J. Phys. C, 2(1), 208, 1968.

10. This method is proposed in assigning edge features in some transition metal fluorides. R. G. Shulman, Y. Yafet, P. Eisenberger and W. E. Blumberg, Proc. Natl. Acad. Sci. USA, 73(5), 1384, 1976.

11. a) A. W. Potts, H. J. Lempka, D. G. Streets and W. C. Price, Philosophical Transactions of the Royal Society, A268, 59, 1970.
b) W. R. Salaneck, H. R. Thomas, C. B. Duke, A. Paton, E. W. Plummer, A. J. Heeger, and A. G. MacDiarmid, J. Chem. Phys., 71(5), 2044, 1979.

12. a) B. K. Teo, P. A. Lee, A. L. Simons, M. Eisenberger and B. M. Kincaid, JACS, 99 3854, 1977;
b) P. A. Lee, B. K. Teo, and A. L. Simons, JACS 99, 3856, 1977;
c) B. K. Teo and P. A. Lee, JACS 101, 2815, 1979.

13. W. H. McMaster, N. Kerr del Grande, J. H. Mullet and J. H. Hubbell, Compilation of X-ray Cross Sections, UCRL-50174, Sec. II Rev. I, NTIS, Springfield, VA 1969.

14. J. Acrivos, San Jose State University, personal communication.

15. K. E. Almin and A. Westgren, Ark. Kemi. Min. Geol., 15(22), 1, 1942.

16. F. B. Clippard, Jr. and L. S. Bartell, Inorg. Chem. 9, 805, 1970.

17. J. A. Ibers, Acta Cryst. 9, 967, 1956.

18. P. Eisenberger and G. S. Brown, Solid State Comm., 29, 481, 1970.

19. S. H. Hunter, Ph.D. Thesis, Stanford University and SSRP report 77/04, 130, 1977.

Table 5-1. Edge Peak Positions

	As(III)	AsF_5	AsF_6^-
As_2O_3	11867.90 67.54 68.16 67.64 67.44 68.09		
AsF_3	67.67 68.45		
AsF_5		11874.25 74.15	
$XeF^+AsF_6^-$			11875.38
$Xe_2F_3^+AsF_6^-$			75.12
$O_2^+AsF_6^-$			75.82 75.43
$Cs^+AsF_6^-$			75.26
$Na^+AsF_6^-$			75.24
$C_{10}F_8^+AsF_6^-$			74.70
$C_6F_6^+AsF_6^-$			75.21

Table 5-2. Radial Distances of Standard Arsenic Compounds

Sample	T(°C)	Fit with $e^{\sigma k^2}$ R (Å)	Fit with amplitude removed R(Å)	Results of other techniques Average R(Å)	N at R(Å)
As_2O_3		1.797 (7)		1.80 (5)[15]	
AsF_3 A		1.699 (7)	1.701 (5)	1.706 (2)	3 1.706 (2)[16]
B		1.709 (5)	1.710 (3)		
AsF_5		1.678 (5)	1.681 (2)	1.678 (2)[16]	3 1.656 (4) 2 1.711 (5)
$XeFAsF_6$		1.727 (6)	1.732 (5)	1.750(10)[2d]	5 1.730(10) 1 1.860(10)
$Xe_2F_3AsF_6$		1.739(10)	1.728 (7)	1.740(20)[2c]	2 1.670(30) 2 1.725(30) 6 1.755(30) 2 1.790(30)
O_2AsF_6		1.723 (5)	1.724 (2)		
$CsAsF_6$		1.726 (5)	1.726 (2)		
$C_{10}F_8AsF_6$		1.732 (5)	1.733 (2)		
$C_6F_6AsF_6$	-93	1.730 (5)	1.731 (2)		
$NaAsF_6$		1.727 (5)	1.726 (3)		
$KAsF_6$				1.800(50)[17]	6 1.800(50)

Table 5-3. Fitting Parameters of Standard Arsenic Compounds

Sample	N	Fit with $e^{\sigma k^2}$ term A	$\sigma^2(Å^2)$	E_o(eV)	Fit with amplitude removal E_o(eV)
				-11800eV	-11800eV
As_2O_3		.3918	-.0024	88 (3)	
AsF_3 A	2.9	.5096	.00011	81 (4)	82 (3)
B	3	.5173	-.00067	86 (3)	87 (2)
AsF_5	4.7	.8444	-.00034	88 (4)	89 (1)
$XeFAsF_6$	4.9	.8274	-.00156	91 (3)	93 (2)
$Xe_2F_3AsF_6$	6.2	1.0352	-.00524	93 (5)	90 (4)
O_2AsF_6	4.6*	.7837	-.00070	89 (3)	90 (1)
$CsAsF_6$	5.8	.9850	-.00144	89 (3)	90 (1)
$C_{10}F_8AsF_6$	5.8	.9698	-.00161	90 (3)	91 (1)
$C_6F_6AsF_6$ -93°C	4.9*	.8243	-.00064	90 (3)	90 (1)
$NaAsF_6$	4.6	.7539	-.00118	88 (3)	89 (2)

*These samples were known to be inhomogeneous, and were expected to have low amplitudes and low values in the number of neighboring fluorines.

Table 5-4. Fitting results for As_2O_3

EXAFS Results

	Peak 1 Fit	Peak 2 Fit
k-range used (1/Å)	5.5 to 13.5	5.5 to 13.5
k weighting	k^3	k^0
Starting E_o (eV)	11886	11923

	Shell 1	Shell 2	Shell 3
Atom Type	O	O	As
E_{oi} (eV)*	11888 (5)	11937	11872
σ_i (Å^2)	-.0024	.0200	.0053
A_i†	.3918	.0432	.0932
R_i (Å)*	1.797 (15)	3.02 (4)	3.22 (2)

Crystal Structure Results

	Radial Distances			
	1	2	3	4
Atom Type	O	O	As	O
N_i	3	3	3	3
R_i (Å)*	1.80 (5)	3.02 (7)	3.23 (1)	3.46 (6)

*The error in the last place is enclosed in parentheses.
†Peak 1 A_i results cannot be compared with Peak 2 results due to different k-weight and fit regions.

Figure 5-1
Edge Region of Arsenic Compounds

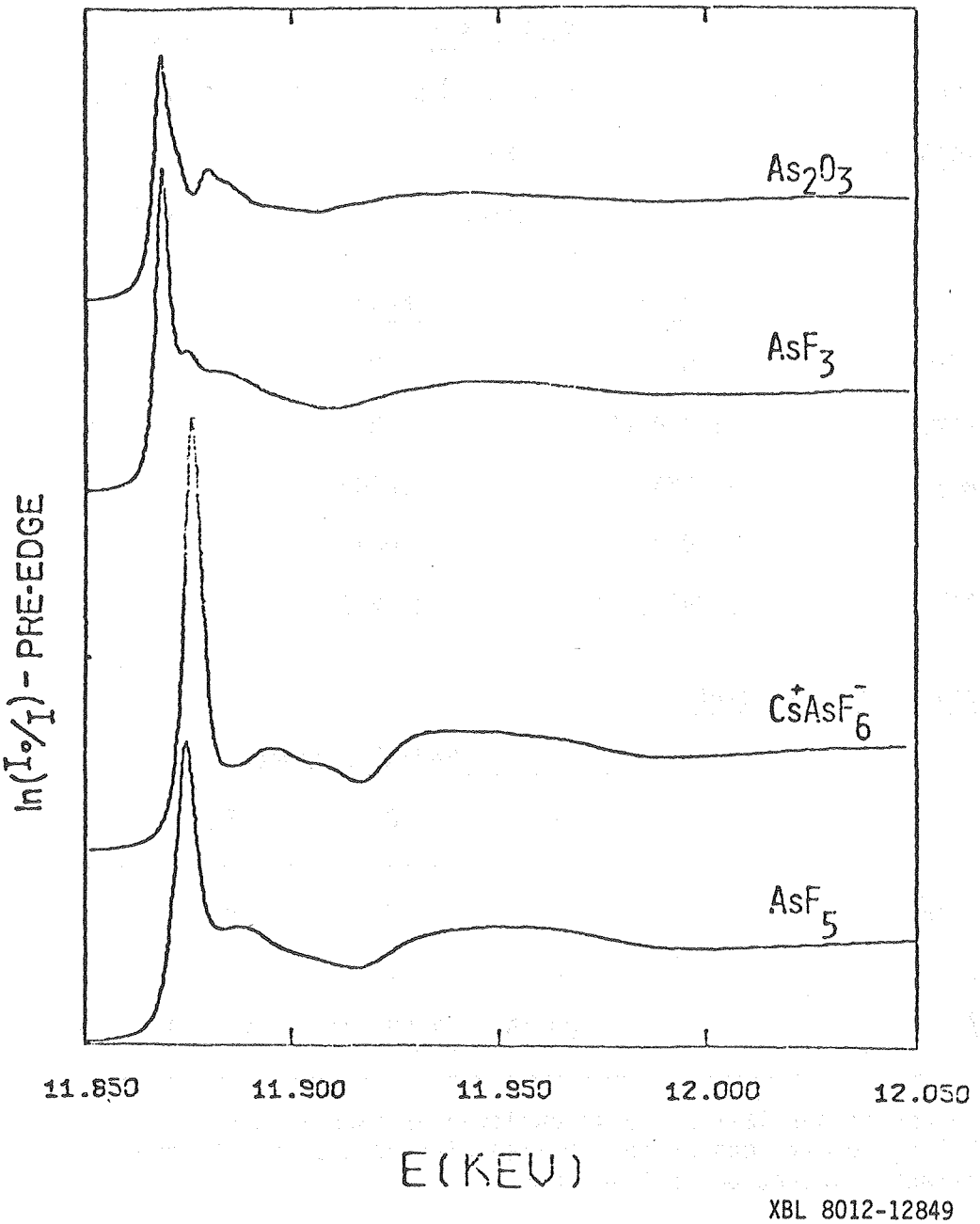

Figure 5-2
Near Edge Region of Arsenic Compounds

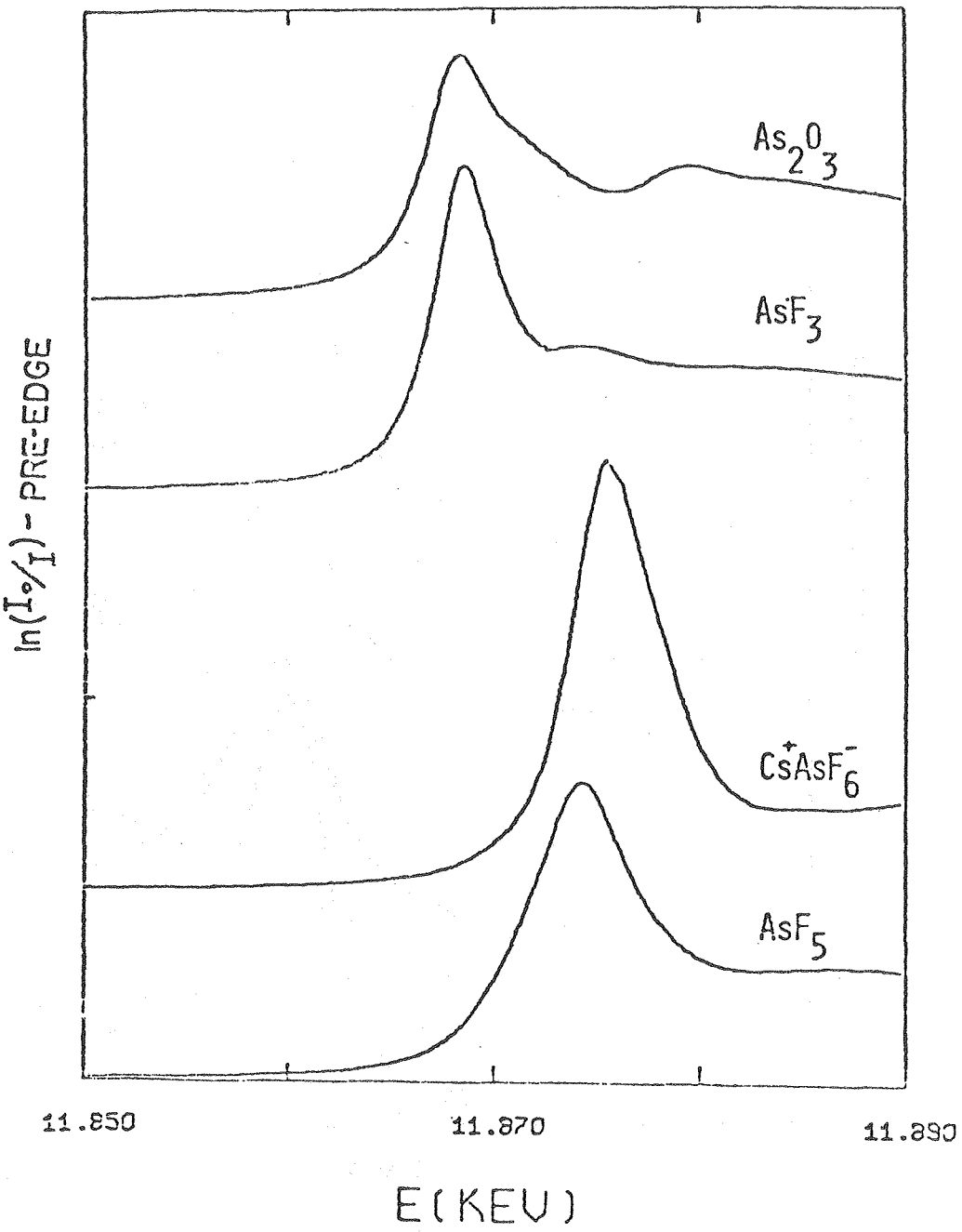

XBL 8012-12846

Figure 5-3
Edge Region of AsF_6^- Compounds

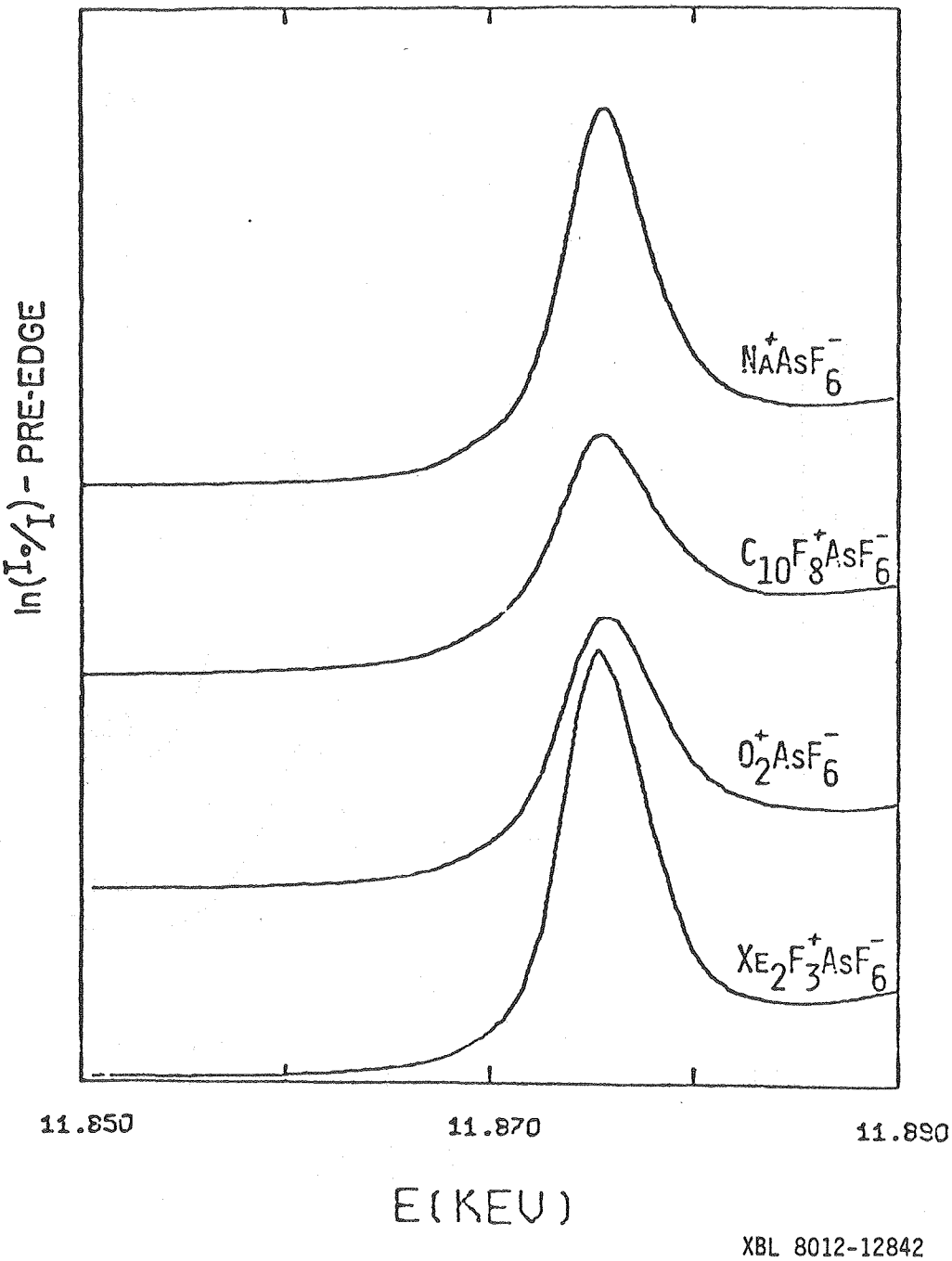

XBL 8012-12842

Figure 5-4
Assignment of Se^{+3} Gaseous Atomic States to AsF_3

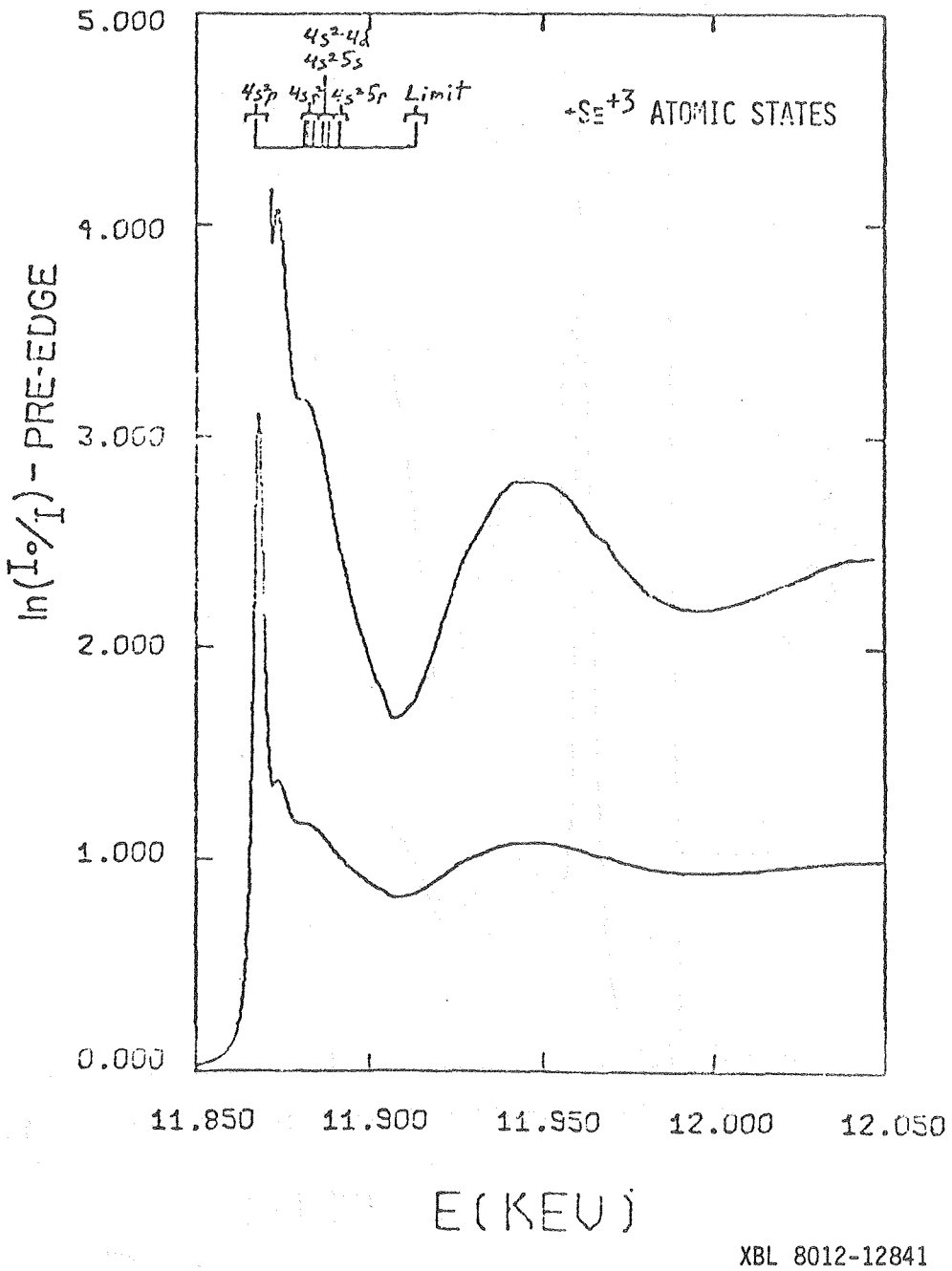

Figure 5-5

Assignment of Se^{+5} Gaseous Atomic States to $Cs^{+}AsF_6^{-}$

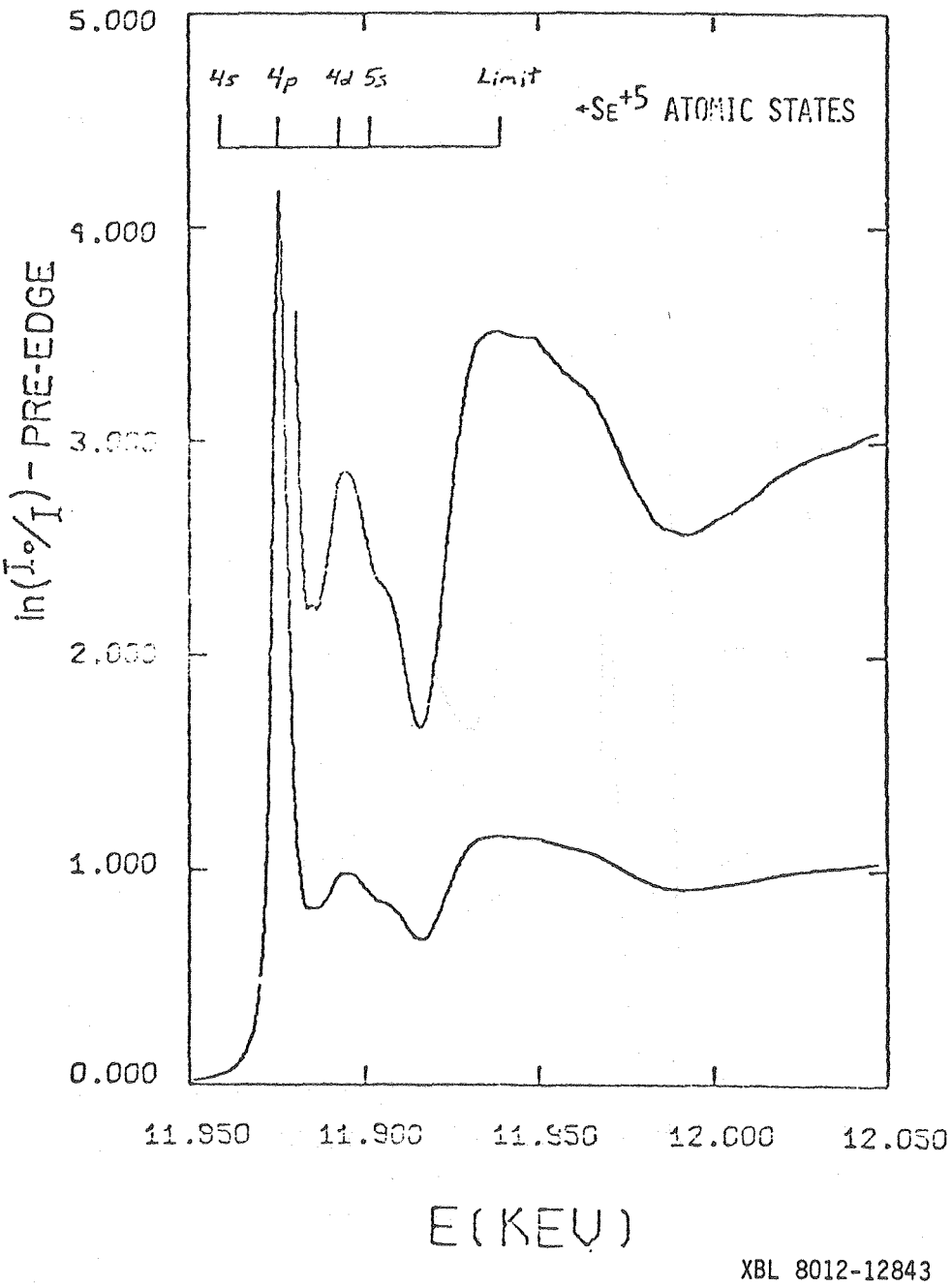

XBL 8012-12843

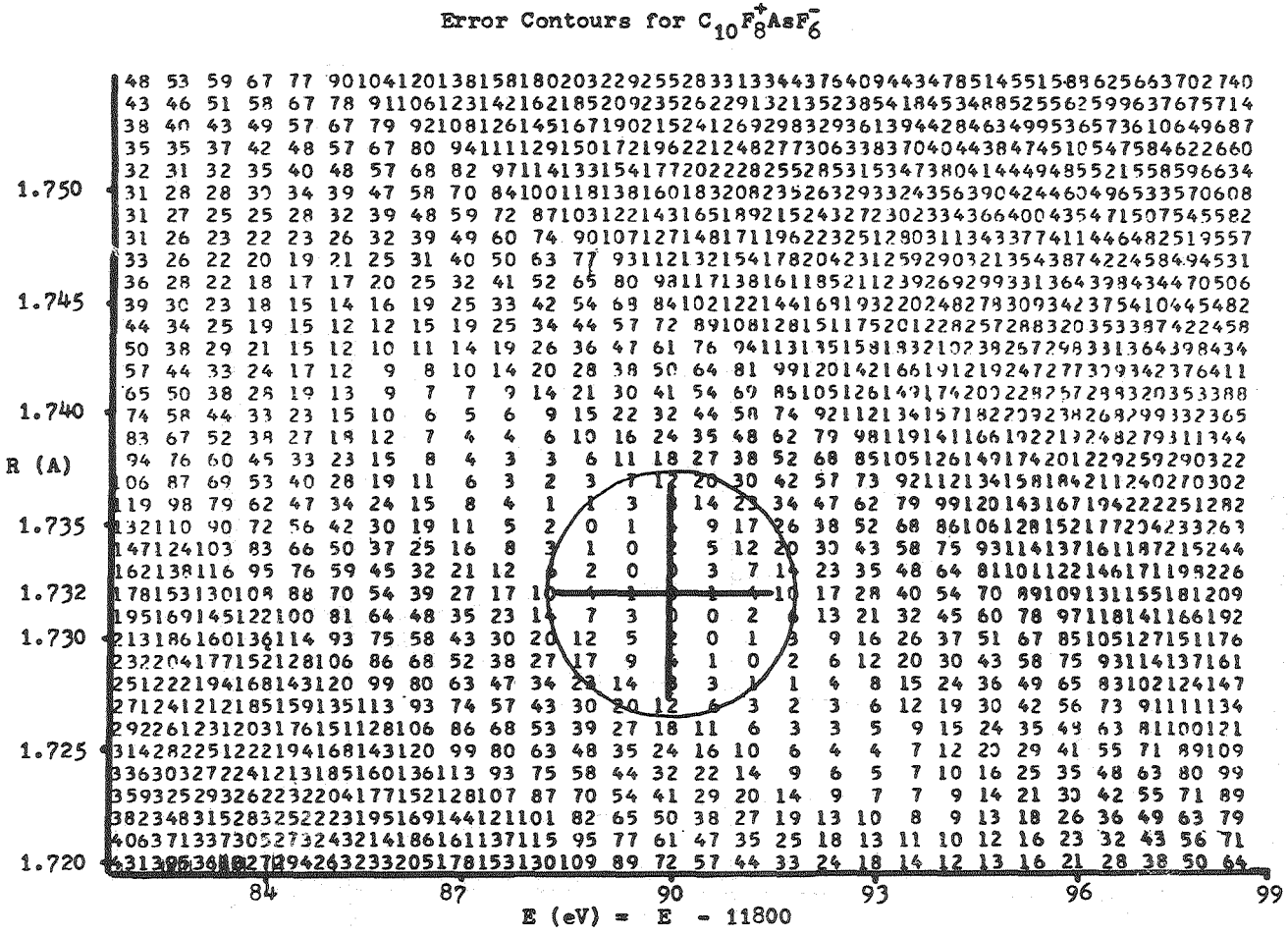

Figure 5-6

XBL 8011-7399A

Contour Plot of Best FCN as a Function of R and E

The value "10" a doubling of the FCN value from the best value given a value "0)

Figure 5-7
Fit of $k^3\chi(k)$ Data to the Calculated Fit
With Amplitude and Debye-Waller Term Present

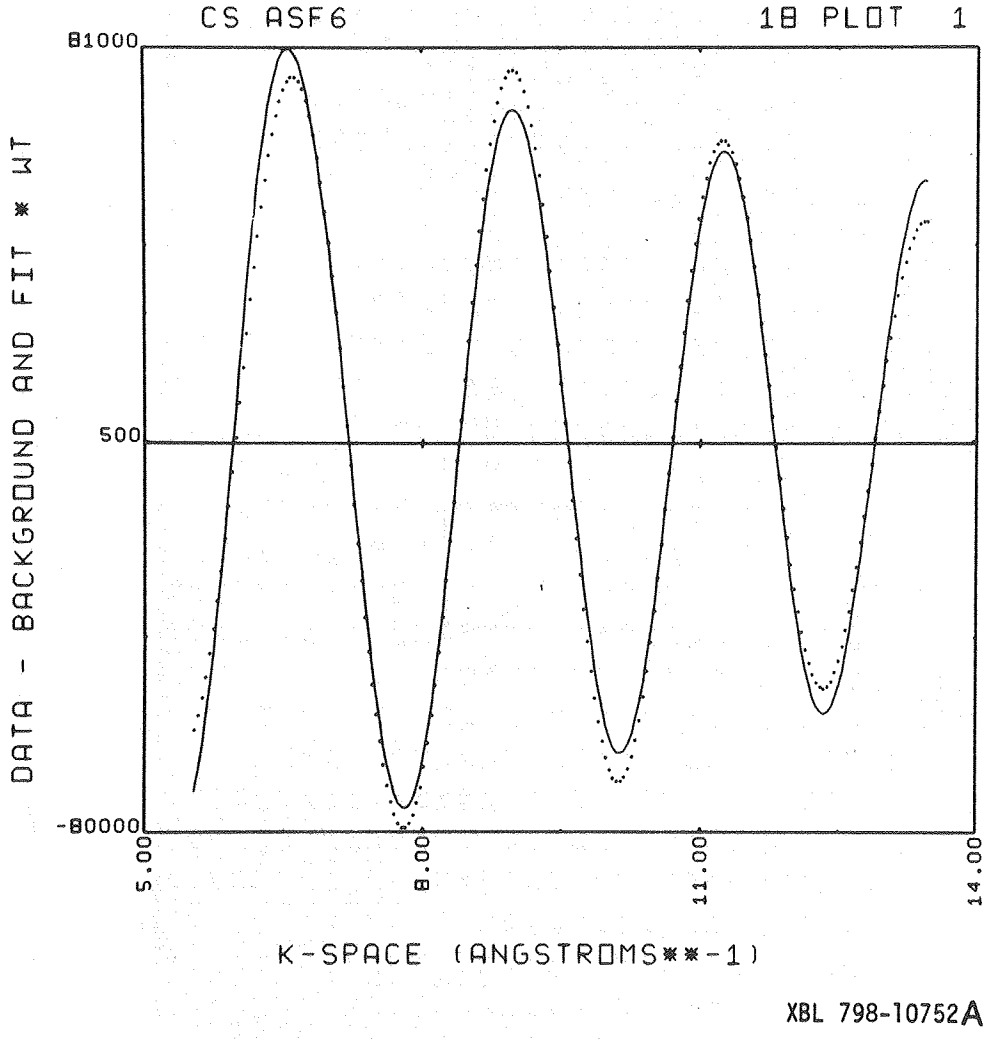

XBL 798-10752A

Figure 5-8
Fit of $k^3 \chi(k)$ Data to the Calculated Fit
With Amplitude and Debye-Waller Term Removed

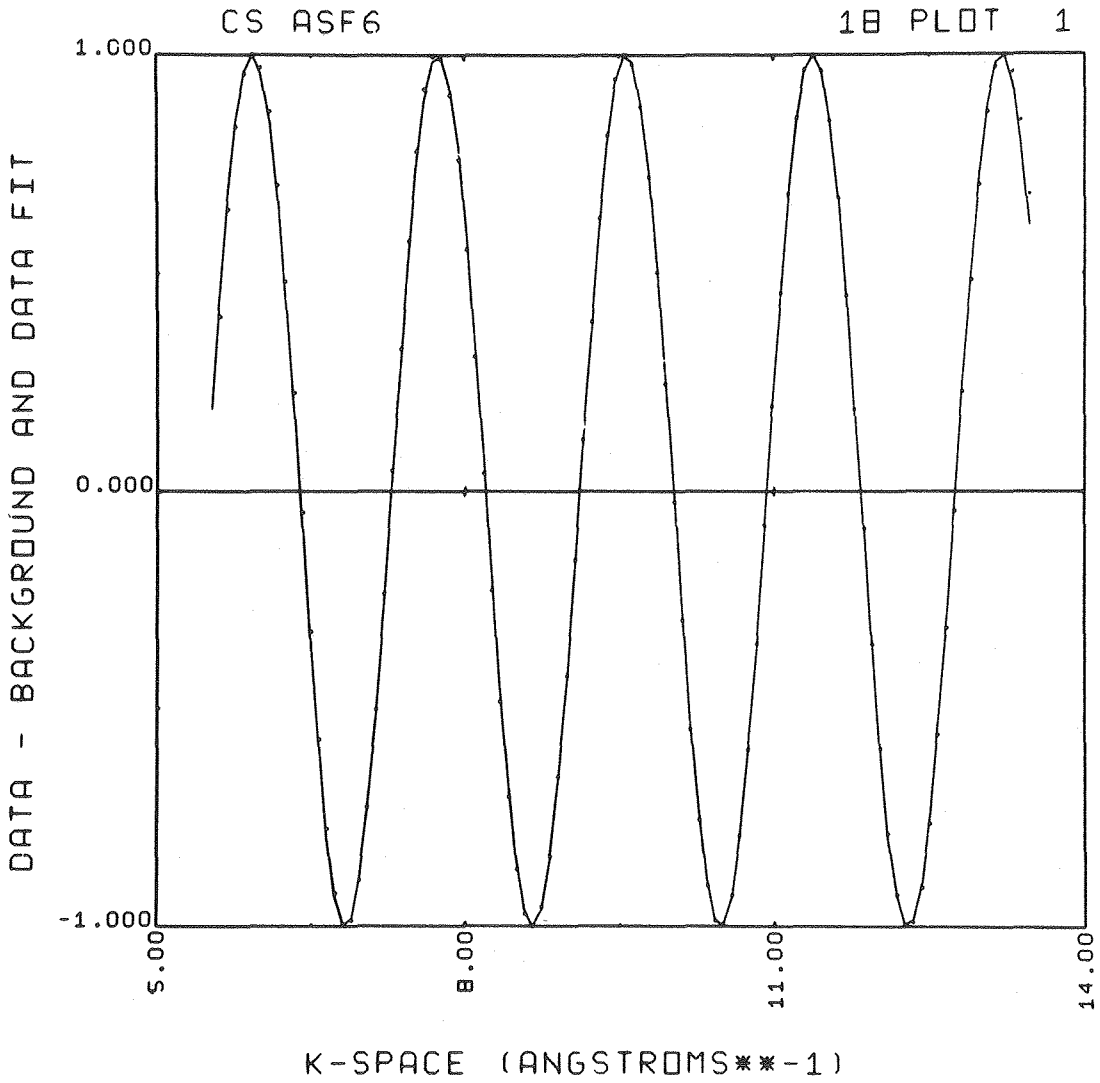

XBL 798-10751A

Figure 5-9

$k^2\chi(k)$ for Selected Arsenic Compounds

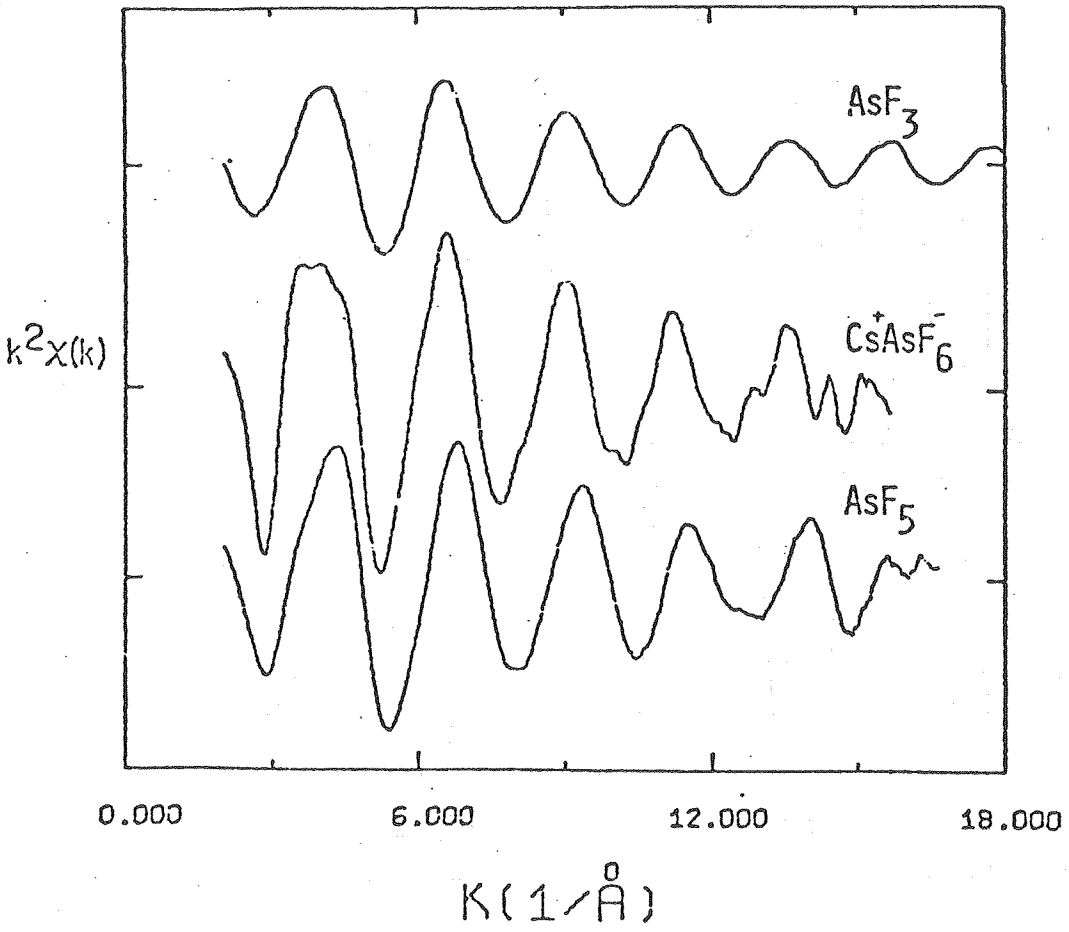

XBL 8012-12844

Figure 5-10

R-Space Transforms from $k^3\chi(k)$ for Selected Compounds

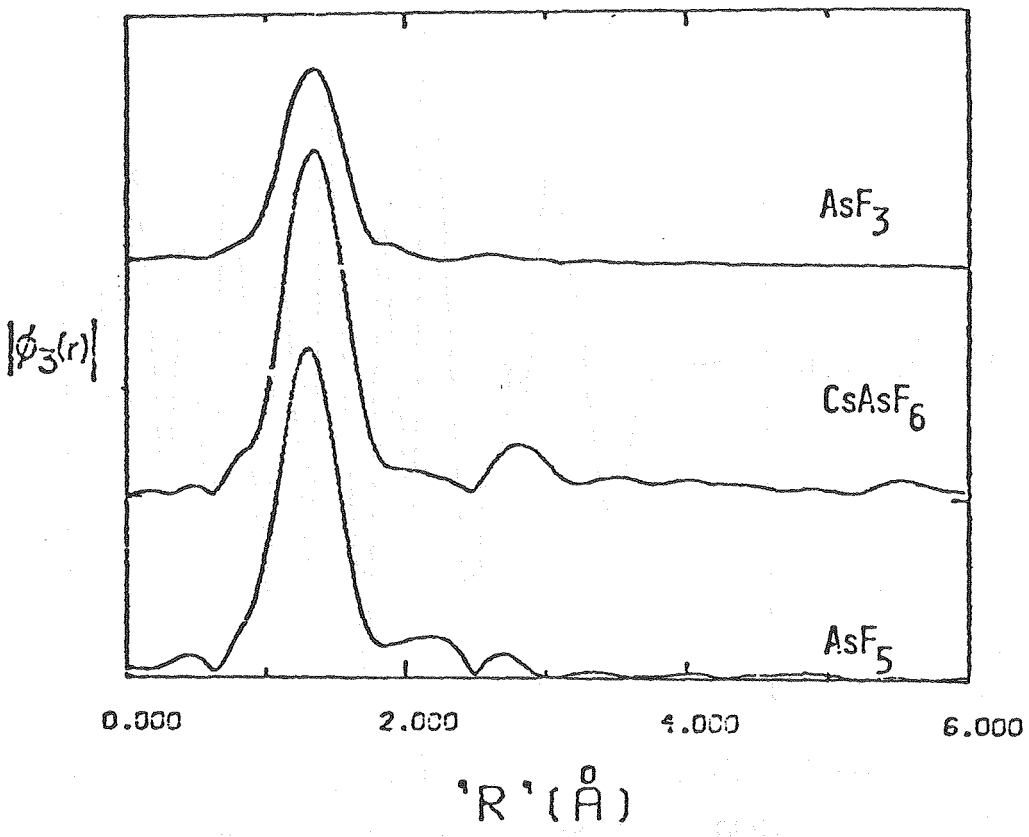

XBL 8012-12845

Figure 5-11
K-Space Data of As_2O_3

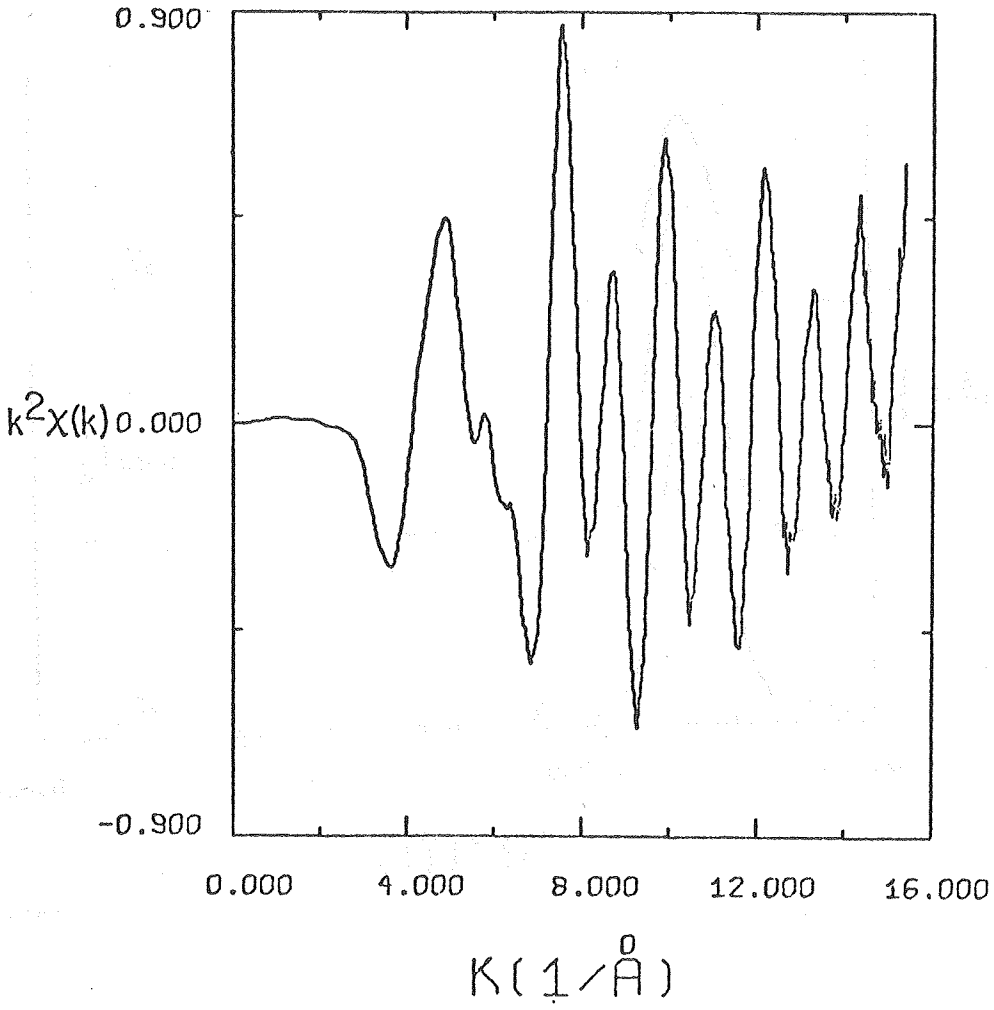

XBL 798-10980A

Figure 5-12

Transforms of $k^3\chi(k)$ (ϕ_3) and $k^1\chi(k)$ (ϕ_1) into R-Space of As_2O_3

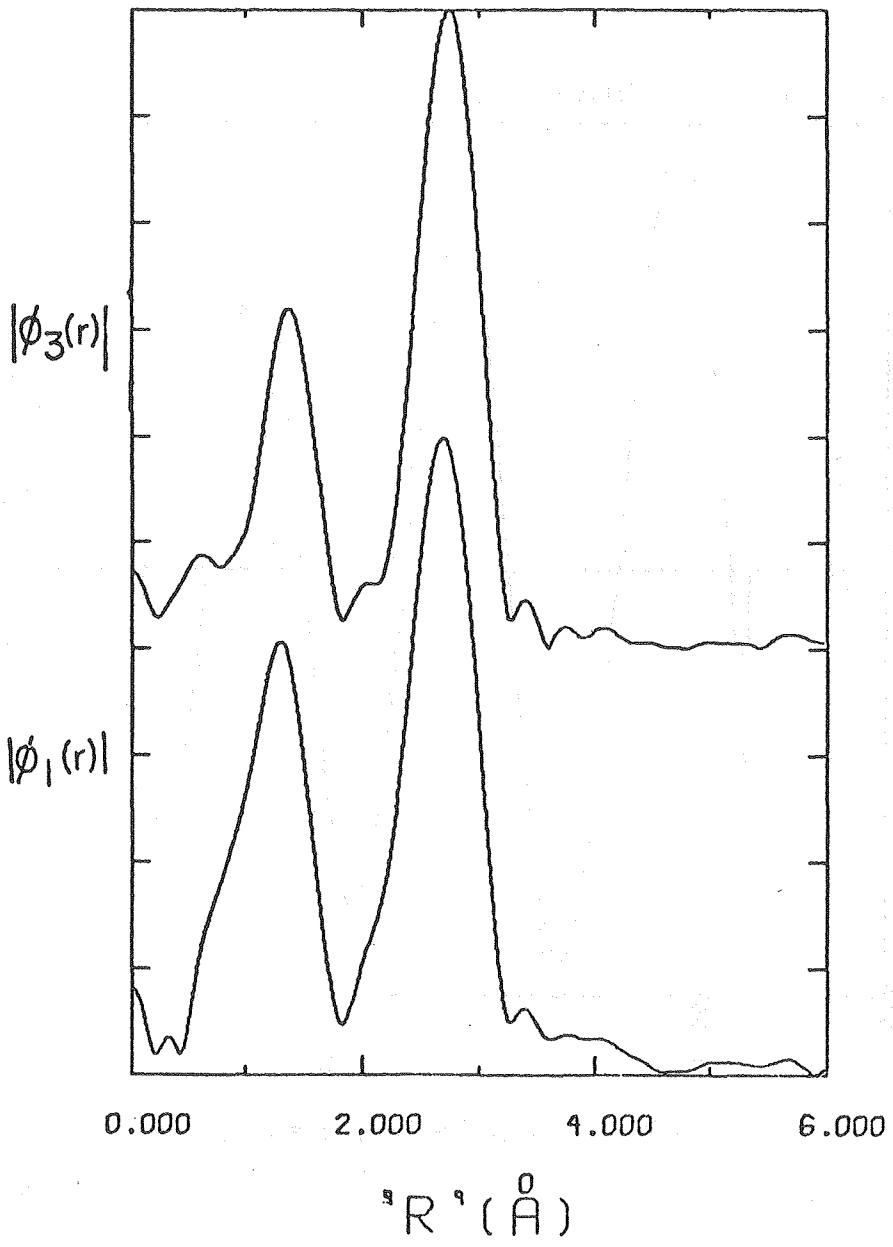

XBL 798-10981A

Figure 5-13

Fit of First Shell As-O $k^3\chi(k)$ to Data

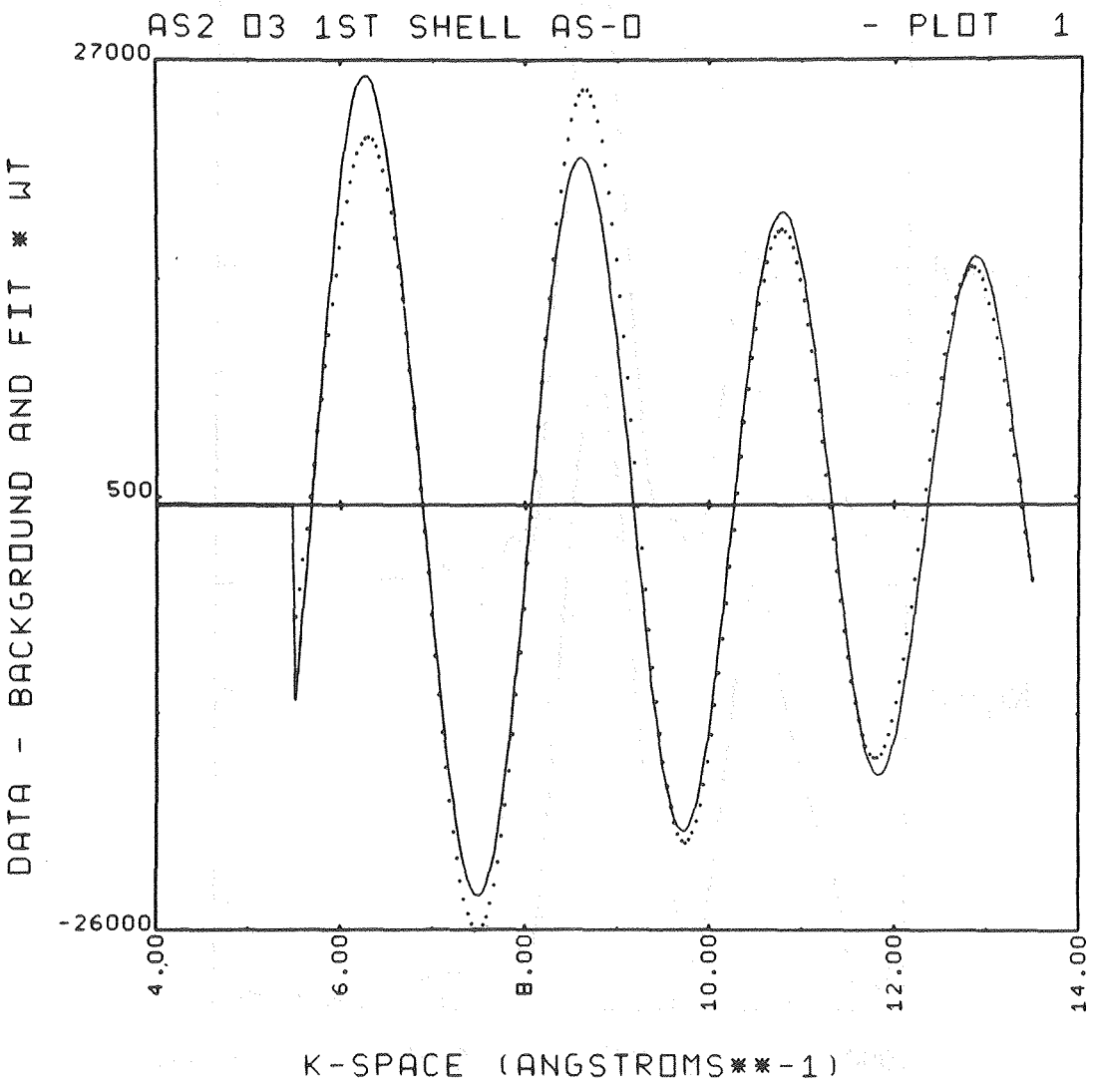

XBL 798-10753A

Figure 5-14
Fit of Second Shell Using Only As-As Parameters

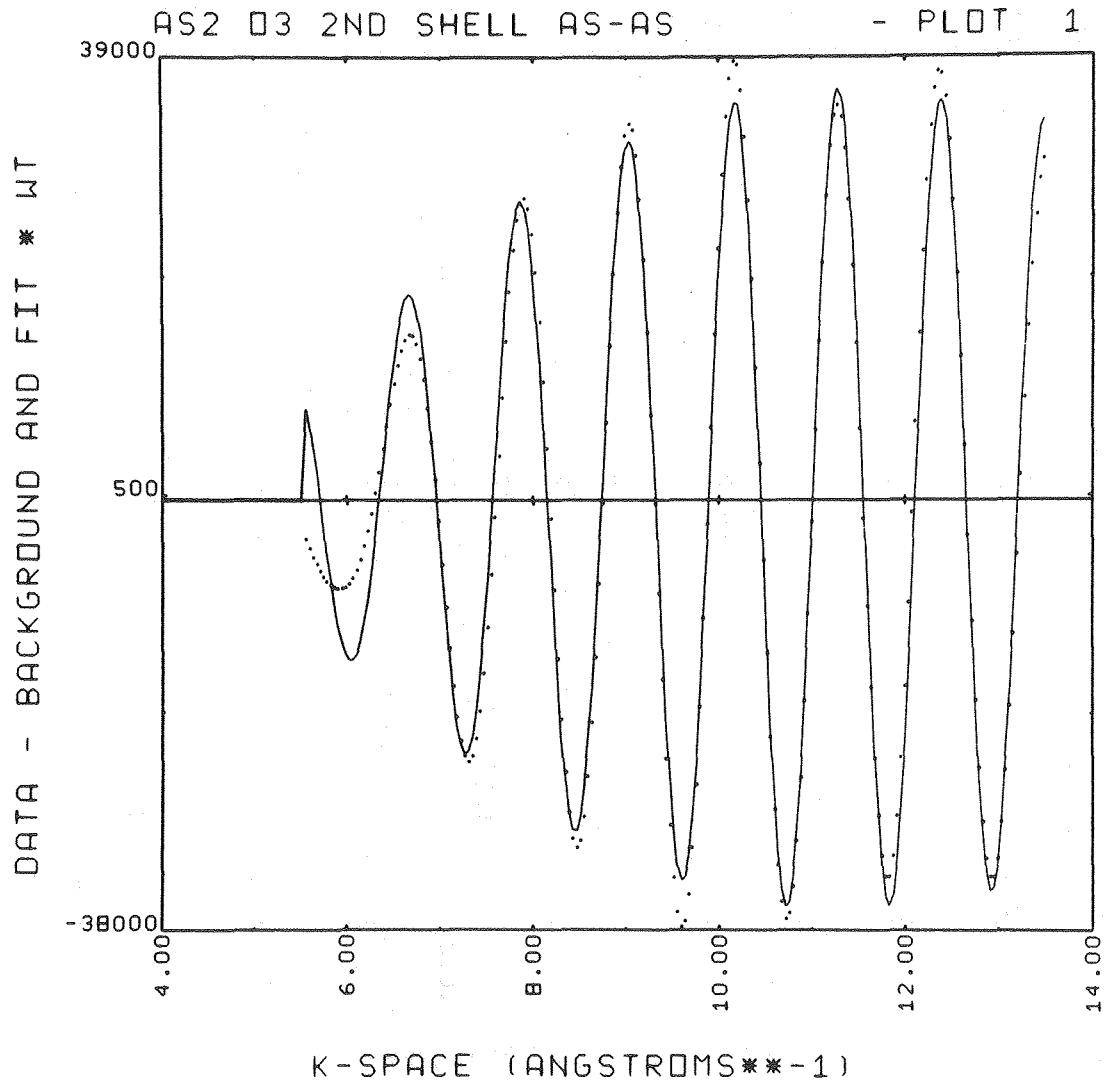

XBL 798-10754A

Figure 5-15
Fit of Second Shell Using As-O and As-As Parameters

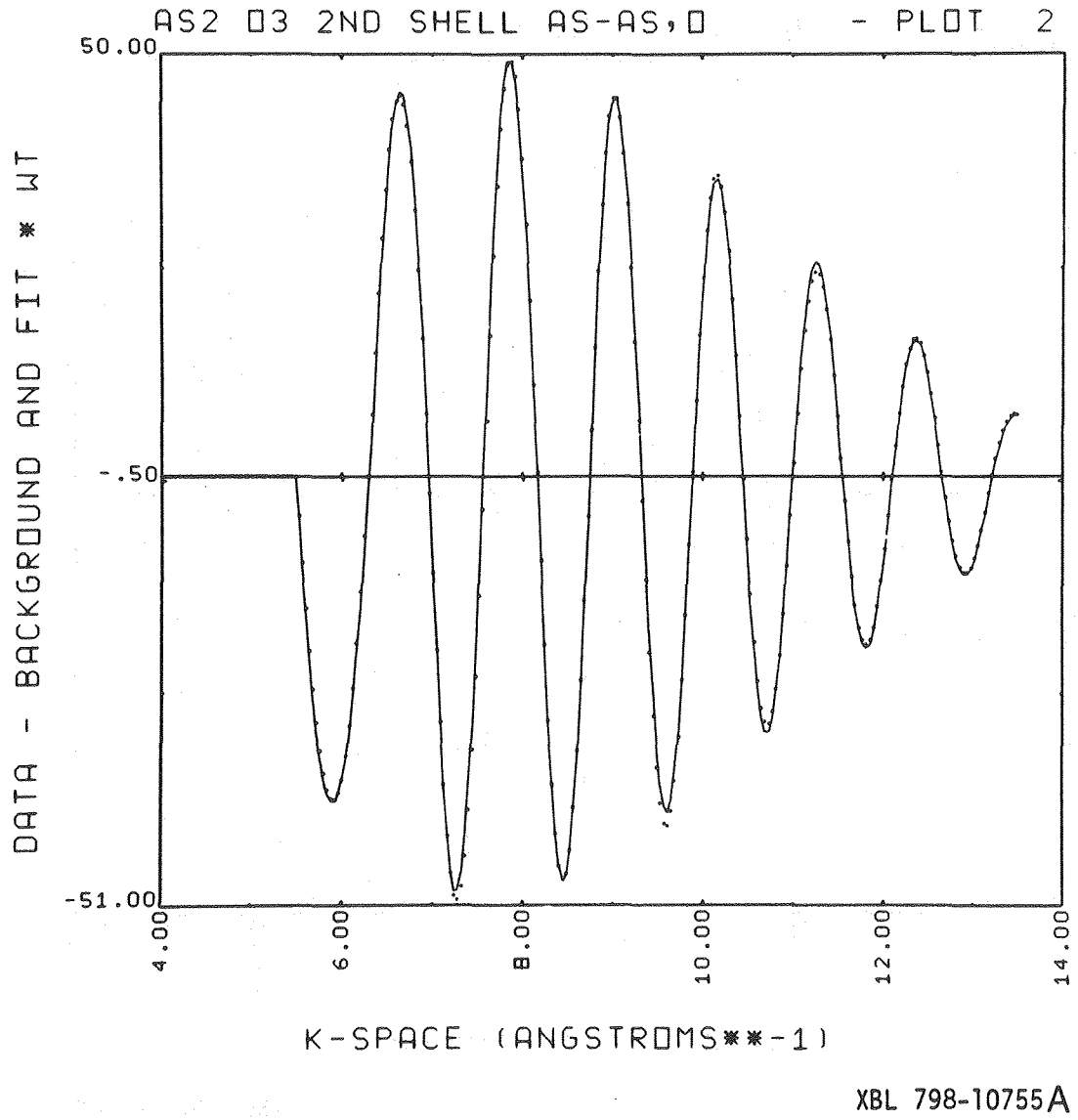

XBL 798-10755A

CHAPTER 6

X-ray Absorption Studies of $C_x^+AsF_6^-$ and "C_xAsF_5"

Introduction

The dramatic changes in electronic properties of graphite[1] and polyacetylene[2] upon reaction with AsF_5 have stirred much interest. Initial researchers presumed that the AsF_5 was present as a neutral, trigonal bipyramidal species within the graphite.[3] Subsequent researchers felt, because some electron withdrawal from the graphite was necessary to cause the dramatic electronic properties, that the AsF_5 was acting as a Lewis acid to attract the carbon π electron density to itself.[4] This Lewis acid (or π acid) proposal has gained wide popularity in explaining a multitude of graphite intercalation reactions which could not be explained otherwise.[5] However, conclusive chemical characterization of the species present, beyond simple elemental analysis and c-axis spacing, is usually meager. In 1978, Bartlett et al. proposed that the AsF_5 reacted with the graphite according to the following known half reaction.

$$3\ AsF_5 + 2\ e^- \rightarrow 2\ AsF_6^- + AsF_3 \quad . \qquad (1)$$

Preliminary As K shell X-ray absorption pre-edge studies supported the proposal that As(III) was formed. Having achieved excellent EXAFS results on a series of known arsenic fluorides, (Chapter 5), extended studies are reported for the X-ray spectroscopic studies of

graphite/AsF_5 and graphite/AsF_6^- compounds. A summary of the present chemical characterization evidence in the literature is also given and compared with the three current models.

Experiment Preparation

Graphite/AsF_5. Pyrolytic graphite was powdered, and 0.2-0.3 g was placed within a quartz reaction vessel attached to a pre-fluorinated 1/4" copper tubing with Teflon Swagelock, capped with a Whitey valve. The entire assembly (including the valve) was leak tested on a He leak detector. The assembly was heated at 100°C overnight under dynamic vacuum, heated with a torch at 10^{-3} torr dynamic vacuum, and then struck with a Tesla coil current to insure an anhydrous condition on all regions which would be in contact with the AsF_5.

AsF_5 (Ozark Mahoning, 99% pure) was condensed at LN_2 into a second quartz tube, and pumped on to remove any possible F_2. The AsF_5 was then warmed and expanded into the graphite tube to achieve a pressure of about 1 atmosphere. For those samples of gravimetry ~ $C_{10}AsF_5$, the final pressure was one atmosphere or less. For the later preparations of C_8AsF_5, more AsF_5 was added to ~ 2 atmospheres until no further pressure drop was observed overnight. The AsF_5 was pumped out quickly (< 2 minutes) and the increase in weight was taken to be from intercalated AsF_5. With the tube at vacuum, the sample was passed into the Vacuum Atmospheres Drilab to load the sample for the EXAFS experiment, X-ray powder diffraction, and carbon analysis. It is generally agreed that graphite/AsF_5 loses AsF_5 under vacuum.

In order to perform a carbon analysis, further pumping had to be done on a very small amount of sample. The carbon analysis always gave a lower composition than gravimetry. Thus the compositions given would indicate a mixed 1st and 2nd stage, while the X-ray powder diffraction only show a first stage material. Chapters 2 and 3 give the analytical results and further characterization.

Graphite AsF_6 was prepared as described earlier.

The earlier samples ($C_{10.8}AsF_5$, $C_{10.8}AsF_6$ and $C_{12}AsF_6$) were simply poured onto the thin teflon windows as uniformly as possible, and the aluminum cell was sealed. In later runs, the same amount of compound was mixed with TFE Teflon powder previously dried at 100°C. The uniform mixture was pressed in an optical die and the resulting compact was placed on the teflon windows and sealed. These compacts later proved to be highly oriented, such that the graphite c-axis was parallel with the X-ray beam propagation. Thus by pressing, we produced a sample which had greater structural integrity, had hopefully more uniformity, and had a highly preferred orientation.

Data were collected at SSRL under the same conditions as mentioned in Chapter 5, and analyzed in the same manner.

Edge Studies

Figure 6-1 shows an assortment of pre-edge white peaks over a range of 50 eV. It is quite apparent that the $C_{10.8}AsF_5$ shows two peaks characteristic of As(III) and As(V). The AsF_5 peak clearly

falls lower in energy than the $C_{12}^{+}AsF_6^{-}$ and the As(V) peak of $C_{10.8}AsF_5$. Table 6-1 gives the white peak energies for a series of compounds, and also shows that the peaks in C_nAsF_5 occur at the AsF_3 and AsF_6^{-} energy positions. Figure 6-2 compares other AsF_6^{-} peaks with the graphite-AsF_6^{-} spectrum.

These peak assignments have been questioned on a variety of grounds. Some have wondered if the low energy peak may be a shake-up satellite due to the core hole excitation. Shake up processes have been shown to be insignificant in K-shell absorption.[6] A shake-up would manifest itself as a small sideable peak above the As(V) peak. This suggestion does not explain the lower energy peak in C_nAsF_5. It would also seem implausible that one would see this "shake-up" only in the graphite/AsF_5, but not in any other arsenic fluoride species studied.

Some have questioned whether the peak ascribed to As(III) might not be As_2O_3 due to air leaks.[7] The EXAFS $\chi(k)$ of As_2O_3 was presented in Fig. 5-11 of Chapter 5, as well as the R space transform which clearly shows two shells, the second of which is the more intense. Later in this Chapter, $\chi(k)$ and R-space transforms will clearly show the presence of only one shell! If As_2O_3 were present in the sizable quantities suggested, it would have appeared in the EXAFS. As_2O_3 is not present in these samples.

Another challenge to the assignment has come from the suggestion that one is seeing a split band.[8] Since this band appears near the arsenic K absorption edge, it must be from As-As or As-C bonding. This suggestion is highly unlikely for several reasons. First, the As(III)

or As(V) orbitals, which are not involved in bonding to fluorine, would be bound close to the highly charged arsenic. Since the nearest carbon, (which is also positive and thus its P_z orbital will be contracted), would be ~ 4.0 Å away, and the next nearest As would be ~ 5.0 Å away, any overlap would be miniscule. Second, later EXAFS data show only one nearest shell (of fluorines), with no hint of an As-C or As-As bond at larger R. Third, the suggestion of a split band would seem to fail to explain why $C_n^+AsF_6^-$ fails to show any sign of a split band, or why the fluorination of C_nAsF_5 removed the lower energy peak. For these reasons, this split band proposal is highly unlikely. The only plausible assignment for these peaks is that of As(III) and As(V).

While not questioning our assignment of these peaks as being As(III) and As(V), some have wondered whether these peaks are truly representative of As(III) and As(V) in ratios of 1:2. In Fig. 6-3 is shown a fit of $AsF_{3(g)}$ and $C_{12}^+AsF_6^-$ as standard files to the $C_{10.8}AsF_5$ unknown file. The result showed 40% AsF_3 and 60% $C_{12}^+AsF_6^-$. The anticipated half reaction would have predicted 33% AsF_3 and 66% $C_{12}^+AsF_6^-$. Fits with AsF_3 and $AsF_{5(g)}$ produced absurdly poor fits. Fits using AsF_3, AsF_5, and $C_{12}^+AsF_6^-$ as standard files gave an insignificant contribution of AsF_5 (< 5%). One should not place too strong a quantitative emphasis on these numbers though. On several other C_nAsF_5 samples, the As(III) peak was reduced relative to the edge pump (Fig. 6-4). The fits gave 20±2% AsF_3 and 80% $C_{12}AsF_6^-$ on all samples. AsF_5 did not contribute significantly in any file (< 5%).

One plausible alternative for the drop in As(III) intensity would be that AsF_3 had been pumped out of the graphite. A test of this idea was made on the compact of $C_{7.8}AsF_5$. After having collected data on the compound, the sample was carefully removed from the cell in the Drilab and placed into a metal can. This sample was then put under dynamic vacuum for three days, in order to pump out some of the intercalant. The intact sample was then reloaded into the cell and more data was collected a week later. The edge jump had decreased substantially (~ 20% to give $C_{10}AsF_5$), thus showing that arsenic had been removed. However, the ratio of white peak heights remained the same. This result is consistent with other reports that the principle volatile from C_8AsF_5 is AsF_5. McCarron has shown that in the initial pumping period, AsF_5 is the principle product.[9] Upon further pumping, the quantity of AsF_3 gradually increases relative to AsF_5. This particular sample may not have been pumped long enough to see a significantly large decrease in the As(III) peak. The experiment does imply that the initial pumping time is not critical to the As(III) peak intensity.

An alternative explanation is the As(III) peak is polarized. This explanation would imply that the AsF_3 molecules are specifically oriented within the graphite layer. Changes in the average orientation of the graphite planes with respect to the polarized X-ray beam wouldbe expected to change the As(III) peak intensity. A piece of graphite (5cm x 1cm x 0.025cm) was reacted with AsF_5 to a composition $C_{8.7}$ AsF_5. This large piece was mounted between Teflon sheets within a rotatable

aluminum cell. The graphite chip was oriented so that the plane was parallel with the electric vector (0 degrees). The chip was then rotated so that the c axis would have a component along the electric vector. In Fig. 6-5 are shown the edge region $\mu_{\theta X}$ for four angles ~. The As(III) peak does not change significantly in amplitude relative to the edge height. The As(III) peak does not change in height depending on its orientation. The most prominent feature is the considerable broadening of the high energy side of the As(V) peak. Because $AsF_{3(g)}$ did not show a second strong white peak in this region, the broadening must be due to an As(V) species molecular orbital. Using the polarization equation

$$\mu_{\theta X} = (\mu_{\parallel}\cos^2\theta + \mu_{\perp}\sin^2\theta)\ t/\cos\theta$$

for $\theta = 0$, $\mu_0 X = \mu_{\parallel} t$ where t is the perpendicular thickness of the graphite-AsF_5 chip. By correcting for the changing path length x, one can isolate $\mu_{90}t$ by subtracting the appropriate files. The resulting $\mu_{90}t$ is shown in Fig. 6-6. The higher energy peak appears prominently. The lower peaks occur at the same positions as in μ_{0X}, as in the earlier data. Table 6-2 gives a summary of the peak positions relative to As_2O_3. Two conclusive results of this polarization study are that the As(III) peak is not polarized, while the As(V) peak has a polarization. This polarization on the As(V) limits the validity of quantitative edge fits to carefully matched standards and unknowns. Since all pressed samples were highly oriented (such as the $C_{12}AsF_6$ used as a standard), and the $AsF_{3(g)}$ has no polarization, fits to the oriented powder C_nAsF_5 using these standards are well matched. The fitting values should be quantitative. A discussion of the significance of the higher energy peak is given below.

EXAFS Results

Figures 6-7 and 6-8 show representative χ(K) spectra and R space transforms for graphite-AsF_5, graphite-AsF_6^- with several standard compounds discussed in Chapter 5. Samples E and F and AsF_3 are probably the samples with the best signal to noise, and data were collected to a higher energy. However, in order to have comparable analyses, all files were used using data only to K = 15. For all samples, Figure 6-8 shows only one prominent peak in R space, and the remainder is background noise. One sees that the worst signal to noise in Figure 5 give the most background noise in R space.

The analysis of the graphite spectra was done in the identical manner as in Chapter 5. The R-space peaks were windowed and inverse Fourier transformed to K-space to create $\chi_3(K)$. $\chi_3(K)$ was then fitted using the method of Teo and Lee[10] which worked so well on the standards. Fits with amplitude both present and removed were made, and error ellipses were calculated.

Table 6-3 shows the As-F distances and error limits for the graphite compounds. All C_nAsF_5 except D show average bond distances ~ 1.705 Å, while $C_{12}^+AsF_6^-$ gives 1.715 Å. We were not able to distinguish AsF_3 and AsF_6^- bond distances in the C_nAsF_5, and we would not expect to do so. In Chapter 5, we failed to distinguish the two distances in AsF_5, which differ by 0.05 Å, whereas in AsF_3 and AsF_6^-, the difference is at most 0.02 Å. The fact that the C_nAsF_5 were generally shorter in distance than $C_n^+AsF_6^-$ is consistent with AsF_3 having slightly shorter bonds than AsF_6^-.

Only ($C_{10.8}AsF_5$) showed a longer bond than the $C^{+}_{10.8}AsF^{-}_{6}$, but $C_{10.8}AsF_5$ had a poorer signal to noise ratio, which may affect the distance. The sample of $C_{10.8}AsF_5 + F_2$ at first appears to have too short a distance compared to $C_{12}AsF_6$, but the 1σ error bars nearly overlap. Since the $C_{10.8}AsF_5 + F_2$ data was taken on a different beam line, with a different monochromator resolution from the rest, variations in the third decimal place may well be expected.

What is most significant in Figure 6-9 with the 1σ error ellipses is that <u>all</u> of the graphite-AsF_5 and graphite-AsF^{-}_{6} distances fall in the region where AsF_3 and AsF^{-}_{6} features occur, and they do not fall in the region of gaseous AsF_5. We feel the results are compelling, on the basis of both As-F bond distances and on pre-edge white peak position, that a "gaseous", trigonal bipyramidal AsF_5 is not present in the graphite. This proposal has been suggested in order to interpret NMR linewidths in graphite-AsF_5 at room temperature.[11] It is also significant that we see no detectable change in bond distance as the temperature is lowered through a phase change reported at ~ 220 K. This phase change and broadened NMR relaxation line width has been ascribed to a more ordered state forming. We can say that, if ordering is occurring, the species which are ordering are the same as those present at room temperature. Thus we can eliminate any temperature dependent equilibrium of $2\ e^{-} + 3\ AsF_{5(g)} \rightarrow 2\ AsF^{-}_{6} + AsF_3$.

As one final point, we fail to see any As-C or As-As bond distance. For $C_nAsF^{-}_{6}$, this absence was not too surprising, since the arsenic is surrounded by fluorines and the next nearest neighbor really is not "seen"

by the arsenic. Because As-As scattering does give about 6 times greater scattering amplitude than As-F, and because there must be ~ 6 As around each As at about 5 Å, one might expect an As-As scattering to be almost equal in intensity to the As-F scattering. That we don't see any As-As bond formation clearly shows that no As-As interaction is present to cause a split band on either C_nAsF_5 or $C_n^+AsF_6^-$. In the C_nAsF_5 case, one might have expected the arsenic of AsF_3 to see the carbon atoms. However, the theoretical scattering of carbon is approximately half that of fluorine. The amplitude of scattering goes as $1/R^2$, so that a carbon ~ 4 Å away would contribute only ~ 18% of the scattering that a single fluorine 1.7 Å away would contribute. Since the amplitude also is a function of the number of scatterers, while there are ~ 5 F/As, there would only be ~ 1C/3 As (1 AsF_3), which would be a 15 fold reduction. These three combined factors would argue that any contribution of As-C to the $\chi(K)$ amplitude would be about 1% of the As-F amplitude contribution, and probably would not be seen. Thus while we cannot eliminate the possibility of As-C bond formation, we do not see any evidence for it. Such bond formation would be implausible chemically. Lone pair donation of electron density back to the carbons is feasible chemically, but we see no evidence to support it.

From the fitting amplitude parameter ($= N \langle \cos^2\theta \rangle / R^2$), the number of nearest neighbors can be calculated. As a quick initial measurement, the ratio of the amplitude of C_nAsF_5 with C_nAsF_6 gives the expected ratio N_1/N_2 of 5/6 in most samples. However, using AsF_3 as a standard reference (as was done in Chapter 5), all values of the number of nearest neighbors

are low. C_nAsF_5 gives 3.7–4.1, and C_nAsF_6 gives 4.5 F per As. A calculation of $\langle \cos^2\theta \rangle$ for a highly oriented pressed Teflon pellet failed to correct the amplitude for the low values of N. Low amplitudes have been shown to be caused by sample inhomogeneity. For instance, 5% pinholes in a sample would give a 20% reduction in amplitude.[12]

One can only presume that sample inhomogeneity in the presssed Teflon samples is the cause of the lowered number of nearest neighbors.

Discussion

A summary of these X-ray results yields a composite picture. The edge features indicate As(III) and As(V) in ratios of approximately 1:4 rather than the 1:2 expected for the AsF_5 half reaction. This factor implies that the half reaction proceeds from 60% of the AsF_5 molecules. The remaining molecules have not been identified conclusively. These molecules are not gaseous trigonal bipyramidal AsF_5 molecules (tbp-AsF_5). The AsF_5 gas peak falls about one eV below the AsF_6^- peak in energy. A tbp-AsF_5 does not have a polarized peak about 2 eV above the initial peak. The fitting routine failed to use a gaseous AsF_5 standard in fitting a C_xAsF_5 sample.

The only chemically plausible species, other than the AsF_3 and AsF_6^-, is a square pyramidal AsF_5 (sp-AsF_5). Only an sp-AsF_5 acts as a Lewis acid by accepting electron density into the empty orbital extending along its fourfold axis. Numerous SbF_5 and $SbCl_5$ adducts with Lewis bases are known where a square pyramidal SbX_5 is formed.[13] The sp-AsF_5 is less well characterized. F_{19}NMR of the CH_3CN-AsF_5 adduct in solution showed

a square pyramidal fluorine arrangement.[14] The octahedral ion AsF_6^- can be considered as the sum of six canonical forms of an sp-AsF_5 coordinating a fluoride ion. To our knowledge, no X-ray structure of a non-fluoride ion donor with AsF_5 is known.

The most plausible orientation of the sp-AsF_5 is with its fourfold axis pointing toward a neighboring fluorine. With this orientation, the sp-AsF_5 can fill a lattice site in a manner similar to an AsF_6^-. This sp-AsF_5 has the same geometry as an AsF_6^- molecule missing a fluoride ion. Alternatave orientations of the fourfold axis along a or c are unlikely. The graphite system has been oxidized, so that it has lost its Lewis basicity. The AsF_5 would not seek to coordinate toward the graphite by orienting along c. The molecule is too thick to coordinate along a unless the arsenic is pushed out of the plane of the fluorines. In this orientation, there exists no base with which to coordinate.

The presence of this oriented sp-AsF_5 is also consistent with the polarized edge data. In this orientation, excitations from the 1s into this empty "acidic" orbital would be seen in all directions due to the orientational disorder around the c-axis. A component of this excitation would be seen at all angles between 0 and 90 degrees, and this As(V) peak appears to be present at all angles. Because this peak is most prominent at 90 degrees, when the electric vector is along c, the sp-AsF_5 must be oriented at an angle closer to the c axis than 54 degrees. At 54 degrees, all orientations would give the same component of this transition, and

thus the spectra would look alike. That the spectra do not look similar as a function of angle can only be explained by a larger component along c than a.

Earlier, an estimate of the degree of oxidation of the graphite was made based on the edge fitting routine. This estimate can only be of qualitative use, because those fits did not take into account the intensity of the sp-AsF_5 transition. A very strong transition would hint that only a small amount of sp-AsF_5 was present, while a weak transition would require a sizable amount of sp-AsF_5. Only if the transition has the same intensity as an AsF_5^- would that estimate of the degree of oxidation be accurate.

The position of this transition above AsF_6^- is also reasonable. If an sp-AsF_5 had its acidic orbital below the Fermi surface, electron donation from the graphite would occur and "AsF_5^-" or "$AsF_5^=$" species would be made. These species are unknown,[15] and magnetic susceptibility showed no evidence for a Curie-Weiss paramagnetic susceptibility of AsF_5^-.[16] AsF_5 is weakly bound within the graphite, as supported by the evidence that it is pumped away from a first stage C_8AsF_5 material. This weak binding is consistent with the transition into the empty orbital. Very little electron donation into the orbital is made. The Lewis acid-base binding would be weak, because the electronegative fluorine would be a poor electron donor. Lastly, theoretical calculations of the valence orbitals of the tbp-AsF_5 and sp-AsF_5 have been performed.[17] These calculations placed two empty orbitals of the sp-AsF_5 above the related tbp-AsF_5 empty orbital. One orbital which is polarized within the plane would fall

under the AsF_6^- peak and would contribute to the AsF_6^- peak at 0 degrees. Upon rotation, this peak should decrease in intensity, as is observed in μx_{90}. The second higher orbital would lie roughly where this polarized transition occurs. A comparison with these calculations can only give qualitative support, because no correction for the core hole was made. The total evidence does make the position of this transition above tbp-AsF_5 reasonable.

The presence of some sp-AsF_5 is also consistent with other data. McCarron has shown that the $C_x^+MF_6^-$ stages as $C_{12n}MF_6$, while C_xAsF_5 stages as $C_{8n}AsF_5$.[9] These staging patterns parallel the degree of oxidation if the AsF_5 half reaction occurs. The AsF_5 half reaction must go to completion at $C_{16}AsF_5$ (C_{24}^+) in order to fit this pattern. However, the half reaction is not required to go to completion at C_8AsF_5. Neutral AsF_5 may fill a part of the galleries along with AsF_3 and AsF_6^- once the galleries have opened up to a first stage. Therefore C_8AsF_5 is not required to be C_{12}^+ because $C_{8n}AsF_5$ is merely the space-filling limit. A second comparison can be made with the oxidation strength of the AsF_5 half reaction (see Chapter 8). The strength of oxidation per electron of the half reaction is 121 kcal. This value falls above the threshold value of ~ 110 kcal, yet below the lowest value for $C_8^+MF_6^-$. While this does not prove that an oxidation up to C_{12}^+ is impossible, it does show that the oxidation reaction may cease before reaching a limiting composition of $C_{12}^+(AsF_6^- \cdot \frac{1}{2}AsF_3)$.

The presence of sp-AsF_5 also provides an alternative path for rapid fluorine exchange.[11] Gaseous AsF_5 is a fluctional molecule and one intermediate geometry is the square pyramid. The electron donation to AsF_5 would stabilize the square pyramid form as the ground state, but the molecule may still be fluctional. Exchange of fluorines on AsF_6^- and sp-AsF_5 could be facile with the sp-AsF_5's acidic orbital pointed toward the fluorine of an AsF_6^- (Figure 6-10). This fluoride could then transfer through an "AsF_5—F^---AsF_5" transition state and become attached to the sp-AsF_5. This mechanism effectively exchanges the sp-AsF_5 and AsF_6^- as well as exchanging the fluorines. Because neutral sp-AsF_5 is present, the oxidation half-reaction must now be near equilibrium with respect to the graphite. This equilibrium implies that there is little thermodynamic contribution to an activation energy of the reverse half reaction. Only kinetic factors, such as an activation energy for rearrangement of fluorines on AsF_3 and AsF_6^- to make sp-AsF_5, can slow such a reversal. This second mechanism of oxidation reversal can exchange the fluorines of As(III) and As(V). One would expect this second mechanism to be slower than the first reaction. Both mechanisms for rapid fluorine exchange must occur if the fluorines on As(III) are not seen on the NMR time scale.[18] Ebert's failure to see rapid fluorine exchange between AsF_3 and AsF_6^- in solution does not satisfy the requirement of a source of electrons (the oxidation reversal mechanism) or of sp-AsF_5 (the As(V) fluorine exchange mechanism.)[19] Temperature dependent studies of the C_nAsF_5 may show these different mechanisms, and the addition of some

sp-AsF_5 (such as in CH_3CN-AsF_5) to some AsF_6^- in solution may show this AsF_5-AsF_6^- exchange.

Lastly, the XPS data on C_nAsF_5 has been interpreted in terms of a tbp-AsF_5 molecule being present within the graphite.[20] Theoretical calculations of tbp-AsF_5 and sp-AsF_5 orbitals place the highest occupied orbitals in the same energy range.[17] A set of XPS peaks assigned to tbp-AsF_5 could be from sp-AsF_5. This "AsF_5" peak disappeared upon pumping, leaving a spectrum of AsF_6^- with AsF_3. This disappearance would be consistent with the weak binding of an sp-AsF_5.

In conclusion, the bulk of the data on C_xAsF_5 is consistent with the proposal that the oxidation half reaction occurs up through $C_{16}AsF_5$, and beyond that stoichiometry some neutral AsF_5 is present. The X-ray edge fits and polarization, as well as the observed chemistry, supports the proposal that the neutral AsF_5 is present in a square pyramidal form which can have a very weak Lewis acid-base interaction with the oxidized graphite. The source of the high conductivity of "C_xAsF_5" must be due to oxidation of the graphite by the proposed half-reaction. Trigonal bipyramidal AsF_5 has not been seen within the graphite.

References for Chapter 6

1. G. M. T. Foley, C. Zeller, E. R. Falardeau, and F. L. Vogel, Solid State Comm. 24, 371. 1977.
2. C. K. Chiang, C. R. Fincher, Jr., Y. W. Park, A. J. Heeger, H. Shirakawa, E. J. Louis, S. C. Gau, and A. G. MacDiarmid, Phys. Rev. Lett. 39, 1089, 1977.
3. Lin Chun-Hsu, H. Selig, M. Rabinovitz, I. Agranat, and S. Sarig, Inorg. Nucl. Chem. Lett., 11(9), 601, 1975.
4. J. E. Fischer and T. E. Thompson, Physics Today, 36, July 1978.
5. A. Herold, Mat. Sci. Engineering, 31, 1, 1977.
6. R. G. Shulman, Y. Yafet, P. Eisenberger, and W. E. Blumberg, Proc. Natl. Acad. Sci., USA, 73(5), 1381, 1976; J. J. Rehr, E. A. Stern, R. L. Martin, and E. R. Davidson, "Contributions to EXAFS from Shake-up and Shake-off Processes", SSRL Users Conference, October 1977.
7. L. V. Interrante, personal communication.
8. A. G. Heeger, personal communication.
9. E. M. McCarron and N. Bartlett, J.C.S. Chem. Comm., 404, 1980.
10. B. K. Teo and P. A. Lee, JACS, 101, 2815, 1979.
11. B. R. Weinberger, J. Kaufer, A. J. Heeger, E. R. Falardeau, and J. E. Fischer, Solid State, 27, 163, 1978.
12. S. H. Hunter, Ph.D. Thesis, Stanford University, 130, 1977 and SSRP Report 77/04, 1977.
13. M. Webster, Chem. Rev. 66, 87, 1966.

17. E. L. Muetterties, T. A. Bither, M. W. Farlow, and D. D. Coffman, J. Inorg. Nucl. Chem., 16, 52, 1960. F. N. Tebbe and E. L. Muetterties, Inorg. Chem. 6(1), 129, 1967.

15. The ion SbF_5^{-2} is known. R. R. Ryan and D. T. Cromer, Inorg. Chem. 11(10), 2322, 1972.

16. B. McQuillan and N. Bartlett, unpublished data.

17. R. S. Berry, M. Tamres, C. J. Ballhausen, and H. Johansen, Acta Chem. Scan., 22, 231, 1968.

18. L. B. Ebert and H. Selig, Mat. Sci. Eng. 31, 177, 1977.

19. L. B. Ebert, personal communication.

20. M. J. Moran, J. E. Fischer, and W. R. Salaneck, J. Chem. Phys. 73(2), 629, 1980.

Table 6-1. Edge Peak Positions

	As(III)	AsF_5	AsF_6^-
As_2O_3	11867.90		
	67.54		
	68.16		
	67.64		
	67.44		
	68.09		
AsF_3	67.67		
	68.45		
AsF_5		11874.25	
		74.15	
$XeF^+AsF_6^-$			11875.38
$Xe_2F_3^+AsF_6^-$			75.12
$O_2^+AsF_6^-$			75.82
			75.43
$Cs^+AsF_6^-$			75.26
$Na^+AsF_6^-$			75.24
$C_{10}F_8^+AsF_6^-$			74.70
$C_6F_6^+AsF_6^-$			75.21
$C_N^+AsF_6^-$			11875.48
			75.37
C_xAsF_5	11868.67		11875.33
	68.24		75.05
	68.80		75.19
	68.96		75.55
$C_{10.8}AsF_5 + F_2$			75.55

Table 6-2. Edge Peak Energies of Oriented C_nAsF_5 Chip

	As(III) energy	(shift from As_2O_3)	As(V) energy	(shift from As_2O_3)
As_2O_3	11863.6	0		
$C_{8.7}AsF_5$				
0 degree	11864.7	1.1	11870.7	7.1
0	11865.0	1.4	11870.9	7.3
15	11865.0	1.4	11871.0	7.4
15	11865.0	1.4	11871.0	7.4
30	11865.0	1.4	11871.4	7.8
45	11865.0	1.4	11870.7 11872.0*	7.1 8.4
45	11865.0	1.4	11870.7 11872.0*	7.1 8.4
$\mu_{90}t$ peaks calculated				
from $\mu_{45}x$	11865.2	1.6	11870.5 11873.6	6.9 10.9
from $\mu_{30}x$	11865.4	1.8	11870.5 11873.2	6.9 9.6

*The fitting routine found two shallow maximums in the original data, separated by 1.3 eV. Only in the subtracted files was the higher energy peak found about three eV above the lower As(V) peak.

Table 6-3. EXAFS Results

	With Amplitude Removed		Without Amplitude Removed				
	R	E_0 -11800	R	E_0 -11800	N	A	σ
$C_{10.8}AsF_5$	1.725(5)	90(2)	1.725(12)	90(2)	(3.7)	.6278	-.00131
-50C					(4.1)	.6955	-.00106
-100C					(3.5)	.5939	-.00022
$C_{9.5}AsF_5$	1.706(3)	90(2)	1.704(11)	88(5)	4.1	.7018	-.00047
$C_{9.5}AsF_5$	1.705(4)	87(2)	1.703(12)	86(5)	4.4	.7685	-.00137
-93C	1.700(5)	86(2)	1.698(13)	85(5)	4.4	.7618	-.00082
$C_{7.8}AsF_5$	1.708(5)	89(2)	1.706(12)	88(5)	3.8	.6598	-.00009
	1.708(5)	89(2)	1.706(12)	88(5)	3.7	.6463	-.00007
-140C	1.707(4)	89(2)	1.705(12)	88(6)	3.6	.6297	.00071
$C_{16.2}AsF_5$	1.712(6)	87(2)	1.711(13)	86(6)	4.4	.7562	-.00080
$C_{10.8}AsF_6$ ($C_{12.8}AsF_5 + F_2$)	1.698(8)	87(4)	1.696(14)	86(8)	(4.2)	.6920	.00024
$C_{12}AsF_6$	1.715(6)	89(2)	1.714(12)	88(5)	4.5	.7781	-.00075
-140C	1.7149(5)	88(2)	1.712(12)	87(5)	4.4	.7479	-.00005

Figure 6-1
As Edge Features of Various Compounds

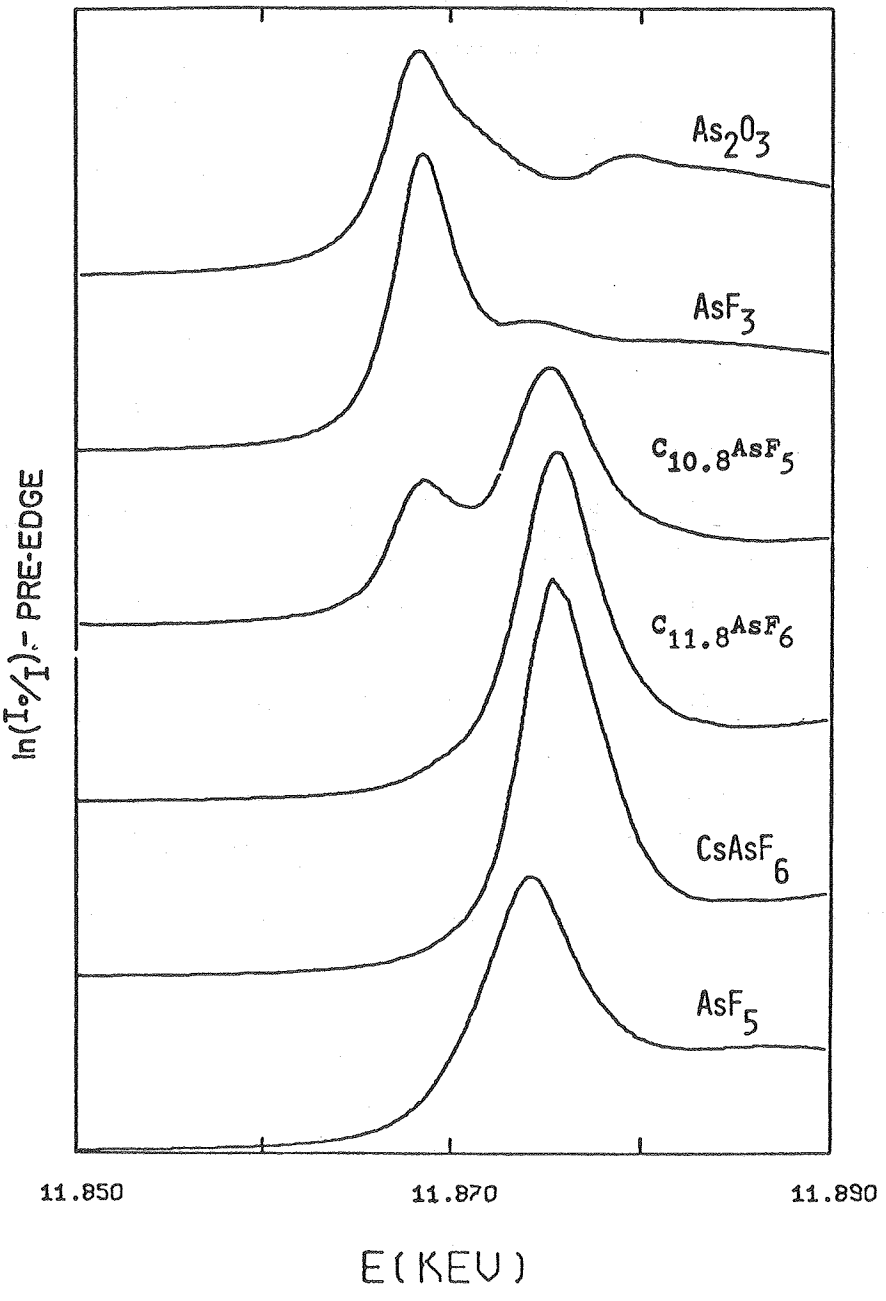

XBL 798-10982A

Figure 6-2

As Edge Features of Various AsF_6^- Compounds

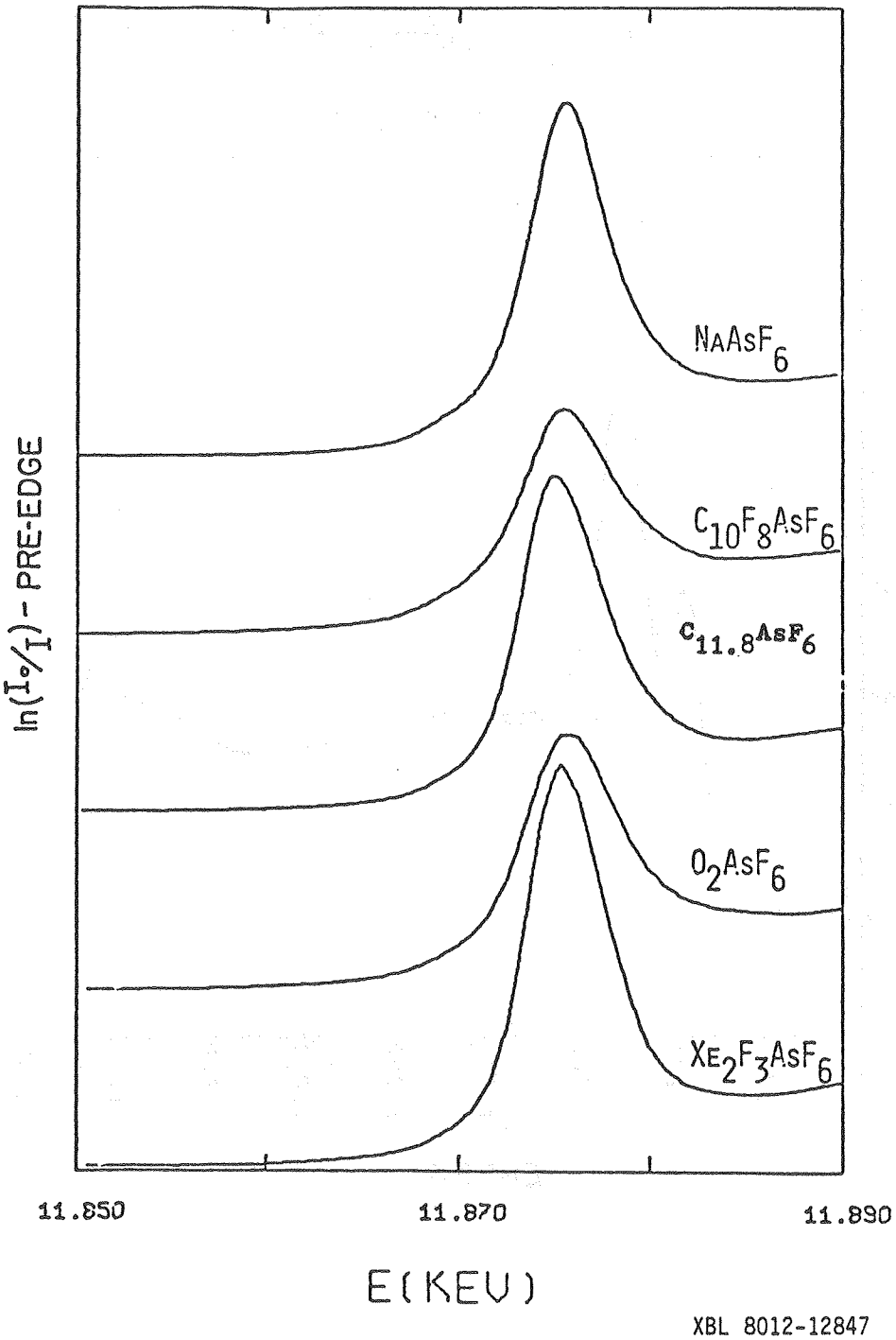

XBL 8012-12847

Figure 6-3

Fit of AsF_3 and $C_{11.8}AsF_6$ Edge Files (.....) to $C_{10.8}AsF_5$ Edge File (——)

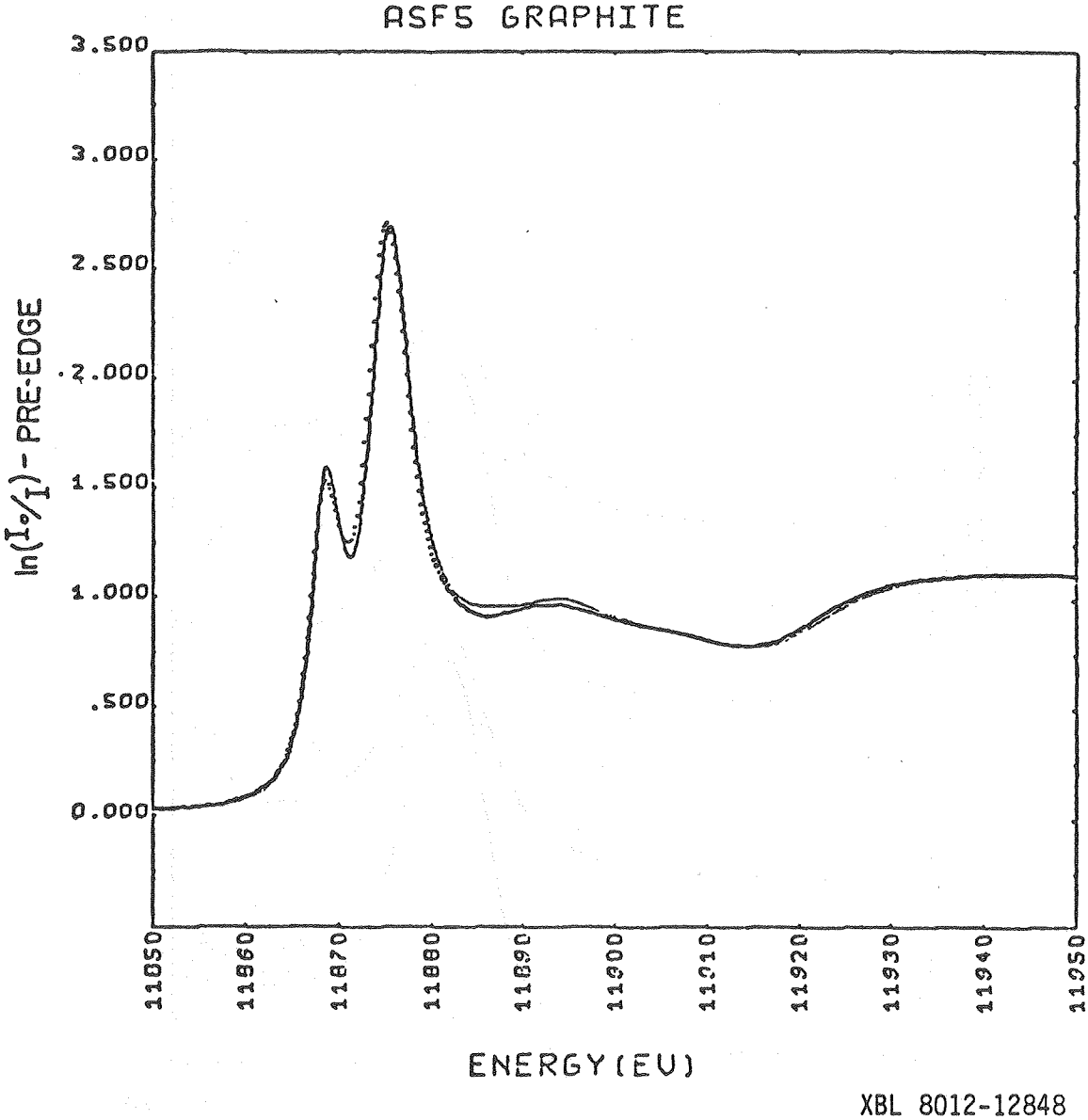

XBL 8012-12848

Figure 6-4

As Edge Region of Several C_nAsF_5 Samples

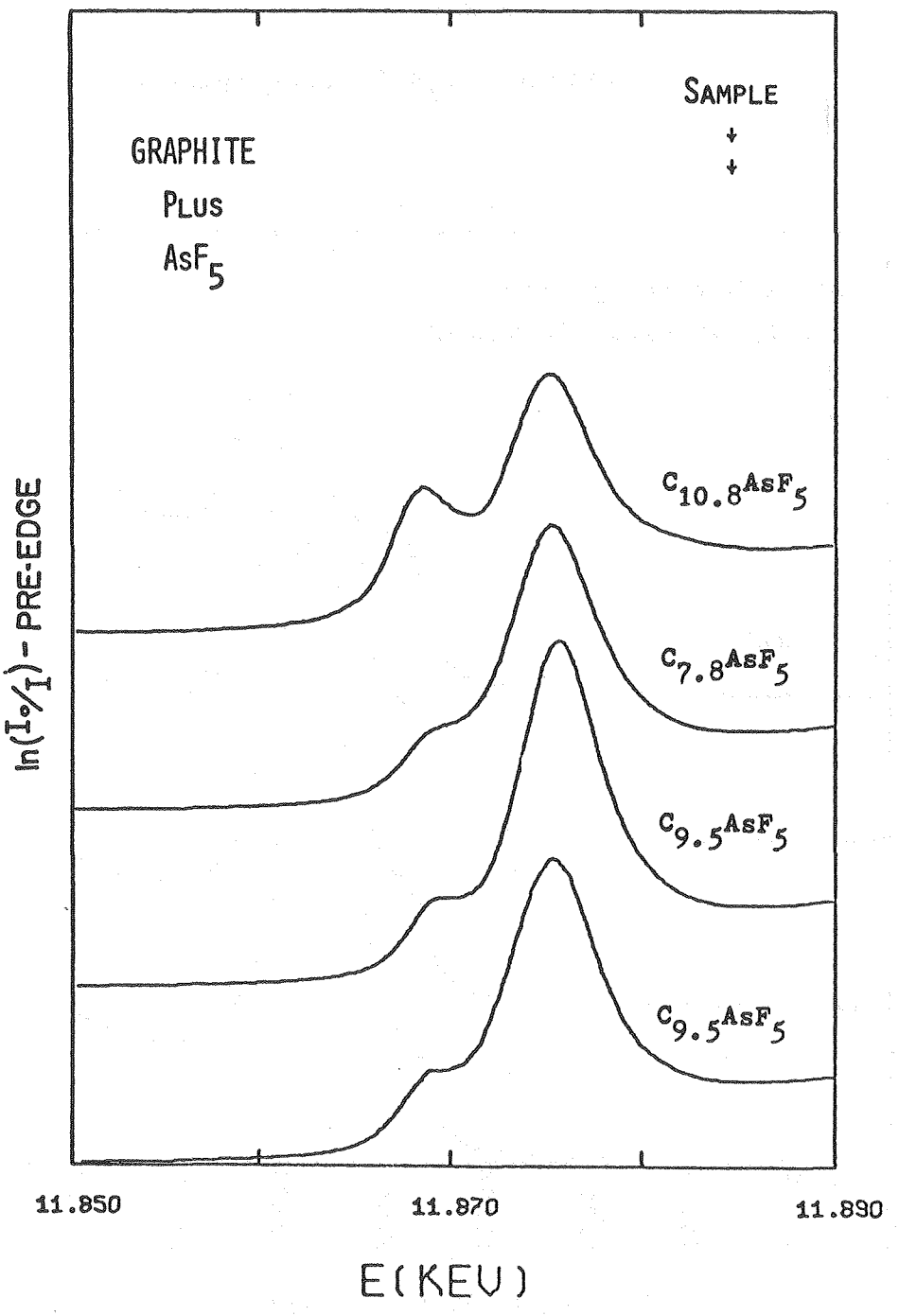

XBL 798-10977A

Figure 6-5

Oriented C_nAsF_5 Edge Spectra

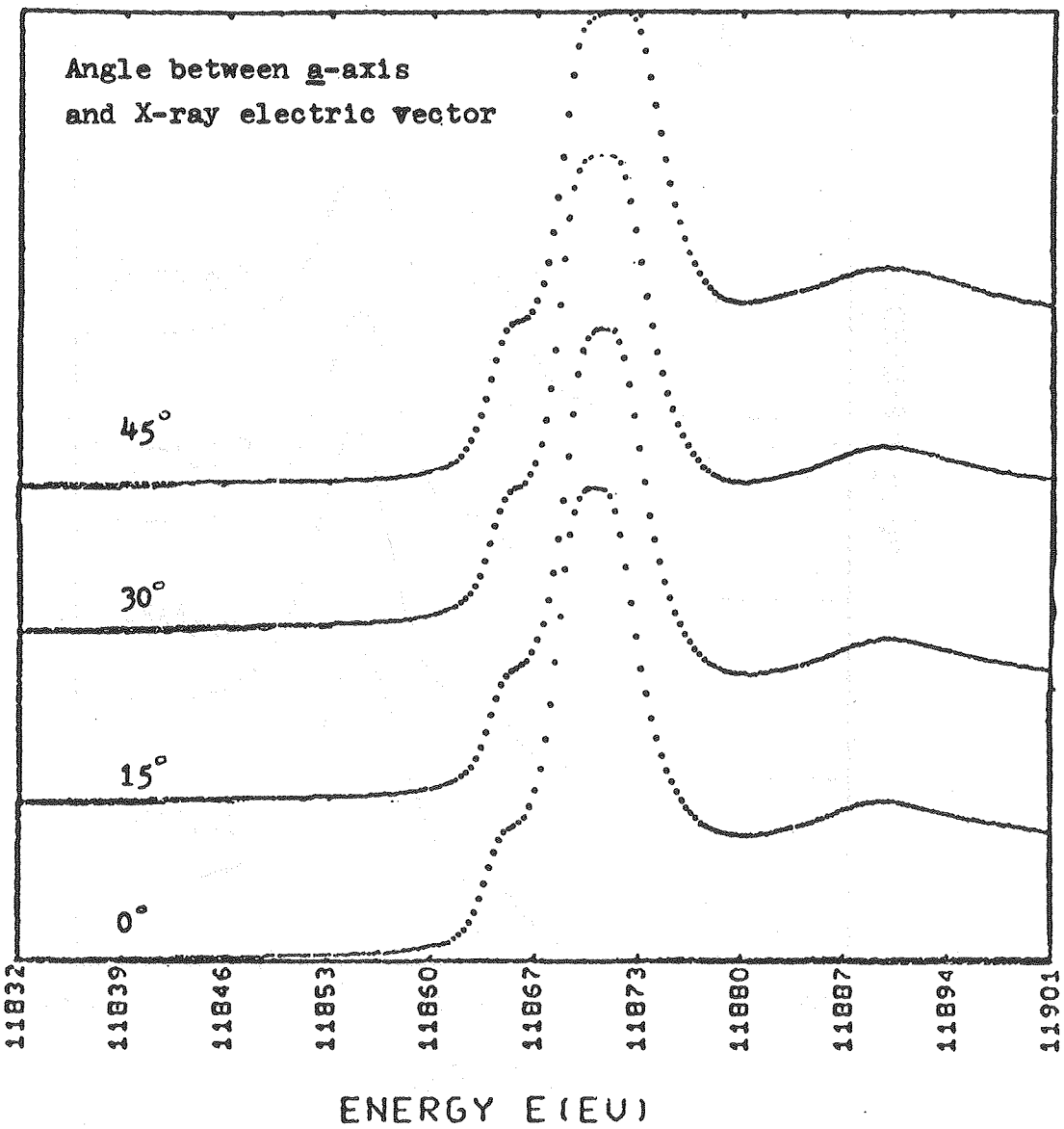

XBL 8012-12856

Figure 6-6

$U_{90}t$ Derived from Oriented C_xAsF_5 Chip

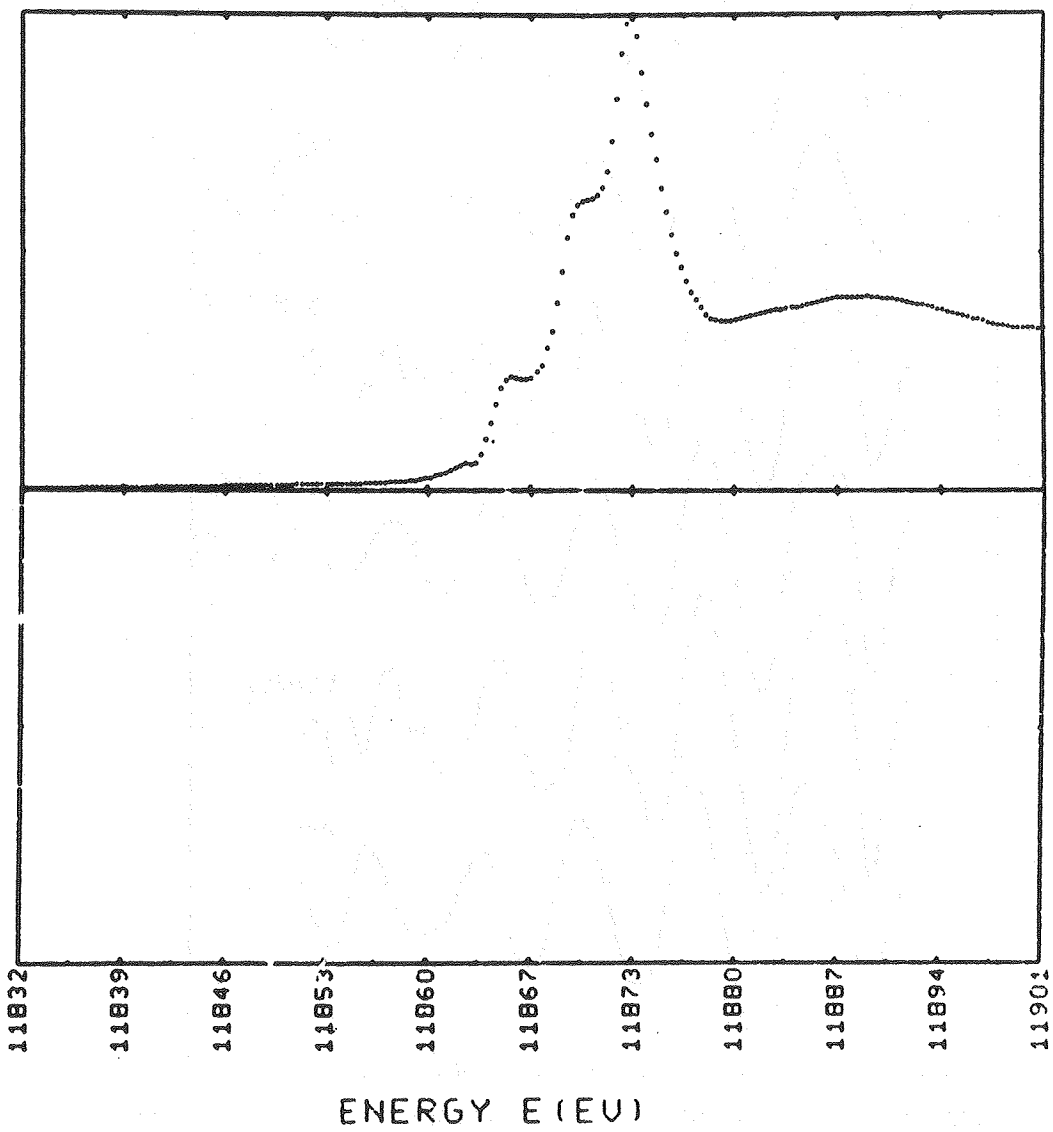

XBL 8012-12855

Figure 6-7

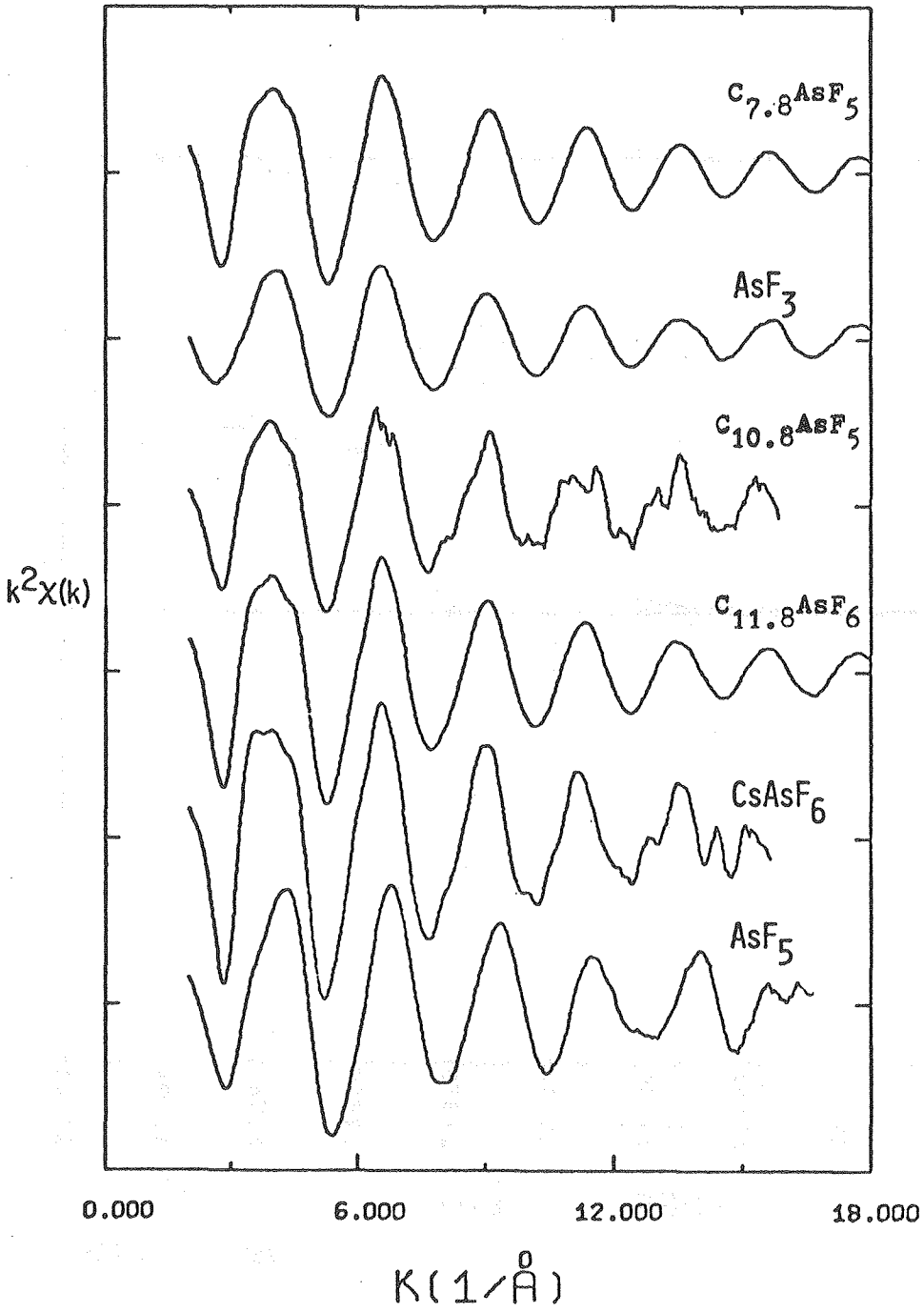

XBL 798-10996A

Figure 6-8

R-SPACE TRANSFORMS OF $K^3\chi(K)$

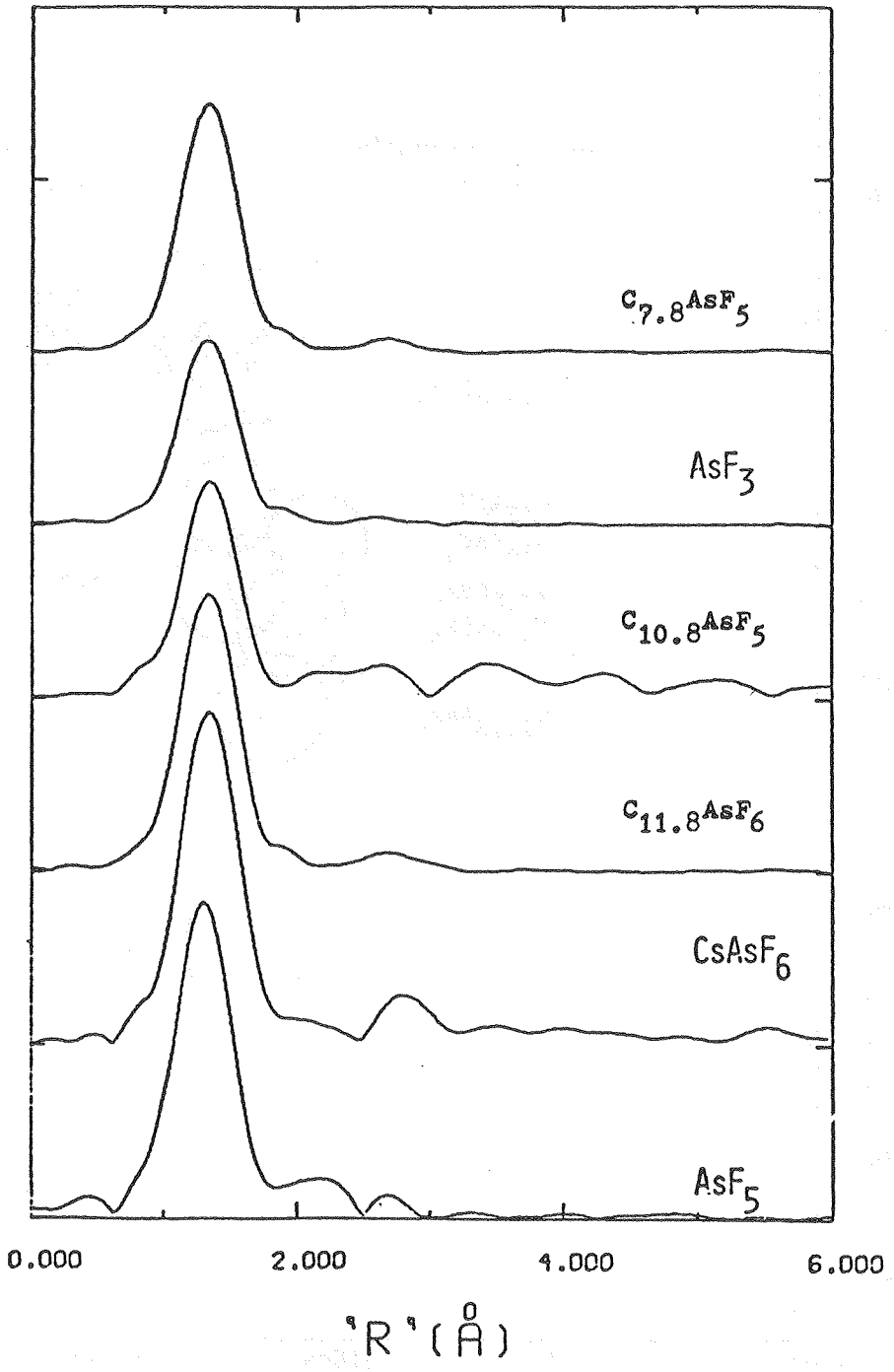

XBL 8012-12850

Figure 6-9

Error Contours

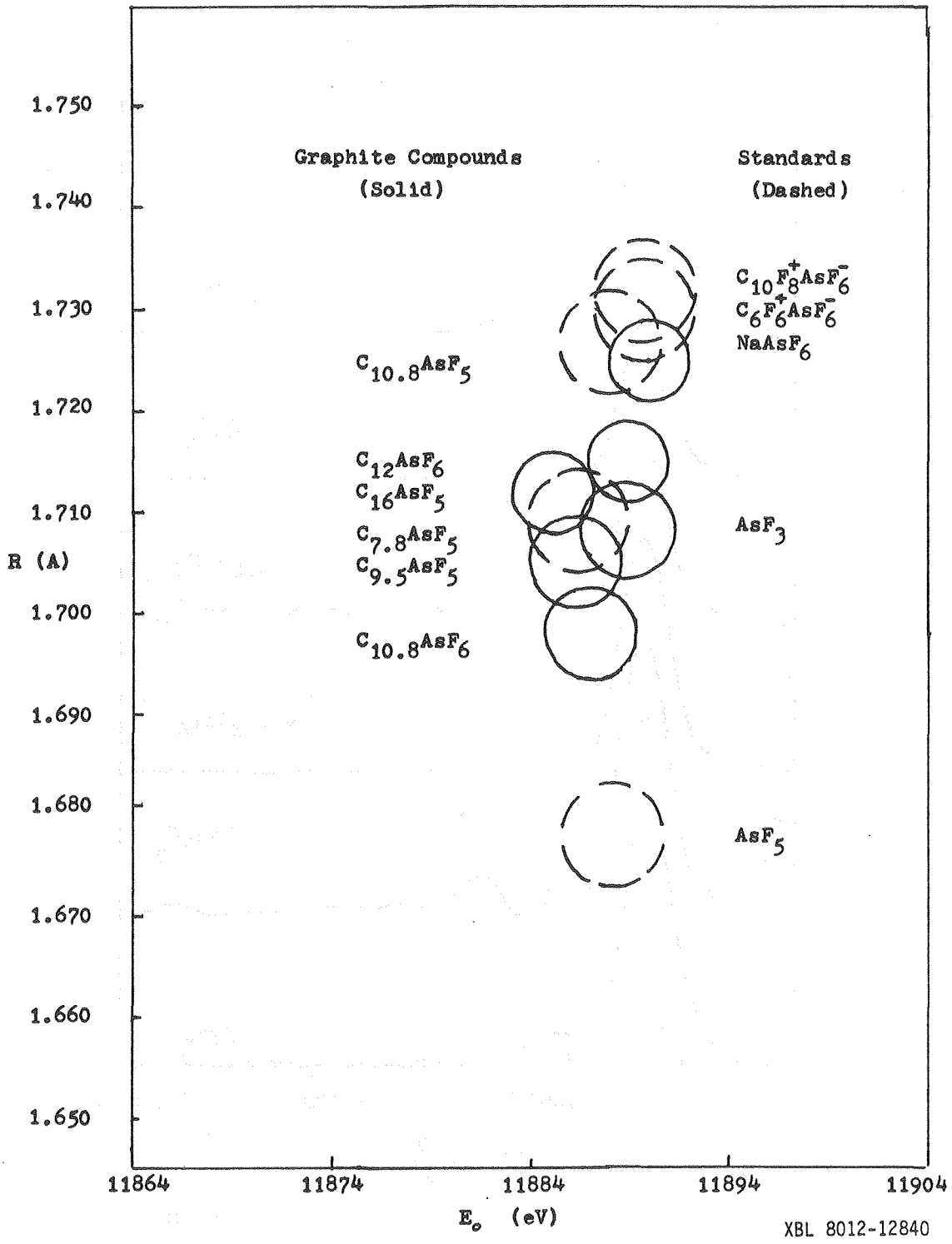

Figure 6-10

C_nAsF_5 Fluorine Exchange Mechanisms

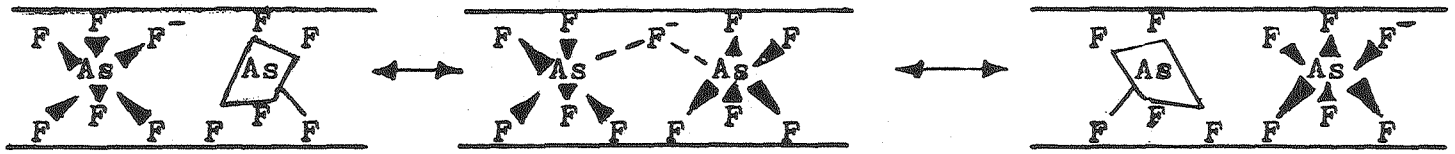

Fluoride Exchange

Reversal of AsF_5 Half Reaction

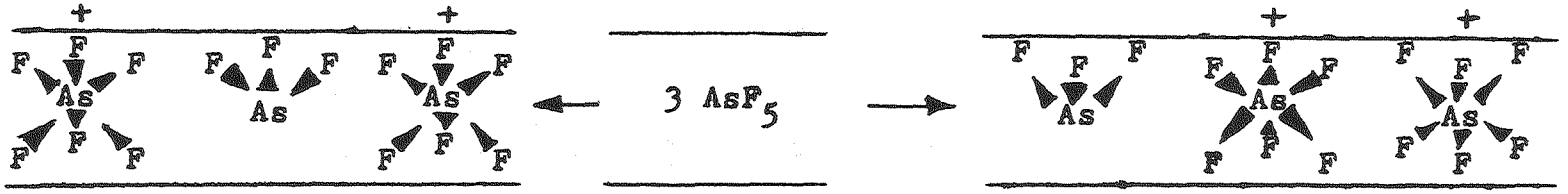

XBL 8012-12854

CHAPTER 7

Preliminary X-ray Absorption Studies of "C_xBrF_3" and C_xGeF_{5-6}

A study of the graphite plus BrF_3 reaction was made in view of the conflicting results from other groups. Work of Opalovskii et al[2] gave evidence that $C_{8.9}BrF_3$ was formed when graphite was immersed in BrF_3 liquid at 0°C. They observed no Br_2 evolution, their F^{19}NMR work implied fluorines on Br(III), and their elemental analysis gave Br:F as 1:3. Parallel work by Nazarov et al[2] with ClF_3 gave Cl:F as 1:4, and they characterized their product as $C_4^+ClF_4^-$. Work of Selig et al[3] with BrF_3 gave very uncertain elemental analysis which yielded a composition "$C_{24}BrF_{13}$". Br_2 was evolved during the reaction, which the authors ascribed to fluorination of the graphite. F^{19} NMR showed a significant shift from BrF_3's signal, in contrast to Opalovskii's result.

An alternative reaction path involving oxidation of the graphite is proposed in this work. This BrF_3 half reaction

$$4BrF_{3(g)} + 3e^- \longrightarrow 3BrF_{4(g)} + 1/2\ Br_{2(g)}$$

is seen in the reaction[4]

$$6KCl + 8BrF_3 \longrightarrow 6KBrF_4 + Br_2 + 3/2\ Cl_2.$$

Apparently this half reaction is at least strong enough to oxidize chloride to chlorine. Estimates of $\Delta H(kcal)/e^-$ (in Chapter 8) give -142 $kcal/e^-$. This value is above the value for the AsF_5 half reaction, and thereby appears to be a plausible oxidation reaction to occur with graphite. It would explain the evolution of Br_2, and the parallel ClF_3 reaction would explain the evidence of ClF_4^- seen by Nazarov. If the Br_2 were retained within the graphite, then a Br:F ratio of 1:3 would be observed.

The use of X-ray absorption seemed ideal to resolve the question which species is present within the graphite. If the graphite were fluorinated, and the Br_2 were retained, then a signal of Br_2 would be expected. Edge shifts of Br(0) and Br(III) should be widely separated, so that if mixtures of the two were present, they would both be visible. Comparisons with previous Br_2[5] and C_xBr[6] X-ray absorption studies could be made. If the edge studies alone could not distinguish BrF_4^- from BrF_3, then the Br-F distances are significantly different (1.89 Å vs 1.78 Å) that the EXAFS analysis should be able to distinguish the species. The experimental plan was to examine $Br_{2(g)}$ as a Br(0) species and uniform Br-Br standard for nearest neighbor determination. BrF_3 has too small a vapor pressure to be a good sample, so $K^+BrF_4^-$ was used as a Br(III) edge sample. $K^+BrO_3^-$ and BrF_5 would be taken as Br(V) standards for edge studies. The BrF_5 would be the uniform sample to derive Br-F EXAFS amplitudes and number of nearest neighbors. If the BrF_5 decomposed, one would still have the bromate

salt as a Br(V) sample. Both in theoretical expectations and in experimental details, the study using X-ray absorption appears quite promising in resolving the question which species is within the graphite.

The samples were prepared in the following manner. $KBrO_3$ and Br_2 were taken from analytical grade samples from Mallinckrodt. These two samples were used without further purification or characterization. Bromine trifluoride was taken from Matheson (98%) and the residual bromine was slowly fluorinated up to golden yellow BrF_3. A slight discoloration of Br_2 was maintained to ensure the absence of BrF_5. The sample was pumped at vacuum at -22°C to remove any trace F_2 or BrF_5. The remaining BrF_3 had a vapor pressure below 20 torr. The room temperature vapor pressure is reported to be 8 torr, while Br_2 and BrF_5 have significantly higher vapor pressures. $KBrF_4$ was made in an Argonne tube by adding BrF_3 to analytical reagent KF (Mallinckrodt). The powder pattern of the solid product after pumping off excess BrF_3 was similar to $K^+AuF_4^-$, [7] and no KF was present. BrF_5 was prepared by fluorinating BrF_3, and separated from the BrF_3 by distillation.

Three graphite samples were prepared (Table 7-1) and two were taken for X-ray absorption studies. One powder was placed within a FEP tube inside an Argonne tube. This arrangement hoped to keep the BrF_3 liquid off the graphite. Some powder escaped from the FEP during removal of the BrF_3 three days later. Much Br_2 was evolved. Gravimetry presumed from weight uptake BrF_3 gave $C_{22}BrF_3$. Elemental analysis for C, H, N, and Br gave a result similar to that observed by Selig. Similarly, the powder pattern showed four lines at 7.07, 5.39, 2.11 and 1.24 Å. The latter two

lines are graphite (100) and (110). The two larger lines may be the (001) and (002) lines of a first and second stage material respectively. This assignment requires c-spacings of 7.07 Å and 10.8 Å for these stages. This assignment would give a thickness of 4.1 Å for the intercalated species in the second stage, and 3.7 Å for the first stage. The breadth of the lines leaves a sizable error in the determination of the actual thickness. The presence of lone pairs on BrF_3 or BrF_4^- makes a quantitative prediction difficult. Due to the uncertain analysis, X-ray absorption studies were not collected on this sample.

A graphite chip was placed in the Argonne tube lengthwise and a small amount of BrF_3 was admitted to the bottom of the tube. Overnight, the solution darkened due to Br_2 evolution. The solution was pumped off, the fresh BrF_3 was added. This process was repeated daily for three days, until no further discoloration occurred. The gravimetry gave "C_6BrF_3", and the sample was a dull blue/grey. This sample was quickly placed into the EXAFS rotating cell in the Drilab. No elemental analysis was performed on this sample.

The value "C_6BrF_3" is interesting for structural reasons. For a BrF_4^- ion, the volume of 4 fluorines is 76 $Å^3$. For a thickness of 4.1 Å, the area taken up by a BrF_4^- would be 18.5 $Å^2$, which would give a limiting composition of $C_7^+BrF_4^-$. A "C_6BrF_3" compound would be a $C_{6.8}BrF_4^-$ by gravimetry. This limiting composition appears odd, though, because a hexafluoride having an area of three fluorides has a limiting composition of

C_8MF_6. It may be that the BrF_4^- are tilted with respect to the graphite plane. In looking at the oxidation strength of the BrF_3 half reaction, which is less than that of IrF_6 (Chap. 8), it is doubtful that BrF_3 could oxidize the graphite completely to C_7^+. One might thus expect to find some BrF_3 left inside the graphite, which would be difficult to pump out due to its low volatility. A mixture of BrF_3 and BrF_4^- would thus appear to be the plausible composition giving a limiting gravimetry of "C_6BrF_3".

The third preparation had graphite powder within a FEP tube with BrF_3. After 7 days, the powder gave gravimetry of "$C_{13}BrF_3$", while elemental analysis gave $C_{13.7}BrF_{4.4}$. The powder pattern showed only one broad band at 6.7 Å which could not be ascribed to the graphite (hk0) lattice. At this point, the prospect of characterizing the reaction product as containing BrF_4^- appeared good.

In Table 7-2 are the X-ray edge peak energies. The BrF_5 sample had clearly decomposed to Br_2, while the $C_{13}BrF_4$ had apparently hydrolyzed to C_xBr. The Br_2 gas standard showed negligible energy shifts. Figure 7-1 shows the edges of representative sample scans. Br(III) and Br(V) are 4.7 and 7.7 eV above the Br_2 white peak. The Br_2 white peak is usually ascribed as a transition to π^*. The "C_6BrF_3" showed neither new peaks nor broadening of its white peak upon rotation. The edge jump at 13480 eV scales as 1/cosθ for the 0° and 45° oriented samples. (134890 eV was the energy at which the Bell Lab's EXAFS analysis picked E = 0 for the photoelectron.) It is apparent that the bromine oxidation state in

"C_6BrF_3" is Br(III), and yet Br_2 was evolved in the preparation of the compound. The proposed half-reaction is consistent with the edge evidence, although the presence of BrF_3 cannot be excluded.

The EXAFS anaylsis was handled in the same manner as the arsenic data except the following four details. First, there was no readily available interactive computer program to remove spikes in the EXAFS. These spikes can come from non-linear responses in the ion chambers to fluctuations in beam intensity. These spikes should not significantly affect the analysis, because the spikes should appear at a radically different position from the windowed R-space region of the bond distance peak. The back Fourier transformed K-space EXAFS signal, on which the fits are performed, showed no evidence of the spikes. Second, the error ellipsoid program, which gave the distance and error in the arsenic case, was not run. For these bromine values, no calculated error estimates are possible. By comparison with the known standards, the errors are taken to be ± 0.010 Å. Third, all values given here are from individual data scans. In the arsenic case, three or more scans were added in order to improve the signal-to-noise. That the R-distance errors are so small on individual data files shows each file to be of high signal-to-noise quality. Lastly, for the bromine compounds, an initial E_o choice was used for a preliminary Bell-Lab's analysis to C_xBrF_3. This E_o generated a better E_o' which was then made the initial E_o choice and the analysis was repeated to give E_o''. When E_o'' varied from E_o' by 2 eV for Br(III) compounds, that E_o' was used for the other compounds. Using that E_o', the final

E_o" values for Br(0) compounds were 7 eV lower in energy, while the Br(V) compounds were 20 eV higher. These shifts in E_o" from E_o' are much more reasonable than those in the arsenic work, where a poor initial E_o guess was used and the program shifted E_o" to 60 eV lower energy. The iterative approach used here gives a more self-consistent E_o". In all other details - background smooths, transform and filter window ranges, etc. - this analysis paralleled the arsenic work.

Table 7-3 gives the values from the EXAFS fits. The fitting function always had slightly lower values for the smoothed background removal than for the Victoreen division. There was no change in the R-value between the two methods, although the amplitude changed slightly. The values for the smoothed background analysis are quoted.

On all the standards, the bond distance found in the EXAFS analysis agree within 0.01 Å. The comparison of observed and calculated fits over the range K = 5.5 to K = 13.5 was excellent. The Bell Lab's theoretical phase parameters worked superbly. The two graphite compounds give distances which differ from those expected distances. In the C_xBr, the distance varies slightly from those EXAFS distances reported previously.[6] However, the Br-Br bond is longer than in gaseous Br_2. The Br-F bond distance in "C_6BrF_3" is not in agreement with the BrF_4^- hypothesis. The bond distance is much closer to the average value for BrF_3.[8] From this limited evidence, the majority of molecules appear to be BrF_3. The amplitude information is very unreliable in giving the number of nearest neighbors. Because the BrF_5 sample decomposed, there was no uniform standard

for the Br-F amplitude. Comparisons using the BrF_4^- salt are tenuous because the sample was not known to be homogeneous. In comparing the 0 and 45 degree sample amplitudes, one finds that they do not scale at $\cos^2$ 45. Since the edge jump did scale properly, the source of this discrepancy is not known. Using the BrF_4^- salt as a standard, one calculates N = 2 or 3.4 for the 0 or 45 degree samples. The amplitudes are reported here so that if a BrF_5 sample is run, its amplitude can be compared with these values.

In summary, the preliminary EXAFS evidence does not conclusively resolve the species present inside the graphite. The proposed half reaction is consistent with the evidence that Br_2 is evolved and a Br(III)-F species is present within the graphite. The Br-F distance implies that a substantial portion of the species is BrF_3. Further work is necessary to definitively characterize the species. Examination of a fluorinated C_xBrF_3 would be useful to insure that one is looking at a BrF_4^- species within the graphite.

Graphite/GeF_{5-6}

An initial X-ray absorption study of the graphite/GeF_4 + F_2 system was also begun. Interest in this system is based on the probable formation of GeF_5^- and GeF_6^{-2} ions within the graphite. While the GeF_5^- ion appears stable to vacuum, the amount of GeF_6^{-2} is fluorine pressure dependent. Thus an equilibrium

$$G_x^+GeF_5^- + 0.5F_2 \longrightarrow C_x^{++}GeF_6^{-2}$$

has been established.[10] In order to characterize these two ions (the GeF_5^- is poorly characterized in the chemical literature), X-ray studies were undertaken to identify the species present within the graphite. One question that might be posed is whether the possible equilibrium

$$2GeF_5^- \longrightarrow GeF_4 + GeF_6^{-2}$$

occurs.

Samples of GeF_4, $n\text{-}Bu_4N^+GeF_5^-$, K_2GeF_6, $(BrF_2^+)GeF_6^{-2}$, C_xGeF_5, C_xGeF_6 under F_2 pressure, and "GeF_2" were prepared and chemically characterized by G. McCarron and T. Mallouk. Sufficient material was loaded into the standard cells to give a path length for $\mu_x = 2$. The C_xGeF_6 was loaded on the Teflon window of a gas IR cell which was then filled with F_2. The Wiggler line at SSRL was used, and data was collected across the edge region in ~ 0.3 eV steps. GeF_4 was used as the energy reference sample and was examined periodically during the day to check for drift in the monochrometer energy across beam dumps. Radiation heating of the crystal monochrometer caused some problems, and may have affected the energy scale slightly.

In Table 7-4 are the energies of the white peaks. Two facts are apparent. First, there was some shifting of the GeF_4 energy reference peak. Since there were few beam dumps, this energy error may be due to heating of the monochrometer crystal. This heating can slightly alter the d-spacing used in the crystal to select the X-ray energy. The crystal may also sightly fall off its rocking curve, which would affect the energy

values. Second, the GeF_5^- and GeF_6^{-2} peaks group near one another about 2.5 eV above the GeF_4 peak. Figure 7-2 gives representative spectra, which also show that GeF_4 falls below the energy of the other Ge(IV) compounds. This energy difference from the GeF_4 is more apparent when the shift from the nearest GeF_4 spectrum is used. With the scatter in the energy shifts, which are only of the order of ± one data point, it is not obvious whether the GeF_5^- peak falls at slightly higher energies than GeF_6^{-2}. In comparing the C_xGeF_5 and C_xGeF_6 samples with the standards, it is clear that GeF_4 is not a significant fraction of the species within either graphite sample.

The "GeF_2" sample gives evidence of being a mixed valence Ge(II)-Ge(IV) species. The X-ray powder pattern did not match the pattern of authentic GeF_2, nor of other reported GeF_x species.[11] The identity of this compound is still undetermined. Attempts to prepare the material again have failed. Most likely, the sample is $GeF^+GeF_5^-$ or $Ge^{++}GeF_6^{=}$ (GeF_3) or $(GeF^+)_2\ GeF_6^{=}$ (Ge_3F_8).

The EXAFS data collected was of insufficient quality to perform an adequate analysis. Further data must be collected.

References for Chapter 7

1. A. A. Opalovskii, A. S. Nazarov, A. A. Uminskii, and Yu. V. Chichagov, Russ. J. Inorg. Chem., 17(9), 1227, 1972.
2. A. S. Nazarov, V. G. Makotchenko, and I. I. Yakoviev, Russ. J. Inorg. Chem., 23(6), 925, 1978.
3. H. Selig, W. A. Sunder, M. J. Vasile, F. A. Stevie, and P. K. Gallagher, J. Fluorine Chem., 12, 397, 1978.
4. L. Stein, "Physical and Chemical Properties of Halogen Fluorides", in Halogen Chemistry, V. Gutmann, Vol. 1, Academic Press, London, 161, 1967.
5. B. M. Kincaid and P. Eisenberger, Phys. Rev. Lett., 34, 1361, 1975.
6. S. M. Heald and E. A. Stern, Phys. Rev. B., 17(10), 4069, 1978; S. M. Heald and E. A. Stern, Synthetic Metals, 1, 249, 1979-80.
7. A. J. Edwards and G. R. Jones, J. Chem. Soc. A 1936, 1969.
8. D. W. Magnuson, J. Chem. Phys. 27, 223, 1957.
9. E. M. McCarron, Ph.D. Thesis, University of California, Berkeley, LBL-11272, 1980.
10. J. C. Taylor and P. W. Wilson, JACS 95(6), 1834, 1973.

Table 7-1. Characterization of C_xBrF_3 Compounds

Final Compound	Details of Synthesis	Elemental Analysis				Powder Pattern d(Å)
		C	H	N	Br	
$C_{25}BrF_{11.9}$	Powder reacted with BrF_3 vapor for four days. Gravimetry gave "$C_{21.9}BrF_3$".	47.11	0.22	3.35	13.12	7.06 b 5.39b 2.11 graphite (100) 1.24 graphite (110)
"C_6BrF_3"	Chip reacted with fresh BrF_3 liquid daily for 3 days.	none				none
$C_{13.7}BrF_{4.4}$	Powder reacted with BrF_3 liquid for 7 days. Gravimetry gave "$C_{13.1}BrF_3$".	48.4	0.14	1.49	24.3	6.76 b 2.13 graphite (100)

Table 7-2. Bromine Peak Energies (-13400 eV)

	Br(0)	Br(III)	Br(V)
$Br_{2(g)}$	63.7		
	63.8		
	63.6		
	63.6		
	63.7		
BrF_5 (decomposed to Br_2)	63.6		
	63.6		
	63.6		
$C_{13.7}BrF_{4.4}$	63.7		
(decomposed to C_xBr)	63.7		
$K^+BrF_4^-$		68.0	
		68.2	
"C_6BrF_3" 0°		68.4	
0°		68.3	
45°		68.5	
$K^+BrO_3^-$			71.4
			71.4

Table 7-3. Bromine EXAFS Results

Compound		Br-Br (Å)	Known Distance	E_o"(-13400)	Amplitude ($N \cos^2\sim/R^2$)
$Br_{2(g)}$		2.287	2.281, 2.29[6]	72	0.266
BrF_5 (Br_2)		2.281		74	0.211
		2.285		73	0.212
		2.283		73	0.17
$C_{13}BrF_{4.4}$		2.299	2.34[6]	74	0.275
(C_xBr)		2.293		72	0.210
		Br-O (Å)			
$K^+BrO_3^-$		1.692	1.68	107	0.0716
		1.686		103	0.107
		Br-F (Å)			
"C_6BrF_3"	0	1.758	1.89 (BrF_4^-)	78	0.431
	0	1.760	1.78 (BrF_3)	79	0.415
	45	1.776		81	0.362
$K^+BrF_4^-$		1.900	1.89[9]	89	0.45
		1.897		87	0.53

Table 7-4. Ge Edge Peak Energies (minus 11100 eV)

	Ge(II)	GeF_4	GeF_5		GeF_6^{-2}	
			Data	Shift from GeF_4	Data	Shift from GeF_4
GeF_4		1.1				
		1.9				
		1.9				
		0.8				
		0.5				
		1.7				
		1.8				
		1.7				
$R_4N^+GeF_5^-$			2.6	1.8		
			3.1	2.2		
			3.1	2.2		
C_xGeF_5			3.4	2.6		
			2.6	1.8		
			3.0	2.2		
			4.3	2.5		
			4.0	2.2		
			4.6	2.8		
			4.6	2.8		
			4.5	2.7		
K_2GeF_6					3.6	1.7
					3.5	1.6
					3.4	1.5
					3.0	1.3
C_xGeF_6					3.1	1.1
					3.6	1.7
					3.6	1.7
					2.5	2.0
					2.5	2.0
					3.7	2.0
"GeF_2"	-4.3		3.0	2.2		
	-4.1		3.1	2.3		
	-4.2		3.1	2.3		

Figure 7-1

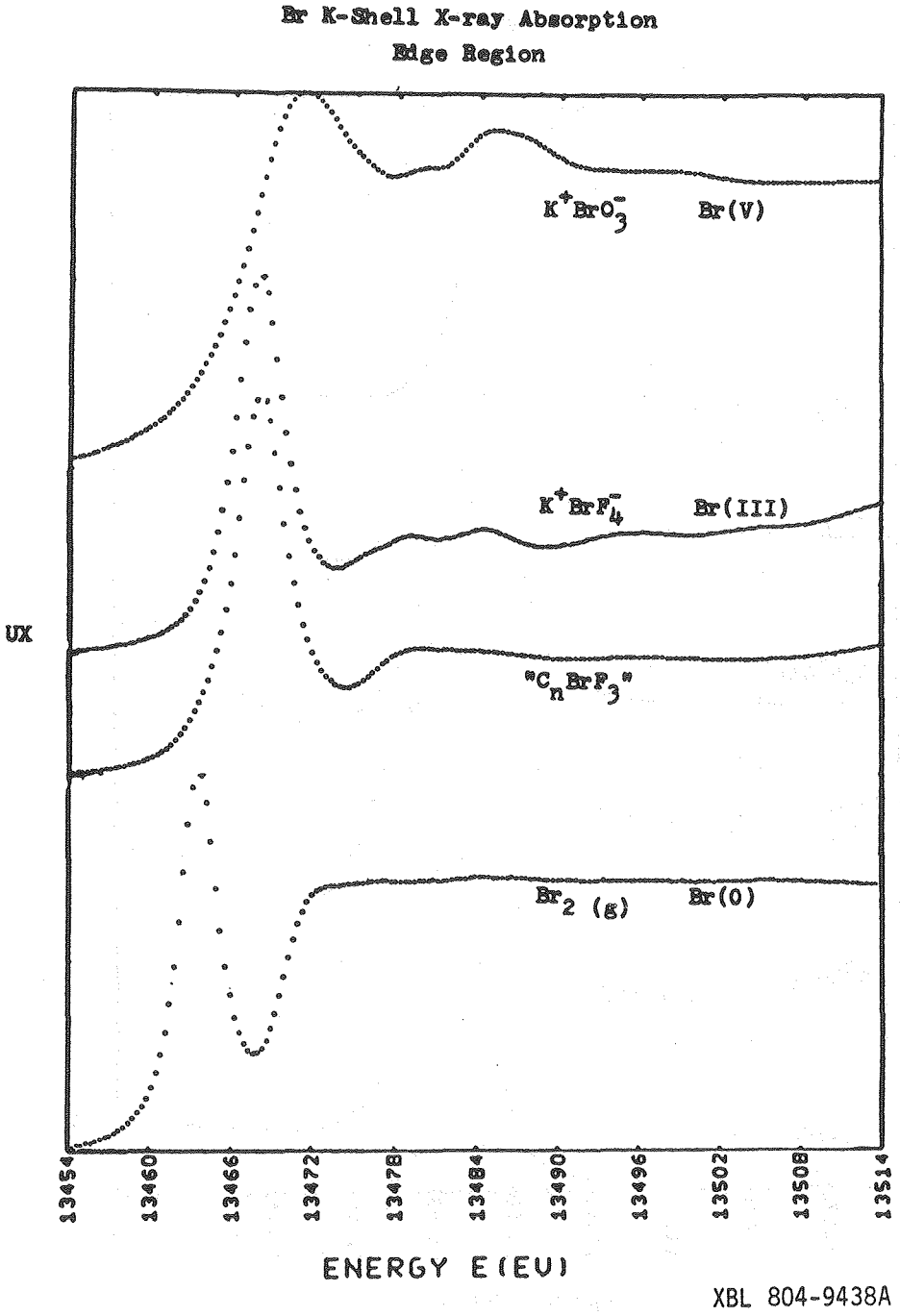

XBL 804-9438A

Figure 7-2

Ge Edge Data

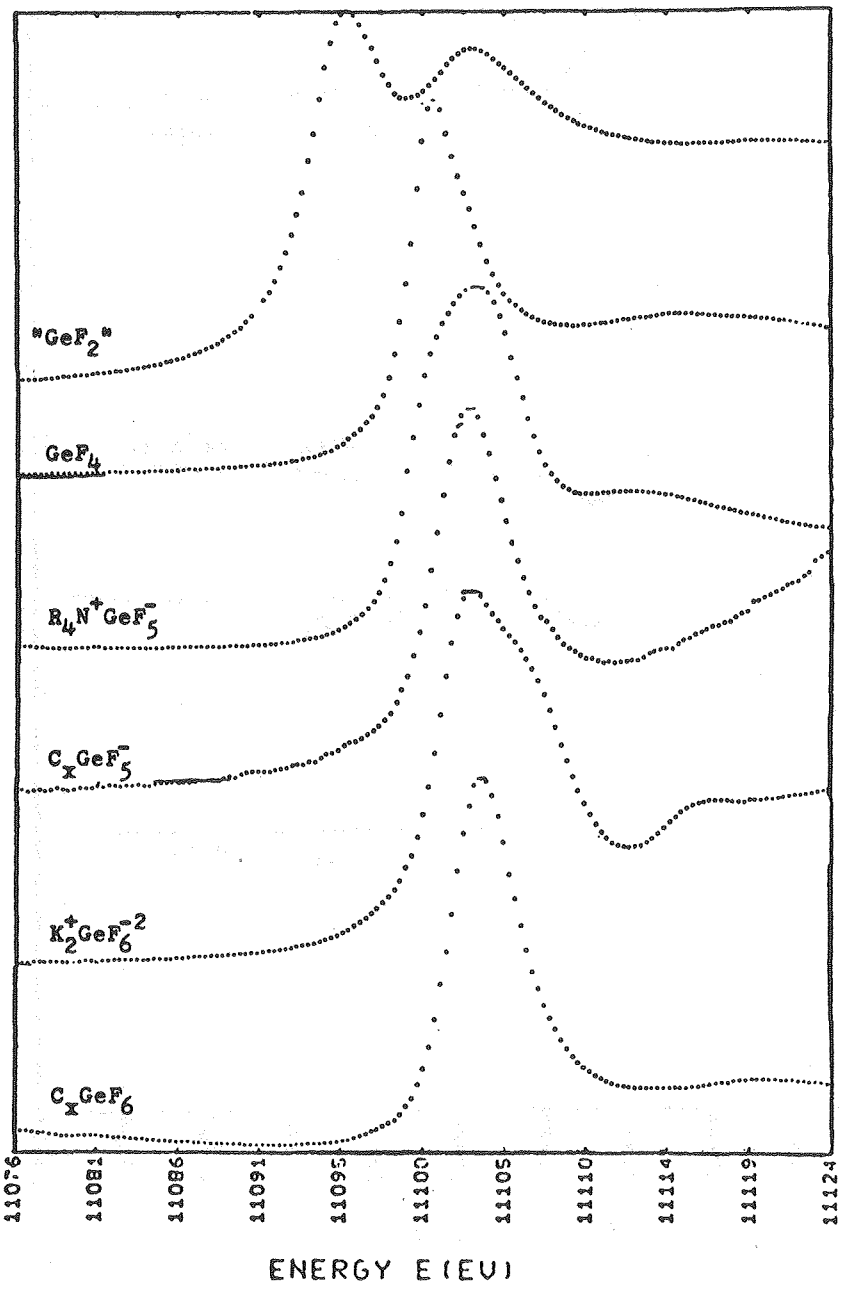

XBL 808-10922A

CHAPTER 8

A Thermodynamic Correlation Between Heats of Oxidation Half-Reactions and Reactivity with Graphite

A variety of substances react with graphite to form intercalation compounds. However, a rationale to predict which substance will react with graphite has not been formulated. This lack of a consistent criteria of reactivity has been most keenly felt among the so-called "acceptor" compounds. Here the intercalating species accepts electron density from the graphite to some unspecified degree. Two generalized models have been developed to explain the reactivity. The first model notices that many, but not all reactants are strong Lewis acids. The acid accepts electron density to an undetermined degree. The second model requires that a formal oxidation reaction, producing known chemical species, is the proper chemical formulation. In this paper, a pattern of chemical reactivity is presented within the "oxidation" model which incorporates the Lewis acid model and removes several discrepancies in the Lewis acid explanation of reactivity.

In Figure 8-1 is shown a generalized thermodynamic cycle which determines the components of the heat of formation of a graphite intercalation compound. W.F. is the work function of the graphite. V.d.W. is the energy needed to separate a layer of graphite from 3.35 Å to a greater distance. U_L is the "lattice energy" of placing a uninegative ion of radius r_- between the expanded graphite layer. For a given set of ions with similar r_-, each of the above terms are equal for each ion. For these similar ions A^-, the only term which varies

is ΔH_{ox}, which is a quantitative measure of the oxidation strength of the molecule. This gas phase measure of oxidation strength can be measured or calculated by alternative thermodynamic cycles. A comparison of similar known compounds' reactivity toward graphite with ΔH_{ox} may indicate a lower limit of $-\Delta H_{ox}$ below which intercalation compound formation is thermodynamically unfavorable.

Reactions of Fluorine Compounds

In Table 8-1 are the electron affinities of some metal hexafluorides. All have thicknesses of ~4.7 Å inside graphite, except for UF_6 which has ~5.1 Å. The $-\Delta H_{ox}$ for MoF_6[1], WF_6[3], and UF_6[7,8] are known from ion cyclotron resonance (ICR) studies.

ReF_6 and OsF_6 are interpolated estimates based on the WF_6 and PtF_6 values. The PtF_6 value comes from the lattice energy calculation and heat of formation of $O_2^+PtF_6^-$.[10] One sees a trend in reactivity depending on the oxidation strength of the metal fluoride. A limiting $-\Delta H_{ox}$ appears to fall somewhere between 105 and 115 kcal.

In Table 8-2 are the heats of oxidation of several Lewis acids with F_2. The values for the pentafluoride monomers and BF_3 are based on thermodynamic cycles, while the WF_6 value is from ICR. The requirement of F_2 for reaction is related to the Lewis acidity of these compounds as shown below:

		ΔH_{ox}(kcal)
(1)	$AsF_5 + F^-_{(g)} \rightarrow AsF^-_{6(g)}$	-106
(2)	$1/2\ F_2 \rightarrow F^-_{(g)}$	- 64
(3)	$AsF_5 + 1/2\ F_2 + e^- \rightarrow AsF^-_{6(g)}$	-170

Reaction (1) reflects the Lewis acidity of AsF_6 as measured by its fluoride ion affinity. Reaction (3) thus contains a measure of the Lewis acidity, while being an oxidation reaction. First, it is significant to note that reactions with graphite are known for all these calculated ΔH_{ox}, and that all values of $-\Delta H_{ox}$ are above the ~110 kcal "border" limit" apparent in the metal hexafluoride series. Second, one can see why WF_6 alone might not react the graphite, while $WF_6 + F_2$ would react because it is a stronger oxidant.

In Table 8-3 are the heats of oxidation of a known pentafluoride disproportionation reaction. This reaction is composed of the $MF_5 + F_2$ reaction and the reduction of MF_5 to $MF_3 + F_2$. A significant point to notice is that the Lewis acidity of PF_5 is virtually as strong as AsF_5, and yet PF_5 alone does not react with graphite while AsF_5 alone does react. Reaction (2) explains this significant difference in reactivity. PF_5 is much more stable relative to PF_3 than is AsF_5 stable relative to AsF_3. AsF_5 has a greater thermodynamic drive to become AsF_3. It is this difference in (2) which distinguishes PF_5 from AsF_5 reactivity. Because 2 e^- are needed in this net reaction, while

the earlier tables required only measuring 1 e^-, a comparison of oxidation strength can only be made by comparing $-\Delta H_{ox}$ per $e^-(E_r)$. In making this comparison one sees that the PF_5 reaction falls below the previously established lower limit of 100 kcal/e^-, while AsF_5 and SbF_5 fall well above the upper limit of ~110 kcal/e^-. In this comparison of PF_5 with AsF_5, the "oxidation" model is clearly more successful in explaining their differences in reactivity than is the "Lewis acid" model.

One must remember, however, that these are thermodynamic quantities, and not mechanistic studies. In writing these two reactions (1) and (2), one is not saying that F_2 is liberated from MF_5 in the process of intercalating graphite. One could just as easily have written

$$2MF_5 + 2F^-_{(g)} \longrightarrow 2MF^-_{6(g)}$$
$$MF_5 + 2e^- \longrightarrow MF_3 + 2F^-_{(g)}$$

$$3MF_5 + 2e^- \longrightarrow 2MF^-_6 + MF_3$$

and achieved the same sum for the half-reaction. All these reactions only give the net energy change made in the reaction.

As a further test of this apparent E_r "border" of reactivity, one can ask whether alternative oxidation reactions can be found for those compounds which fail to react, and whether E_r for these alternative reactions remain below the border. In Table 8-4 are listed alternative possible reactions for unreactive fluorides. In most cases, one alternative product is allowed to be in the solid state, in order to further

drive the oxidation toward the right. In none of these reactions does E_r pass above the border, which is consistent with the observed non-reactivity of these compounds.

A further test of the significance of this oxidation model is to look at the alternative reaction for AsF_5

$$6AsF_5 + 5e^- \longrightarrow 5AsF_{6(g)}^- + As_{(s)}.$$

The E_r is 108 kcal, which appears be strong enough to be a plausible reaction. However, the half-reaction of Table 8-3 shows a larger E_r, and thus would be the preferred reaction. This alternative reaction is not observed, while the formation of AsF_3 has been observed.

All the reactions given above created spherical uninegative metal fluoride ions with thicknesses of ~4.7Å, and therefore a direct comparison of E_r is valid. A "border" in E_r appears in the neighborhood of 110 kcal/e^-. This approach has proposed a solution to the non-reactivity or reactivity of several reagents with graphite.

Reactions of Other Halide Compounds

A brief look at metal chloride systems is warranted. In Table 8-5 are shown possible reactions of MCl_3 species. Comparing (1) with the Al reaction of (3), one sees that $FeCl_3$ and $AlCl_3$ must have similar Lewis acidity. Yet $FeCl_3$ alone reacts with graphite, while $AlCl_3$requires Cl_2 in order to react. Reaction (2) supplies part of the answer. Iron has a stable +2 oxidation state, while Al has no such state. Thus (2) is a plausible oxidation reaction to explain the intercalation reaction. The value of E_r is certainly well above the previously established "border". All the remaining MCl_3 species show E_r which would assert

that compounds do exist. Such compounds do exist in the presence of Cl_2. In the absence of Cl_2, the alternative reactions are less favored, and fall below the "border" previously established. Here again, this oxidation approach can explain the different reactivities among $FeCl_3$ and $AlCl_3$, $AlCl_3$, and $AlCl_3 + Cl_2$, and $GaCl_3$ and $GaCl_3 + Cl_2$ in a manner that the Lewis acid model cannot explain.

Table 8-5 compares the gas phase E_r of $AlBr_3$ and $GaBr_3$. Again a border of reactivity/non-reactivity appears. However, the reported compositions and characterization are made more difficult because Br_2 does react with graphite and excess Br is apparently present in these compounds. In summary though, this brief look at chloride and bromides shows that limiting values of E_r must exist.

The above calculations were for reactions which all produced spherical uninegative ions. This restriction permitted a Kapustinskii lattice energy calculation using a plausible thermochemical radius. A look at non-spherical uninegative ions can also be made. However, the lattice energy calculation is liable to have greater error within it, due to the lack of a plausible criteria for a thermochemical radius. A Yatsimirskii calculation can give a radius, but the calculation can be susceptible to very large errors in radius based on small errors in a Born-Haber cycle. The E_r values given for the following reactions carry a larger potential for error than those previously calculated.

The reactivity of the halogens and interhalogens have been used to argue that a simple oxidation does not solely account for the graphite reactions. In Table 8-6 are shown E_r for various possible product species. One immediately notes that for F_2 and I_2, for which no

reaction occurs near room temperature, all values of E_r are below ~110 kcal. The E_r values for Cl_3^- and Br_3^- are more questionable, although their E_r do hint that these ions may be among the product ions. The sizable limits on the E_r of Br_3^- shows how E_r is prone to errors from choosing a thermochemical radius. Recent EXAFS results on $(SN)_x^+Br_3^-$ [43] and C_xBr [44] imply that some Br_3^- is present within the graphite. The values for ICl and IBr are susceptible to the same errors, but are consistent with the thesis that an E_r threshold must be exceeded. The excess chlorine in the ICl and excess Br in the IBr reactions gives support to the argument that some ICl_2^- and IBr_2^- are present along with the interhalogen. The strength of oxidation gives support to the thesis that an oxidation is required for reaction.

Calculations of E_r have also been made for the reactions of HX plus 1/2 X_2 to make the bihalide ions. It had been puzzling that F_2 does not react with graphite at ordinary temperatures unless HF were present. A comparison of the E_rs for formation of the fluoride and bifluoride ions supports that thesis that HF_2^- is a final product of this reaction. The failure of the other halides with their respective acids is also supported by the E_r values.

Lastly, the reaction of BrF_3 with graphite can be mentioned. From the known reaction[45]

$$3KCl + 4BrF_3 \longrightarrow 3/2\ Cl_2 + 3K^+BrF_4^- + 1/2\ Br_{2(\ell)}$$

one can see that the E_r for the reaction

$$4BrF_3 + 3e^- \longrightarrow 3BrF_{4(g)}^- + 1/2\ Br_{2(1)}$$

is at least strong enough to oxidize chloride to chlorine (58 kcal). From the reactions

$$3BrF_3 + 3/2F_2 + 3e^- \longrightarrow 3BrF_4^- \qquad \Delta H = -372 \text{ kcal}^*$$

$$BrF_3 \longrightarrow 3/2\ F_2 + 1/2\ Br_2 \qquad \Delta H = -62 \text{ kcal}^{19}$$

$$4BrF_3 + 3e^- \longrightarrow 3BrF_4^- + 1/2Br_{2(1)} \qquad \Delta H = -434 \text{ kcal}$$

$$E_r = 145 \text{ kcal}$$

one can see that this E_r exceeds the threshold for reaction.

Discussion

Having established that, for a given family of reactants, there exists a limiting E_r below which no reaction with graphite occurs, one can ask whether this limit is a thermodynamic or kinetic limit. Because this border lies near ~110 kcal for the hexaflourides, and the work function of graphite is about 106 kcal, it is tempting to speculate that a kinetic barrier of ~106 kcal limits graphite's reactivity. One can propose that an initial first step towards intercalation is the removal of an electron from the graphite basal plane, followed by the galleries opening up to admit ions or neutral molecules. This proposal has several merits. First, it would explain why the stoichiometry of many reactions support

---

*This value is calculated from the heat of reaction $KF + BrF_3 \longrightarrow KBrF_4$, (-4.1 kcal),[46] the lattice energy of KF (194 kcal),[21] and an estimated lattice energy of $KBrF_4$ of 138 kcal which lies midway between those of KBF_4 (152 kcal)[47] and $KAsF_6$(125 kcal).[47]

the presence of many neutral species. The reaction of ferric chloride shows a Cl:Fe ratio slightly above 3:1. The ICl reaction hints at only a small proportion of ICl_2^-.[37] $C_xMCl_{3.5}$[26,27] hints that the species present may be $Al_2Cl_7^-$ or Al_2Cl_6 plus two $AlCl_4^-$. The neutral molecules may diffuse from the gas phase into the layers at high temperatures. Upon cooling, the neutrals do not have sufficient vapor pressure to come out, or they polymerize with the ions to form larger species ($Fe_2Cl_7^-$ for instance.) Second, this proposal is consistent with other observations that a trace of sufficiently strong oxidant initiates a complete intercalation. For instance, Ubbelohde noted that in dilute HNO_3, the electrochemical synthesis began only after reaching a certain threshold voltage.[48] The reaction then continued without any applied voltage. H_2SO_4 does not intercalate unless initiated with a known oxidant or via electrochemical oxidation. These E_r values for the halides can be used to support the kinetic barrier argument.

The thermodynamic argument is not without support. In order to complete this argument, an estimation of the lattice energy of a graphite intercalation compound must be made, as well as the subsidiary terms in the Born-Haber cycle. Following Salzano and Aronson,[49] a crude lattice energy calculation using image force theory for point charges has been done for MF_6^- and MCl_4^-. The assumption here is that the principle attractive force of the ion with the graphite sheet is the same force which attracts a point charge toward a "neutral" metallic sheet. Table 8-7 shows the calculation for the hexafluorides for various stages $C_{12n}^+MF_6^-$. A C_{72} unit was chosen arbitrarily so that sixth, third, second and

first stage C_{12n} units as well as a C_8 unit can be calculated. The sixth stage was used to estimate the limiting bonding in the dilute limit where intercalation must begin. Using Salzano's estimated values for the work function (106 kcal), changes in the work function upon oxidation (23.06 x $\sqrt{4.4x}$ x/72 kcal), the Van der Waals energy to separate a C_{12} layer (18 kcal), and the lattice energy terms for attractive and repulsive interactions, one can estimate the minimum E_r necessary to have $\Delta H = 0$. For the MF_6^- case the limiting E_r falls ~90 kcal. For the MCl_4^- case, where a larger c-spacing is required, the limiting E_r is ~100 kcal.

These values for a minimum heat of oxidation assuming only ions are packed within the sheet appear reasonable. These values are sufficiently close to the phenomenological thresholds so as to appear plausible. Packing of neutrals would lower the repulsive terms between ions in the same sheet, and would slightly lower the minimum E_r. The difference between this limiting value and the phenomenological limiting E_r may well be taken up in an entropy term. If there is a thermodynamic limitation, then ΔG and not ΔH is the significant term. An entropy term ΔS has not been considered in calculating the gas phase oxidation strengths, nor the ΔS for the formation of the solid. The sum of these two entropy terms must be unfavorable, since a gas phase species is being placed within a lattice. E_r would have to be larger than the minimum E_r required by the Born-Haber calculation. If the $T\Delta S$ term were approximately 20 kcal, then the limiting E_r would be ~110 kcal for the MF_6^- and 120 kcal for MCl_4^-. The effect of an entropy term may explain the reaction of

Cl_2 with graphite. The compound is only stable below -20C, and no reaction is seen at room temperature. The $T\Delta S$ term may be small enough at -20C to form a stable compound. While Salzano's calculation of the various energy terms are only approximate, they give support to the thermodynamic explanation of a limiting E_r.

In the course of this work on the halides, two apparent contradictions to the oxidation strength model appeared. While the stronger oxidant of the family does fit the pattern, the weaker member fails to fit the criteria. In comparing SiF_4 with GeF_4, the fluoride ion affinity of SiF_4 appears to be too large. Simple salts SiF_5^- are unknown, due to the large lattice energy gain to form $SiF_6^=$ salts. The SiF_4 plus F_2 value in Table 8-8 is based on Beauchamp's ICR results,[50] which imply SiF_4 is slightly weaker than BF_3 as a fluoride ion acceptor. The large value of E_r is in contradiction with McCarron's observation that SiF_4 plus F_2 does not react with graphite.[51] Rudorff observed a reaction of HF plus F_2 in a glass vessel to make a graphite compound with a lattice spacing of 8.06 Å.[52] This thickness appears to be that of a hexafluoride ($SiF_6^=$) or SiF_5^-. The SiF_4 precursor may have been made by HF attack on the glass. Since the 8 Å spacing appears to be too large for a bifluoride ion itself (unless it is oriented lengthwise along c), the only other possible species would be an $H_4F_5^-$ tetrahedral ion. This ion is too large to create this lattice expansion without distorting itself.[53] The principle point is that there is some data which can support the reaction of SiF_4 plus F_2 with graphite.

McCarron's observation is difficult to reconcile with the ICR prediction. McCarron observed that the WF_6 plus F_2 reaction was very slow. One can propose that stable tetrahedral (SiF_4) and octahedral (WF_6) molecules may have an activation barrier to reorganization of their fluorines in order to accept another fluoride. This barrier may have slowed the reactions of WF_6 and SiF_4 with fluorine. In an HF solution, this reorganization may be more facile for SiF_4 and Rudorff's observed reaction could occur. The other metal hexafluorides did not have to reorganize their fluorines, and thereby reacted quickly. GeF_4 plus F_2 reacts quickly because its oxidation strength is sufficiently stronger to drive the reaction, and may have a lower barrier to reorganization. While the failure of SiF_4 with F_2 to react with graphite appears anomalous, further work must be done to verify this lack of reactivity under varying conditions.

The second anomaly occurs in a comparison of PCl_5 and $SbCl_5$ in Table 8-8. $SbCl_5$ reacts spontaneously with graphite, as would be expected from its sizable E_r.[56] The comparable E_r values for PCl_5 appear to cause difficulty, because PCl_5 plus Cl_2 might be expected to react. This range of E_r values comes from several related reactions. The stability of $KPCl_6$, made from the reaction of $K^+ICl_2^-$ and $PCl_4^+ICl_2^-$, requires that the E_r of PCl_5 plus Cl_2 be greater than 110 kcal.[57] Since KCl plus PCl_5 did not form this solid at high temperatures, one may assume that the entropy term is preventing the reaction. This entropy limit would place an upper limit of E_r approximately 20 kcal above at 130 kcal. When NOCl reacts with PCl_5, $NCl_{3(l)}$ and $OPCl_{3(l)}$ are formed rather than $NO^+PCl_6^-$.

If this alternative reaction is the thermodynamically stable reaction, then $NO^+PCl_6^-$ is unstable relative to these products.[19] This places an upper limit on the E_r of 120 kcal. These calculations appear to be self consistent, and place the heat of reaction $PCl_5 + Cl_2$ between 110 and 120 kcal. This value falls above the threshold value for the hexafluorides, and yet several workers have failed to obtain any reaction with graphite.

The most plausible solution to this anomaly is that this oxidation strength is too close to the threshold. In the lattice calculation of MCl_4^-, which would have almost the same thickness as MCl_6^-, the minimum required oxidation strength was about 10 kcal above that of the MF_6^- ions. An MF_6^- barrier of 110 kcal would become a barrier of 120 kcal for the MCl_4^- and MCl_6^- ions. All other chloride reactions found fall above a 120 kcal limit. Because this reaction of PCl_5 plus Cl_2 involves two gaseous species, the change in entropy upon intercalation would be unfavorable. Any consideration of entropy or changing thresholds implies the threshold is a thermodynamic limit. The failure of PCl_5 plus Cl_2 to react with graphite gives support to the contention that this threshold is of thermodynamic origin.

In summary, an impressive correlation occurs between the reactions of graphite with various halides and the gas phase oxidation strengths of these halides. The proposed requirement of an oxidation reaction for intercalation is given further support. Whether this oxidation requirement reflects a kinetic or thermodynamic threshold is unclear, although all the evidence can be interpreted on the thermodynamic model. However,

the gas phase oxidation strengths do provide a phenomenological criteria for the synthesis of further compounds. Table 8-9 gives a list of proposed reactions and their expected reactivity. Several predictions have been confirmed since this list was composed. ClF does react with BF_3 and PF_5 to place BF_4^- and PF_6^- ions into graphite.[60] The product "C_xVF_5" has been mentioned,[61] although no mention of its synthesis has been reported to our knowledge. Cyanogen does not react with graphite.[66] The phenomenological utility of this gas phase oxidation strength model to predict chemical reactivity gives the synthetic chemist a new tool to guide synthesis of new compounds.

References for Chapter 8

1. B. K. Annis and S. Datz, J. Chem. Phys., 66(10) (1977) 4468.
2. A. A. Opalovskii, Z. M. Kuznetsova, Y. N. Chigagov, A. S. Nazarov, and A. A. Uminskii, Russ. J. Inorg. Chem. 19(8) (1974) 1134.
3. P. M. George and J. L. Beauchamp, Chem. Phys., 36 (1979) 345.
4. N. Bartlett, E. M. McCarron, B. W. McQuillan, and T. E. Thompson, Synthetic Metals, 1 (1979/80)221.
5. N. Bartlett, R. N. Biagioni, B. W. McQuillan, A. S. Robertson, and A. C. Thompson, J. C. S. Chem. Comm., (1978) 200.
6. J. Binenboym, H. Selig, and S. Sarig, J. Inorg. Nucl. Chem., 38 (1976) 2313.
7. J. L. Beauchamp, J. Chem. Phys., 64(3) (1976) 929.
8. R. N. Compton, J. Chem. Phys., 66(10) (1977) 4478.
9. P. Plurieu, J. Chatelet, M. Luce, and P. Rigny, 7th International Symposium on Fluorine Chemistry, Santa Cruz, California, July 1973, Abstract.
10. P. Barberi and N. Bartlett, to be published.
11. N. Bartlett, Angew. Chem. Int. Ed., 7(6) (1968) 433.
12. A. P. Altshuller, JACS, 77 (1955) 6187.
13. J. L. Bills and F. A. Cotton, J. Phys. Chem., 64 (1960) 1477.
14. A. D. Cohen, French Patent 2.291.151 (1975).
15. D. D. Gibler, Ph.D. thesis from the University of California, Berkeley, (1973).
16. Unpublished results of E. M. McCarron and N. Bartlett.
17. a) P. A. G. O'Hare, quoted by L. Stein, Science, 168 (1970) 362.

17. b) P. A. G. O'Hare and W. N. Hubbard, J. Phys. Chem., 70 (1966) 3353.

18. E. Rudzitis, E. H. Van Deventer and W. N. Hubbard, J. Chem. Thermodynamics, 2 (1970) 221.

19. [NBS Technical Note 270-3 (1969.]

20. A. A. Woolf, J. Fluorine Chem., 15(6) (1980), 533.

21. P. A. G. O'Hare and W. N. Hubbard, Trans. Faraday Soc., 62 (1966) 2709.

22. a) C. M. Cook, and W. E. Dunn, J. Phys. Chem., 65 (1961) 1505.

22. b) D. Cubicciotti, J. Chem. Phys. 34 (1961) 2189.

22. c) H. D. B. Jenkins and R. P. Thakur, J. Chem. Ed., 56 (1979) 576.

23. H. D. B. Jenkins, R. F. Pratt, G. Mairesse, P. Barbier, and J. P. Wignacourt, Inorg. Chem. 19(10) (1979) 2796. The gas phase chloride ion affinity should be 357 kJ, not 257 kJ.

24. H. D. B. Jenkins, Inorg. Chem. 15(1) (1976) 241.

25. R. C. Gearhart, J. D. Beck, and R. H. Wood, Inorg. Chem., 14(10) (1975) 2413.

26. B. Bach and A. R. Ubbelohde, Proc. Royal Soc. London, Ser A 325 (1971) 437.

27. B. Bach and A. R. Ubbelohde, J. Chem. Soc. A (1971) 3669.

28. T. Sasa, Y. Takahashi, and T. Mukaido, Bull. Chem. Soc. Japan, 45 (1972) 2250.

29. C. Balestreri, R. Vangelisti, J. Melin and A. Herold, Comptes Rendues Acad. Sci., 279 (1974) 279.

30. W. A. Chupka, J. Berkowitz, and D. Gutman, J. Chem. Phys., 55(6), (1971) 2724.

31. L. R. Morss, J. Chem. Thermodynamics, 7 (1975) 709.

32. Quoted by T. C. Waddington, in Adv. in Inorg. Chem. and Radiochem., Academic Press, NY 1(1959), 157.

33. A. Finch, P. N. Gates, and S. J. Peake, Thermochemica Acta 19 (1977) 213.

34. L. E. Topol, Inorg. Chem., 10(4) (1971) 736.

35. A. Finch, P. N. Gates, and S. J. Peake, J. C. S. Dalton (1977) 397.

36. G. Furdin, M. Lelaurain, E. McRae, J. F. Marcehe, and A. Herold, Carbon, 17, (1979) 329.

37. B. Bach and A. Herold, C. R. Acad. Sci., 257 (1963) 1706.

38. G. Colin and A. Herold, Bull. Soc. Chim. Fr., (1972) 3345.

39. S. A. Harrell and D. H. McDaniel, JACS, 86 (20) (1964) 4497.

40. H, D. B. Jenkins and K. F. Pratt, JCS Faraday Trans. II, 73 (6) (1977) 812.

41. D. H. McDaniel and R. E. Valee, Inorg. Chem., 2 (5) (1963) 996.

42. W. Rudorff and G. Rudorff, Chem. Ber. 80 (1947) 413; W. Rudorff, Z. Anorg. J. Allgem. Chem. 254 (1947) 319.

43. H. Morawitz, P. Bagus, T. Clarke, W. Gill, P. Grant, G. B. Street, and D. Sayers, Synthetic Metals 1, 267, 1979-80.

44. S. M. Heald and E. A. Stern, Phys. Rev. B., 17(10), 4069, 1978; S. M. Heald and E. A. Stern, Synthetic Metals, 1, 249, 1979-80; S. M. Heald and E. A. Stern, 2nd International Conference on Intercalation Compounds of Graphite, Provincetown, MA, May 1980 (to be published by Synthetic Metals).

45. L. Stein, "Physical and Chemical Properties of Halogen Fluorides" in Halogen Chemistry, ed. V. Gutmann, Vol. 1, Academic Press, London, 161, 1967.

46. JANAF Thermochemical Tables, Dow, Midland, MI, 1960-63.

47. Ref. [15], p. 42; Radius of K^+ = 1.33 Å.

48. A. R. Ubbelohde, Proc. Roy. Soc. A. 309, 297, 1969.

49. F. J. Salzano and S. Aronson, J. Chem. Phys. 44(11), 4320, 1966.

50. M. K. Murphy and J. L. Beauchamp, JACS 99(15), 4992, 1977.

51. E. M. McCarron, Ph.D. thesis, University of California, Berkeley, LBL report 11272, 1980, p. 49.

52. W. Rudorff, Z. Anorg. Chemie, 254, 22, 1947.

53. B. A. Coyle, L. W. Schroeder, and J. A. Ibers, J. Solid State Chem., 1, 386, 1970.

54. J. C. Haartz and D. H. McDaniel, JACS, 95(26), 8562, 1973.

55. N. Bartlett and T. Mallouk, unpublished work.

56. J. G. Ballard and T. Birchall, JCS Dalton, 18, 1859, 1976.

57. V. Gutmann, Monatschrefte, 83, 39, 1952.

58. L. Brewer, L. A. Bromley, P. W. Gites, and N. L. Lofgren, Thermodynamic Properties of the Halides, 1946; JANAF Tables (1968) give 27 kcal.

59. D. D. Wagman, W. H. Evans, I. Halow, V. B. Parker and R. H. Schumm, Selected Values of Chemical Thermodynamic Properties, NBS Tech. Note 270-1, 1965.

60. L. Ebert, 2nd International Conference on Intercalative Compounds of Graphite, Provincetown, MA, May 1980. Based on $\Delta H_f(CIF)$ = -13.6 kcal from Ref. [46].

61. L. B. Ebert and H. Selig, Mat. Sci. Eng., 31, 177, 1977.

62. Based on $NOF + VF_5 \quad NO^+VF_6^-$ ΔH of -18 kcal, H. C. Clark and H. J. Emeleus, J. Chem. Soc. 190, 1958, using lattice energy estimate of 140-150 kcal for NO^+ VF_6.

63. This estimate is based on $\Delta H < 0$ $2VF_4 \rightarrow VF_5 + VF_3$ at 100°C. $\Delta H_f(VF_5)$ = -343 kcal from G. K. Johnson and W. N. Hubbard, J. Chem. Thermodynamics 6, 59, 1974. $\Delta H_f(VF_4)$ = -321 kcal from R. G. Carell and H. C. Clark, Trans. Faraday Soc. 59, 2706, 1963.

64. R. N. Compton, P. W. Reinhardt, and C. D. Cooper, J. Chem. Phys. 68(5), 2023, 1978.

65. J. Berkowitz, W. A. Chupka, and T. A. Walter, J. Chem. Phys. 50, 1497, 1969 and references quoted in J. A. Kerr, Chem. Rev. 66, 465, 1966.

66. Personal communication from R. Setton.

Table 8-1. Electron Affinities[a] (Kcal mole^{-1})

$MF_6 + e^-$	$MF_6^-(g)$ (N.R. means no reaction with graphite)			
MoF_6				
117[b]				
C_8MoF_6[c]				
WF_6	ReF_6	OsF_6	IrF_6	PtF_6
81[d]	107[a]	135[a]	161[a]	188[a]
N.R.[e]	N.R.[e]	$C_8^+OsF_6^-$[f]	$C_8IfF_6^-$[g]	$C_{12}^+PtF_6^=$[h]
UF_6				
113[a]				
C_9UF_6[i]				

(a) The oxidative chemistry of the third transition series hexafluorides had established a smooth increase in oxidizing capability from W to Pt and Bartlett [11] had estimated that the electron affinity increases by ~1 eV for each unit increase in atomic number across the series. There has, however, been much uncertainty about the absolute values of the electron affinities $A(MF_6)$, some of this uncertainty springing from uncertainties in evaluations of lattice energies for salts, such $NO^+MF_6^-$ and $O_2^+PtF_6^-$. Here, we have, for the first time, tied $A(MF_6)$ to $A(UF_6)$. Two independent measurements for $A(UF_6)$ give 113 [7] and 117 [8] kcal mole^{-1}. The former value derives from ion-cyclotron resonance studies, from which studies a rather precise value is also available for $A(WF_6)$, hence we take it as our fixed point for $A(UF_6)$.

Table 8-1 (continued)

Calorimetric studies [9] give $\Delta H^\circ(NO(g) + UF_{6(g)} \rightarrow NO^+UF^-_{6(c)}) = -52$ kcal mole^{-1}. Since the first ionization potential, I(NO), is 213 cal mole^{-1}, and $A(UF_6) =$ 113 kcal mole^{-1}, it follows that the lattice energy $U(NO^+UF^-_{6(c)}) = -152$ kcal mole^{-1}. A similar calorimetric study [10] gas given $\Delta H^\circ(O_{2(g)} + PtF_{6(g)} \rightarrow O_2^+PtF^-_{6(g)}) = -60$ kcal mole^{-1}. Therefore, because $U(O_2^+PtF^-_{6(g)})$ must be slightly more exothermic than $U(NO^+UF^-_{6(c)})$, since PtF^-_6 is smaller than UF^-_6, the electron affinity of PtF_6 must be slightly greater than $I(O_2) + U(NO^+UF^-_{6(c)}) - \Delta H^\circ(O_{2(g)} + PtF_{6(g)} \rightarrow O_2^+PtF^-_{6(c)}) = (278 - 152 + 60)$ kcal mole^{-1}. Accordingly we set the electron affinity of PtF_6 at 188 kcal mole^{-1}. Since $A(WF_6)$, derived from ion-cyclotron resonance studies [3], is in harmony with less precise evaluations [11] from other experiments, and is also compatible with the known oxidative chemistry of WF_6, we accept this value as our other fixed point for the third transition series. The estimates of $A(MF_6)$ for PtF_6, OsF_6 and IrF_6 have been derived, assuming a smooth increase with atomic number of M, between $A(WF_6) = 81$ kcal and $A(PtF_6) = 188$ kcal mole^{-1}. Although the lattice energy $U(O_2^+PtF_{6(c)}) = -154$ kcal^{-1} is higher than that derived from a Kapustinskii lattice energy, the $A(MF_6)$ based on the higher lattice energy are in excellent agreement with the known oxidative chemistry. (b) see 1; (c) see 2; (d) see 3; (e) see 4; (f) see 5; (g) see 4; (h) see 4; (i) see 6.

Table 8-2. Gas Phase Electron Affinity (E_r) - Limiting Composition of Graphite Salt

$E_r(BF_3 + 1/2\ F_2 + e^- \rightarrow BF_4)$[a]	C_nBF_4[b]
155 (kcal/mole e^-)	
$E_r(MF_{5(g)} + 1/2\ F_2 + e^- \rightarrow MF_6$	
M	
P 158[c]	$C_8^+PF_6$[d]
As 170[c]	$C_8^+AsF_6$[e]
Sb 193[f]	$C_n^+SbF_6^-$[d] (~<12)
$E_r(WF_6 + 1/2\ F_2 + e^- \rightarrow WF_7)$	$C_n^+WF_7$[g]
141	

(a) In all calculations, $\Delta H_f(F^-_{(g)}) = -64$ kcal. There are two reports of the value of $\Delta H(BF_{3(g)} + F^-_{(g)} \rightarrow BF^-_{4(g)})$ [12] gives a value of -71 kcal, while [13] gives -91 kcal. We prefer the -91 kcal value because it is compatible with the marginal stability of $O_2^+BF^-_{4(c)}$. All other values of fluoride ion affinities are based on the -91 kcal value for BF^-_4. These fluoride ion affinities also depend upon the lattice energy evaluations which are no more precise than ±10 kcal $mole^{-1}$.

(b) See 14; (c) See 15; (d) See 16 (e) See 5.

Table 8-2 (continued)

(f) See 15. The value given is for SbF_5 liquid.

(g) See 3. Their reported $\Delta H_f(WF_{7(g)}^-)$ has been lowered to -552 ±10 kcal, based on our use of -91 kcal rather than -71 kcal for the fluoride ion affinity of $BF_{3(g)}$.

Table 8-3. Electron affinity for the reaction $3MF_5 + 2e^- \rightarrow 2MF_6^- + MF_3$[a]

		P	As	Sb
1	$-2E_r(2MF_5 + F_2 + 2e^- \rightarrow 2MF_{6(g)}^-)$[b]	≤ -316	≤ -340	≤ -386
2	ΔH $MF_5 \longleftrightarrow MF_3 + F_2$	152[c]	98[d]	90[e]
	$3MF_5 + 2e^- \rightarrow 2MF_6^- + MF_3$	≤ -164	≤ -242	≤ -296
	E_r	≥ 82	≥ 121[f]	≥ 148
		N.R.	"C_8AsF_5"	"C_nSbF_5"

(N.R. means NO REACTION with graphite)

(a) The values for "P" and "As" species are for the gas phase species. For "Sb", reaction (1) is for polymeric liquid SbF_5, and reaction (2) is for polymeric liquid SbF_5 forming solid SbF_3. Since the heat of vaporization and the heat to form the gaseous monomer SbF_5 are both endothermic, the Sb value for the monomer must be more exothermic than this value.

(b) See Table 8-2

(c) See 18

(d) See 20

(e) See 17a

(f) For a possible alternative oxidation ($6AsF_{5(g)} + 5e^- \rightarrow 5AsF_{6(g)}^- + As_{(c)}$), E_r = 108 kcal/mole e^-.

Table 8-4. Some other possible half reactions for fluorides which, alone, do not intercalate graphite

	E_r (kcal/mole e^-)
$2WF_{6(g)} + e^- \rightarrow WF_7^-(g) + WF_{5(c)}$ [a]	76
$7WF_{6(g)} + 6e^- \rightarrow 6WF_7^-(g) + WF_{(c)}$ [a]	72
$6PF_{5(g)} + 5e^- \rightarrow 5PF_6^-(g) + P_{(c)}$ [b]	79
$4BF_{3(g)} + 3e^- \rightarrow 3BF_4^-(g) + B_{(c)}$ [c]	64

(a) See 17b $\Delta H_f(WF_{5(c)}) = -346$ kcal

See $\Delta H_f(WF_6) = -411.5$ kcal

(b) See 18

(c) See 19 $\Delta H_f(BF_3) = -272$ kcal

Table 8-5. Gas phase heats of reaction of assorted metal halides[a]

	E_r
(1) $FeCl_{3(g)} + 1/2\ Cl_2 + e^- \rightarrow FeCl^-_{4(g)}$	+161[b]
$FeCl_{3(g)} \rightarrow FeCl_{2(c)} + 1/2\ Cl_2$	- 22
(2) $2FeCl_{3(g)} + e^- \rightarrow FeCl_{2(c)} + FeCl^-_{4(g)}$	+139

All compounds below require Cl_2 to react with graphite

	E_r		
	M = Al	Ga	In
(3) $MCl_{3(g)} + 1/2\ Cl_2 + e^- \rightarrow MCl^-_{4(g)}$	145[c]	143[d]	156[e]
	$C_9AlCl_{3.5}$[f]	$C_9GaCl_{3.5}$[g]	$C_{18}InCl_{3.5}$[g]
$M_2Cl_{6(g)} + Cl_2 + 2e^- \rightarrow 2MCl^-_{4(g)}$	128	133	

Extreme Alternative Reactions in the Absence of Cl_2

$4MCl_{3(g)} + 3e^- \rightarrow 3MCl^-_{4(g)} + M_{(c)}$	97	107
$2M_2Cl_{6(g)} + 3e^- \rightarrow 3MCl_{4(g)} + M_{(c)}$	77	95

All Compounds Below Require Br_2 to React with Graphite

	E_r	
	Al	Ga
$MBr_{3(g)} + 1/2\ Br_2 + e^- \rightarrow MBr_{4(g)}$	133[e]	128[e]
	$C_9AlBr_3 \cdot Br_2$[h]	$C_{13}GaBr_{3.5} \cdot Br_2$[i]

Extreme Alternative Reactions in the Absence of Br_2

(4) $MBr_{3(g)} + 3e^- \rightarrow 3MBr^-_{4(g)} + M_{(c)}$	99	105

(Continued)

Footnotes to Table 8-5

(a) All ΔH_f of metal halide species are taken from [19].

(b) Calculated from the ΔH of the reaction of KCl or $NaCl_{(c)}$ with $FeCl_{3(c)}$ to make $K^+FeCl_4^-(c)$ or $Na^+FeCl_4^-(c)$ in [22a], the lattice energy of NaCl in [22b], and a Kapustinskii radius of 3.58 Å in [22c]. This radius appears a bit larger than expected from the tetrachlorides listed. A lowering by 0.4Å increases the lattice energy and decreases the chloride ion affinity by 13 kcal.

(c) See 23; (d) See 24; (e) See 25; (f) See 26; (g) See 27; (h) See 28; (i) See 29.

Table 8-6.

	Energy (kcal)			
X =	F	Cl	Br	I
$1/2X_{2(g)} + e^- \rightarrow X^-_{(g)}$ (a)	64	58	63	61
$X^-_{2(g)}$ (b)	71	55	58	60
X_3^-	Unknown	(73)[c,d]	(73–145)[c,d,e]	80[c,f]
	N.R. at room temperature	Reaction only below room temperature[g]	C_8Br	N.R.
$2IX \rightarrow IX_2^- + 1/2I_{2(g)}$		135[h]	140[i]	
		"$C_8I_{0.9}Cl_{1.1}$" [j]	$C_8I_{0.45}Br_{0.55}$ [k]	
$1/2X_2 + HX \rightarrow HX_2^-$	101,[d] 106[l]	72[m]	76[m]	73[m]
	rxn[n]	N.R.	ambiguous since Br_2 reacts with graphite	N.R.

(continued)

Footnotes for Table 8-6.

(a) Ref. [19] (b) Ref. [30].

(c) The values for X_3^- and IX_2^- carry considerable potential for error due to the uncertainty in determining a suitable thermochemical radius for the Kapustinskii lattice energy. The use of the Yatsimirskii-Kapustinskii procedure to determine an empirical X_3^- radius can be very sensitive to small differences (or errors) in large energy terms. For non-spherical ions, the assumptions of the Kapustinskii formula become more uncertain.

(d) ΔH for $Et_4N^+Cl^-_{3(c)} \rightarrow Et_4N^+Cl^-_{(c)} + Cl_{2(g)}$ = 17 kcal [31]. Assuming the lattice energies of the salts are equal, one has $Cl^-_{3(g)} \rightarrow Cl^-_{(g)} + Cl_{2(g)}$ = 17 kcal from which the value in this table is derived. This value should be considered a lower limit, due to the lattice energy approximation.

(e) $\Delta H_f(CsBr_{3(c)}$ = 103.8 kcal [31], and $\Delta H_f(NH_4^+Br^-_{3(c)})$ = - 67.5 kcal [19]. A Yatsimirskii calculation using MBr lattice energies of Cubicciotti [22b] or Waddington [32] give $r(Br_3^-)$ = ~ 2.5 Å or > 6 Å. A radius of 2.5 Å, which is also consistent for a sphere of the same value as $3Br^-$, gives a lattice energy of 135 kcal for $NH_4^+Br_3^-$, and 3/2 $Br_2 + e^- \; Br_3^-$ = - 84 kcal. Using the radius 4.04 Å of IBr_2^- [33] for Br_3^- gives 3/2 $Br_2 + e^- \rightarrow Br_3^-$ + 129 kcal . The 6.0 Å radius gives a lattice energy of 74 kcal, and 3/2 $Br_2 + e^- \rightarrow Br_3^-$ = 145 kcal. Assuming the lattice energies of NH_4Br_3 and NH_4Br are equal, one has a minimum value of -73 kcal for 3/2 $Br_{(g)} + e \rightarrow Br^-_{3(g)}$.

(continued)

Footnotes for Table 8.6.

(f) Topol's value [34] appears reasonable with a radius of 2.45 Å. However, Finch's [35] value of $\Delta H_f(I^-_{3(g)}) = -117.5$ kcal, which is dependent on the Yatsmirskii equations' radius of 6.01 Å, would give $3/2\ I_{2(g)} + e^- \rightarrow I^-_3$ $\Delta H = -140$ kcal.

(g) See Ref. [36] for the latest work on this system.

(h) $\Delta H_f(ICl^-_{2(g)}) = -145$ kcal from [35] was devised from a Yatsmirskii radius of 4.66 Å, which appears very large. A smaller radius would give a smaller ΔH for $2ICl_{(g)} + e^- \rightarrow ICl^-_2 + 1/2\ I_{2(g)}$.

(i) The 140 kcal value is from [33], using a radius of 4.04 Å and a $\Delta H_f(IBr^-_2) = -120$ kcal. Again the authors radius appears larger, and perhaps inconsistent with their ICl^-_2 radius of 4.66 Å in [35].

(j) Ref. [37] The composition given here appears implausible as there is not sufficient room in the "C_4" graphite gallery to accommodate this amount of halogen.

(k) Ref. [38].

(l) Ref. [39]. Uses 37 kcal for $F^- + HF \rightarrow HF^-_2$. Theoretical calculations [40] give the fluoride ion affinity as -42 kcal.

(m) Ref. [41] (n)

Ref. [42].

Table 8-7. Salzano's and Aronson's Thermodynamics Model

$$H_f = \text{W.F.} + (\Delta\text{W.F.}) + \text{V.d.W.} + \Delta H_{ox} + (U_1 + U_2) \quad (1)$$

$$= (106.5)X + 5.7\sqrt{X} + (18)X + (\Delta H_{ox})X + (3.0)X + -\frac{112.95}{r}\left(1 - \frac{0.3}{r}\right)X \quad (2)$$

$$= (85.57)X + 5.7\sqrt{X} + (\Delta H_{ox})\,X \quad (3)$$

Where (3) is calculated for a radius r of 2.35 Å for a MF_6^- ion, and X is from the composition $C_{72}^{+x}xA^-$. The C_{72} is chosen because the MF_6^- intercalates have been shown to stage as $C_{12n}MF_6$, and C_{72} allows for a calculation of 1^{st}, 2^{nd}, 3^{rd}, and 6^{th} stages with X = 6,3,2, and 1 respectively.

With X = 9, and by adding 3.7 kcal to the 85.57, one will have the equation for the 1^{st} stage $C_8^+MF_6^-$ composition.

	A^-	A^- A^-	A^- A^- A^-	A^- A^- A^- A^- A^- A^-	$A^-\frac{1}{2}A^-$ $A^-\frac{1}{2}A^-$ $A^-\frac{1}{2}A^-$ $A^-\frac{1}{2}A^-$ $A^-\frac{1}{2}A^-$ $A^-\frac{1}{2}A^-$
X = 0	1	2	3	6	9
ΔH_f =	$92.3 + \Delta H_{ox}$	$179.2 + 2\Delta H_{ox}$	$266.6 + 3\Delta H_{ox}$	$527.4 + 6\Delta H_{ox}$	$829.5 + 9\Delta H_{ox}$
Minimum $-\Delta H_{ox}/e^-$ Required (kcal)	92.3	89.6	88.9	87.9	92.2

Table 8-8. Heats of Reaction for Anomolous Reactions

	M =	Si	Ge
$MF_4 + 1/2\ F_2 + e^- \rightarrow MF_5^-$		125-152 [a]	165 [c]
		N.R.[b]	$C_x^+GeF_5^-$ [b]
	M =	P	Sb
$MCl_5 + 1/2\ Cl_2 + e^- \rightarrow MCl_6^-$		110-120 [d]	153 [e]
			$C_n^+SbCl_6^-$ [f]
$3MCl_5 + 2e^- \rightarrow 2MCl_6^- + MCl_3$		99-109 [g]	146 [g]
		N.R.	"C_nSbCl_5" [h]

(a) 152 kcal is an upper limit based on Beauchamp's[50] finding that SiF_4 is almost as strong a fluoride acceptor as BF_3. The 125 kcal limit is an average value from McDaniel et al[54] which placed the fluoride ion affinity between -37 kcal (for HCl) and BF_3 (which we place at -91 kcal rather than his -71 kcal).

(b) Results of E. McCarron, PhD thesis, UC Berkeley, 1980.

(c) Based on the heat of dissociation of $ClO_2^+GeF_5^-$ of 29 kcal, compared to that of $ClO_2^+BF_4^-$ of -24 kcal. Work of T. Mallouk and N. Bartlett.[55]

(d) Limits based on several reactions found in text. Calculations based on the results of V. Gutmann.[57]

(continued)

Footnotes for Table 8-8.

(e) The value 153 kcal is a lower limit to E_r based on the stability of the salt $KSbCl_6$ made from KCl and $SbCl_5$.

(f) This reaction is difficult to document because $SbCl_5$ alone reacts with graphite and the species within the graphite have not been characterized.

(g) Based on the heats of $MCl_{5(g)} \rightarrow MCl_3 + Cl_2$ of 22 kcal for $PCl_{3(g)}$ [58] and 14 kcal for $SbCl_{3(s)}$.[59]

(h) See Ref. [56].

Table 8-9. Predictions of Reactivity with Graphite

Reaction	E_r (kcal)	
$VF_5 + 1/2\ F_2 + e \rightarrow VF_6^-$	120-130[62]	Should react
$ClF + SiF_4 + e^- \rightarrow SiF_5^- + 1/2\ Cl_2$	111-138	Should react
$ClF + PF_5 + e^- \rightarrow PF_6^- + 1/2\ Cl_2$	142[a,60]	Should react
$ClF + BF_3 + e^- \rightarrow Bf_4^- + 1/2\ Cl_2$	138[a,60]	Should react
$ClF + WF_6 + e^- \rightarrow WF_7^- + 1/2\ Cl_2$	122	Should react
$3PF_5 + 1/2\ O_2 + 2e \rightarrow POF_3 + 2PF_6^-$	112	Reaction likely
$HCl + 1/2\ F_2 + e^- \rightarrow HClF^-$	110[54]	Reaction likely
$3VF_5 + 2e^- \rightarrow 2VF_6^- + VF_{3(s)}$	98-108[b,63]	Reaction likely
$HCl + ClF + e^- \rightarrow HClF^- + 1/2\ Cl_2$	97[54]	Undecided
$HF + ClF + e^- \rightarrow HF_2^- + 1/2\ Cl_2$	84[54]	Reaction unlikely
$TeF_6 + e^- \rightarrow TeF_6^-$	74[c]	Reaction unlikely
$SeF_6 + e^- \rightarrow SeF_6^-$	69[c]	Reaction unlikely
$SF_6 + e^- \rightarrow SF_6^-$	16-33	Reaction unlikely
$(CN)_2 + 2e^- \rightarrow 2CN^-$	30[d]	No reaction[66]

(a) Reaction reported by Ebert, Second International Conference on Intercalation Compounds of Graphite, Provincetown, MA, May 1980.

(b) Mentioned by Ebert et al, Ref. [61].

(c) Values given in Refs. [1] and [64].

(d) Value in Ref. [65], after removing the C-C bond strength. R. Setton informed me that no reaction occurred between cyanogen and graphite.

Figure 8-1

Generalized Thermodynamic Cycle for Graphite Intercalation

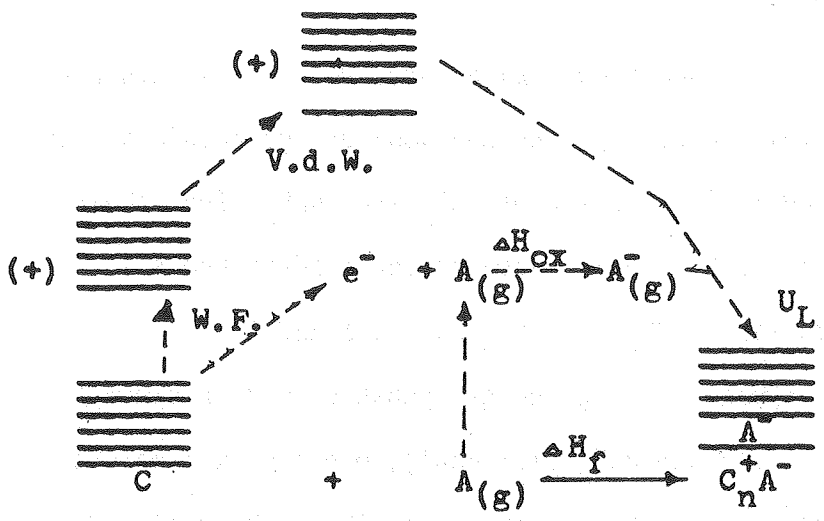

W.F. is the work function of graphite, plus any changes in the work function as oxidation proceeds.

V.d.W. is the Van der Waals energy needed to separate a sheet of carbons away from 3.35 A separation.

U_l is the "lattice energy" for placing an A^- species within the positively charged graphite layers.

CHAPTER 9

XeF_2:$XeF_5^+AsF_6^-$ Adducts

In order to pursue electrochemical oxidations, robust solvents were needed. To exemplify this necessity, one can look at the required potentials for the electrochemical oxidation of PtF_6 and "AuF_6" from their MF_6^- ions. In anhydrous HF, O'Donnell measured the electrochemical potential for the oxidation of WF_6^- and MoF_6^- as -0.11 and 0.92 volts vs a Cu/CuF_2 electrode.[1] Using the gas phase oxidation strengths (Chapter 8) of WF_6 (81 kcal) and MoF_6 (117 kcal), one can extrapolate what potential is necessary for the oxidation of PtF_6^- (188 kcal) and AuF_6^- (220 kcal). Assuming the solvation in HF is similar for all MF_6^-, one finds values of 2.95 volts for PtF_6^- and 3.86 volts for AuF_6^-. However, in this HF solvent, fluorine is produced at ~2.7 volts at this reference electrode.[2] A preferable solvent would be a low melting, highly oxidized salt. The work of Zemva[3] on making 1:2, 1:1, and 2:1 adducts of XeF_2:$XeF_5^+AsF_6^-$ had hinted that at "1.3:1" compositions, the system might be liquid near room temperature. A study of the $XeF_2/XeF_5^+AsF_6^-$ phase diagram was undertaken to attempt to define the system, and particularly the eutectics, more precisely.

Experimental

A FEP container was constructed in order to perform the melting point measurement. A copper-constantine thermocouple was made of 40 gauge wires, which were then sheathed within FEP spaghetti tubing. This thermocouple was heat sealed through the bottom of a 3/8" FEP tube until the seal was vacuum-tight. This arrangement placed the thermocouple 1/4" above

the bottom of the FEP tube, with a 0.010" FEP wall separating the melt from the thermocouple. A stainless steel Swagelock union and cap were then attached to the top of the 2-3" long FEP tube. This container could be filled quickly with about 1/2-1 gram amounts of XeF_2 and $XeF_5^+AsF_6^-$. The tube was then capped, and totally immersed in an oil bath to melt the two solids into a homogeneous mixture.

This experimental arrangement had several advantages over alternative designs:

(1) The thermocouple was very close to the melt while not being attacked by the melt. This design with FEP spaghetti tubing insured that the thermocouple would measure the melt temperature at each moment. With the thermocouple and potentiometer, accurate temperature measurement of $\pm 0.2^{\circ}C$ were possible.

(2) The transparent FEP tube would allow visual observation of the melt as it passed from white crystals to a transparent liquid. Raman spectra could also be taken through the FEP walls.

(3) By using a large diameter FEP tube, larger amounts of material could be weighed accurately than could be weighed into a small capillary. This larger capacity allowed for greater accuracy in the determination of the composition. With the FEP, formation of $XeOF_4$ or XeO_3 was minimal. In quartz capillaries, these oxides could form and contaminate the mixture. This larger tube would also allow one to see how viscous was the melt.

(4) The FEP tube was sufficiently short so as to be completely immersible in the heating oil. This total immersion prevented any sublimation toward a cooler end and thus eliminated changes in the melt composition.

The thermocouple was connected in opposition to an identical thermocouple maintained at ice temperature in distilled water. The difference in voltage was read on the Leeds and Northrup Model 8686 millivolt potentiometer with galvanometer. Several standards (ice, phenanthrene, and naphthalene) were measured in the tube, and gave accurate melting points within ±0.5°C of reported values when the temperature was raised through the melting point. Upon cooling, one occasionally saw evidence of supercooling with the standards and with the adducts. For this reason, the xenon salt adduct's melting points were always measured upon raising the temperature through the melting point at a rate of 1-2°C/min. The liquidus temperatures given here are for the temperature at which the last bit of solid melted. This point was sometimes difficult to determine visually, and may be in error by 0.5°C.

XeF_2 was prepared by the routine photolysis of Xe and F_2 in a pyrex bulb. $XeF_5^+AsF_6^-$ was prepared by heating a prefluorinated monel bomb with XeF_2, a 50% excess AsF_5, and a 100% excess of F_2. Several preparations were made before discovering in powder patterns that the copper gasket was attacked and CuF_2 was in the final product. By nickel plating the gasket, followed by subliming the product at 120°C in a water-cooled

monel can, pure samples of $XeF_5^+AsF_6^-$ were made. Their purity was checked by Raman spectroscopy, X-ray powder patterns, and melting point (130°C).[4]

In order to clarify descriptions throughout the following discussion, the following notation will be used. Mole ratio compositions based on the relative mole amounts of XeF_2 and $XeF_5^+AsF_5^-$ will be denoted "A:1". Well characterized or proposed units having the composition $C(XeF_2)$ plus $B(XeF_5^+AsF_6^-)$ will be denoted C:B. This distinction can be demonstrated by two examples. First, a mixture of 2 mmole XeF_2 and 1 mmole $XeF_5^+AsF_6^-$ is "2:1", and the crystal structure shows this mixture to be $2XeF_2$ molecules each bridge-bonding to an XeF_5^+ ion[3]. Thus the compound is designated 2:1. In the second case, a mixture of 1.5 mmole XeF_2 and 1 mmole XeF_5^+ AsF_6^- is "1.5:1". However, the Raman data will be interpreted in terms of three different XeF_2 molecules interacting with two XeF_5^+ units, and will be designated 3:2. In all cases, the "A:1" is always the correct proportion, while the assigned formula unit C:B may require further investigation to characterize definitively.

Melting Point and Raman Results

When this phase study was begun, the three compositions 1:2, 1:1, and 2:1 had been well characterized by Raman spectroscopy and single crystal structures.[3] During the study, three other Raman spectra were observed either in pure form or in mixtures together with previously established adducts. All six spectra are shown in Figures 9-1 and 9-2, and the peak positions and assignments are summarized in Table 9-1. In order to facilitate discussion of these three new complexes, they have been tentatively labeled 3:2, 2:1M, and 3:1. The reasons supporting this labeling will be

given throughout the discussion, although the labeling is not conclusively established as correct. The 2:1M is designated as such to distinguish it from the 2:1 already characterized. The 3:1 may be another 2:1 complex, but the 3:1 will be used to simplify the labeling of the complex.

A "0.56:1" mixture was prepared to check Wechsberg's "0.542:1" (1:2) composition,[5] for which he gave a sharp melting point of 65°C. The melting behavior of the 0.56:1 mixture was quite different. The onset of melting began at 42°C, and yet the solid was only half melted at 60°C. Some solid specks were still visible at 80°C. The Raman spectra taken after one melting showed predominently the 1:2 compound, with some $XeF_5^+AsF_6^-$. It is probable that the observed melting point behavior was due to an inhomogeneous mixing of the components. Wechsberg's 65°C will be taken for the phase diagram.

A "1.00:1" mixture was made in order to verify the 1:1 composition previously determined. Wechsberg reported a range of melting point 54-57°C, and proposed an incongruent melt.[5] The melting point observed here was sharper, at 57-58°C. Several Raman spectra taken after various melts all gave the reported 1:1 spectra. Both the 1:2 and 1:1 reported by Wechsberg are confirmed. No further work was done across this composition interval since Wechsberg noted only mixtures of these two adducts over that interval.

Until this study, no investigation had been made on the XeF_2 rich side of "2:1". Three molar ratios were studied: "2.89:1", "3.04:1", and "4.08:1". The "2.89:1" was formed from the "1.87:1" (to be discussed below) by the addition of more XeF_2. After the initial melts and cooling to 0°C, the Raman showed the new spectra of 2:1M (which will be discussed

under the "1.90:1" composition) along with excess XeF_2. Upon melting again, and quenching in liquid nitrogen, the Raman showed the previously established 2:1 and XeF_2. This behavior of the established adduct forming upon rapid liquid nitrogen quenching, while the newer adducts appearing upon milder quenching to 0°C, appears repeatedly in these new studies. This pattern is consistent with Wechsberg's and Zemva's results in finding the 2:1 after quenching in liquid nitrogen or liquid air. Complete melting (taken on the 2:1M plus XeF_2) occurred between 70 and 75°C, but the onset occurred at 39°C. The bulk had melted by 49°C. The last solid to melt was probably XeF_2. The 70°C value will be used as the liquidus point of the "2.89:1" compound, with an onset of melting at 39°C.

The "3.04:1" and "4.08:1" compositions both have identical spectra of the 3:1 species and XeF_2. Much of the "4.08:1" material melted in the 50–70°C range, but much solid (probably XeF_2) remained at 103°C. The "3.04:1" mixture changed from white to off-white at 44–45°C, indicating the beginning of melting. By 60°C, much of the material was molten. On two occasions, it appeared that the last fine threads of solid disappeared at 80°C, while on a subsequent melting one bit of solid appeared to remain above 100°C. The 80°C value will be used as a liquidus point, although it may simply be difficult to tell visually where the last bits of XeF_2 finally disappeared. From these results, it appears that there is a new 3:1 species which only appeared above the 2:1 composition. Because there was a large excess of XeF_2 and the melting point rose dramatically, it is doubtful that there are any other species beyond a "3:1" composition.

The bulk of the investigation was spent in the interval between 1:1 and 2:1. Compositions "1.2:1", "1.35:1", "1.50:1", "1.87:1", and "1.90:1" were prepared in order to uniformly span the interval. This region behaved in a very complex and bewildering manner. Upon varying the temperature or cooling rates, the same sample would yield uniquely different Raman spectra of various species. Supercooling of the melts by 10-20°C was common and prevented measuring the freezing point reliably. The possibility of nucleation and precipitation of kinetically stable species cannot be excluded. However, the total picture across this region appears more self-consistent, as seen in Table 9-2.

After some initial melts of "1.50:1", which showed 2:1 and 1:2 species in the Raman, the new phase 3:2 appeared. This 3:2 appeared upon quenching with liquid nitrogen after the 1.5:1 had been kept at 45°C where a partial melt had occurred. Following another partial melt, a slow cooling overnight to a glass, and then a quenching at 0°C, the spectrum in Figure 9-2 was taken. After going to a full melt, maintaining the glass at 40°C for two days, and then quenching with LN_2, the 2:1 and 1:1 appeared. A melting point study at this point showed a color change white to off-white at 32°C, the onset of melting at 39-40°C, and complete melting at 49°C. It is tempting to ascribe the 32°C transition to a phase change 1:1 + 2:1 to 3:2. The 3:2 appeared upon going to a partial melt at 45°C, followed by a mild quenching with ice. Upon more severe quenching in LN_2 from the glass, 1:1 and 2:1 precipitated. It may be that the milder quench keeps the temperature at which precipitation occurs above 32°C, so that the 3:2 is seen. A more severe quench causes nucleation of the 1:1 and 2:1 species

seen below 32°C. An alternative explanation of the 32°C observation is simply that the 1:1 and 2:1 are forming a glass of undetermined composition at the crystal interfaces. Further studies as a function of temperature are needed to outline the various phase regions.

The peculiar behavior of "1.5:1" was also seen in two preparations of "1.35:1". Both preparations were made in quartz NMR or ESR tubes rather than the FEP container. The first preparation showed 1:2 plus 2:1 during the early melts. It quickly became apparent that this composition supercooled to a glass at room temperature. The Raman peaks were broadened considerably. Upon quenching, the crystalline solid remained solid at room temperature. Two months later, the solid showed the 1:1 plus 3:2. The melting point gave 52-53°C. After melting this composition again, the compound remained glassy at room temperature for more than 18 months, with an index of refraction very close to that of the quartz. The glass is apparently kinetically stable at room temperature.

The second preparation also gave 2:1 plus 1:2 initially, along with a 771 peak which Zemva ascribed to 1:1.[3] Upon further melting, followed by quenching with LN_2, 2:1 and 1:1 appeared. However, no sign of the 771 peak was present. Upon remelting and slow cooling of the glass, followed by a 0°C quench, 2:1 plus 3:2 appeared in the Raman spectrum. This combination cannot be a thermodynamically stable mixture and the mixture cannot be homogeneously 2:1 plus 3:2. Soon after the spectrum was taken, the NMR tube broke or detonated. The 771 peak which Zemva ascribed to AsF_6^- was XeO_3. $XeOF_4$ was never observed in these melts at an intermediate, nor did any 771 peak appear in any of the samples prepared in FEP.

Due to the impurity, one can make few quantitative conclusions based on this preparation. The qualitative features of the cooling rate are consistent with the species seen in other compositions and in the initial preparation of "1.35:1".

The mixture of composition "1.23:1" showed the 1:1 and 3:2 phases also. The final liquidus point occurred in the range 58-62°C, which appears high considering the 1:1 melts at 57-58°C and the 3:2 at 49°C. It may be that the composition was not at its thermodynamically correct mixture of 1:1 and 3:2 when the melt was taken.

The complexity of melts in this region is also continued in the three compositions "1.87:1", "1.87:1", and "1.90:1". One "1.87:1" gave a Raman of 3:2 plus XeF_2. The second preparation, quenched from the melt to 0°C, showed mostly 2:1 with a trace of 1:1. Traces of melt appeared at 43-44°C, but the bulk of the melt occurred at 50-55°C. The final liquidus point of 57°C was accurately determined. The "1.90:1" showed the 2:1M phase previously mentioned in the "2.87:1" composition. The melting point was 59-61°C. (These limits are due to calibration errors due to a failing recorder battery.) Upon cooling, the "1.90:1" showed a pronounced supercooling down to 32°C where it solidified. No Raman was taken at this 32°C precipitation. It is tempting to speculate that this is the same point where the formation of 1:1 and 2:1 occurs in the "1.5:1" composition.

Conclusions on the Species Found in the Melts

The Raman spectra of the 3:2, 2:1M, and 3:1 adducts permits some discussion of their possible structures in light of Zemva's Raman and crystal structures of the 1:2, 1:1, and 2:1 complexes, as well as $XeF_5^+AsF_6^-$

and $XeF^+AsF_6^-$. The XeF_5^+ commonly has three or four bridging fluorines approaching its square base. In $XeF_5^+AsF_6^-$, three bridging fluorines from two neighboring AsF_6^- are arranged in a near three-fold symmetry about the cation's pseudo four-fold axis at an average distance of 2.7 Å. This three-fold arrangement about the cation's four-fold axis is apparently due to the steric repulsion of the non-bonding electron pair which forms the sixth coordination site of the pseudo octahedral XeF_5^+. This electron pair lies along the four-fold axis, and the bridging fluorines crowd around the lone pair. The steric effect of the lone pair always prevents a single direct axial approach of a bridging fluorine to the XeF_5^+. In any XeF_5^+ salt, one would expect a three or four-fold coordination of bridging fluorines at the base of the XeF_5^+ ion.

Secondly, the angle formed at the bridging fluorine is generally found to be about 130±20. In $XeF_5^+AsF_6^-$, the angles are found to be 110, 114, and 158. In $XeF^+AsF_6^-$, the Xe-F-As angle is 134.8°.

Third, when one of the fluorines of XeF_2 is a bridging ligand, the canonical form $F\text{-}Xe^+\text{--}F\text{—}MF_5^-$ makes a significant contribution. The terminal Xe-F has a shortened bond, while the distance to the bridging fluorine is lengthened. The breaking of the local center of symmetry about the XeF_2 splits the symmetric Raman peak at 496 cm^{-1} into a high frequency $Xe\text{-}F^+$ stretch and a low frequency Xe—F stretch. These two peaks are approximately equidistant from 500 cm^{-1}. In the highly distorted $XeF^+AsF_6^-$, the short bond is 1.87 Å and appears at 610 cm^{-1}. The bridging Xe—F distance is 2.18 Å, and appears at 346 cm^{-1}. For salts with less distorted XeF_2 molecules, the bond distances would become more

similar and the peak splitting would decrease to zero near 500 cm^{-1}. These three factors - the number of bridging fluorines approaching the XeF_5^+, the angle at the bridging fluorines, and the degree of distortion of the XeF_2 - are expected to be significant structural features of $XeF_2:XeF_5^+AsF_6^-$ adducts.

The Raman spectra of the 1:2, 1:1, and 2:1 adducts are consistent with these expectations based on their crystal structures. The 1:2 compound shows only one stretch in the XeF_2 region at 498 cm^{-1}. This peak implies a symmetrically bridged XeF_2, and the crystal structure has a center of symmetry at this XeF_2 which bridges two XeF_5^+ ions (Figure 9-3). The Xe(II)-F bond is slightly lengthened from that of XeF_2 (2.00 Å). As expected, each XeF_5^+ has three bridging fluorines arranged about the four-fold axis. The other two fluorines come from two neighboring AsF_5^-.

The Raman spectrum of the 1:1 compound shows two XeF_2 peaks at 555 and 433 cm^{-1}. The crystal structure shows a single XeF_2 sharing one of its fluorines with the XeF_5^+ (Figure 9-4). In this particular compound, there are only two bridging fluorines around the base of the XeF_5^+. The second fluorine comes from an AsF_6^-. This low coordination has been observed in the tetramer portion of the cubic form of XeF_6, which is largely $XeF_5^+F^-$.[6]

From the Raman peaks at 550, 542, and 479 cm^{-1}, the 2:1 adduct shows two distinct XeF_2. The crystal structure shows two distinct XeF_2 (Figure 9-5). The two different XeF_2 have different XeF^+ distances, which will give the different high frequency vibrations. The third coordination site beneath the XeF_5^+ is occupied by a fluorine of an AsF_6^-.

The Raman features of the 2:1M species show it to be similar to the known 2:1. While the 2:1 shows two high frequency vibrations and only one low frequency vibration for XeF_2, the 2:1M shows two low frequency vibrations at 452 and 423 cm^{-1} and only one high frequency vibration at 555 cm^{-1}. One of the two XeF_2 must interact more strongly with the XeF_5^+, and thus gives a spectrum (and presumably bond distances) similar to the 1:1. The other XeF_2 would be somewhat more symmetric, and would look like those in the 2:1. For both XeF_2, the Xe-F^+ bond length would be expected to be very similar. Based on the melting point behaviors, it may be that 2:1M is a high temperature phase of 2:1. Wechsberg had noted that the 1:2 was dimorphic with a transition near 40°C. One might expect the 2:1M to be similar in structural features to the 2:1.

The 3:2 adduct shows a Raman peak at 509 cm^{-1} in addition to the two unsymmetric XeF_2 peak pairs. One would expect two different distorted XeF_2 and one symmetric XeF_2 for a 3:2 composition. The triplet at 673, 667, and 662 indicate two distorted AsF_6^- and two distinct XeF_5^+ which are overlapping in that region. The proposed structure in Figure 9-6 satisfies these requirements, as well as maintaining three bridging fluorines arranged about the pseudo-four-fold axis of the XeF_5^+. The structure maintains bent Xe(VI)-F-Xe(II) bonds, and maintains one bridging fluorine from each AsF_6^-.

The most unsettling aspect of assigning the 3:2 compound as a pure compound is that the melting point appears to occur at a minimum, while a pure compound would be expected to manifest a local maximum in melting point. The widespread appearance of the 3:2 in all the melts between 1:1

and 2:1 hints that the 3:2 has some thermodynamic stability relative to the 1:1 and 2:1. Presumably at low temperatures, the 3:2 is unstable relative to 2:1 plus 1:1, but 3:2 is stable about ~35°C. This idea is appealing in view of the cooling rate evidence, although it in itself does not explain the minimum in the melting point. An incongruent melting of the 3:2 to 2:1 and 1:1 species in the melt would permit a minimum. The broad melting range 40-49°C would support this incongruent melting proposal.

A second possibility is that the "1.5:1" spectrum is not a 3:2 species, but a mixture of several other compounds. Several possible alternative mixtures are conceivable. Because the equilibrium $XeF_2 + XeF_6 \rightleftharpoons 2XeF_4$ is near unity, one can propose alternative compositions with XeF_4 or XeF_3^+. However, XeF_4 is not a sufficiently good fluoride donor to form $XeF_3^+AsF_6^-$.[7] This combination forming $XeF_3^+AsF_6^-$ can be discounted. Similarly, attempts to make the $Xe_2F_7^+AsF_6^-$ species can be discounted due to the greater stability of the 1:1. From a similar argument, one could propose the formation of an XeF_2:XeF_4 adduct, along with the formation of $As_2F_{11}^-$ from the free AsF_5. The Raman spectrum rules out the presence of XeF_2:XeF_4.[8] Secondly, the low thermal stability of $As_2F_{11}^-$ makes this proposal improbable. The fact that $XeF^+AsF_6^-$ rearranges to $Xe_2F_3^+AsF_6^-$ plus AsF_5 [9] (rather than $Xe_2F_3^+As_2F_{11}^-$) shows that XeF_2 is too good a fluoride donor to allow $As_2F_{11}^-$ to exist in its presence. This factor would eliminate the coexistance of any loosely complexed XeF_2 such as in XeF_2:XeF_4 with $As_2F_{11}^-$. $2XeF_2$ would react with $M^+As_2F_{11}^-$ to make $M^+AsF_6^-$ and $Xe_2F_3^+AsF_6^-$. A one-to-one mixture of $XeF_5^+AsF_6^-$ and $Xe_2F_3^+AsF_6^-$, which melted at 70°C, gave

a Raman consisting only of the original salts. Sladky also noted that these two salts were formed in BrF_5 solvent from XeF_2 plus XeF_6 plus AsF_5.[7] Lastly, the formation of XeF_2 plus $Xe_2F_3^+AsF_6^-$ plus $Xe_2F_{11}^+$ AsF_6^- is possible. However, the Raman spectra bears no resemblance to any of these compounds.[9,5] The improbable fluoride ion transfer from AsF_6^- to XeF_5^+ in the presence of XeF_2 eliminates the species XeF_4, XeF_3^+, $Xe_2F_7^+$, or $As_2F_{11}^-$ from possible consideration. One is forced to conclude that the 3:2 species is the only plausible alternative composition.

The Raman spectra of the "3.04:1" and "4.08:1" compounds show identical 3:1 spectra plus excess XeF_2. The peak assignments are fairly straightforward, although the true composition of this 3:1 species is not known. Based on the admittedly crude estimate that the $XeF_{2(c)}$ peak roughly doubles in intensity relative to the 3:1 species in passing from "3.04:1" to "4.08:1", one might speculate that the 3:1 species is really another 2:1 species. One interesting feature is the absence of any significant peak splittings in the XeF_2 region 550 to 430 cm^{-1}. Only one broad peak at 513±10 cm^{-1} can be seen near the strong $XeF_{2(c)}$ peak at 496 cm^{-1}. This strong peak obscures any possible peaks in the region 505–485 cm^{-1}. It is noteworthy that the 3:2 species had a similar peak at 509 cm^{-1}, which was assigned to a symmetrically bridging XeF_2. However, it is improbable that a structure with three symmetric XeF_2 can be constructed. Even if this species were another 2:1 (or 4:2), placing four bridging XeF_2 between two XeF_5^+ along with two AsF_6^- is improbable. An alternative explanation is that the spectrum truly reflects a 3:1. Most

likely, a very weak unsymmetric XeF_2 - XeF_5^+ interaction is present, which does not split the XeF_2 Raman peak drastically. The breadth of the 513 peak may reflect a small distribution of XeF_2 peaks. With this weak interaction, one could have three XeF_2 bridging to the XeF_5^+. Whether the AsF_6^- also bridges with one fluorine is debatable. With four bridging fluorines, the XeF_2 molecules would be further from the XeF_5^+, and thus there would be a weaker interaction. However, three coordination to the XeF_5^+ is common in the AsF_6^- salts and adducts. Further work must be done to characterize this 3:1 species.

References for Chapter 9

1. T. A. O'Donnell, J. Fluorine Chem., 11, 467, 1978; A. M. Bond, I. Irvine, and T. A. O'Donnell, Inorg. Chem., 14(10), 2408, 1975.
2. J. P. Masson, J. Devynck, and B. Tremillon, Electroanalytical Chem. and Interfacial Electrochemistry, 54, 232, 1974.
3. N. Bartlett, B. Zemva, D. Templeton and A. Zalkin, to be published.
4. N. Bartlett and F. O. Sladky, "The Chemistry of Krypton, Xenon, and Radon", Comprehensive Inorganic Chemistry, Volume 1, Pergamon Press, New York, 1972, 252-8.
5. N. Bartlett and M. Wechsberg, Zeitschrift fur Anorganische und Allgemeine Chem., 385, 5, 1971.
6. R. D. Burbank and G. R. Jones, Science, 168, 248, 1970.
7. N. Bartlett and F. O. Sladky, JACS, 90(19), 5316, 1968.
8. C. J. Adams, J. Environmental Spectroscopy, 8, 478, 1973.
9. F. O. Sladky, P. A. Bulliner, and N. Bartlett, J. Chem. Soc. A, 2179, 1969.

Table 9-1. Raman Spectral Assignments of New Adducts.

Compositions (Intensity)			Assignments		
3:2	2:1	3:1	XeF_5^+	XeF_2	AsF_6^-
718(10)		724(4)			ν_3
705(10)					
673(100)[a]	678(15)	679(50)	ν_1		
667(100)	666(100)	661(100)			ν_1
662(100)	651(15)		ν_1 ν_7		
615(140)	607(75)	616(70)	ν_2		
609(140)					
600(sh)	600(50)	598(15)	ν_4		
	564(sh)	576(15)			ν_2
555(120)	555(100)	550(20,b)		Xe–F	
	551(sh)			Xe–F	
537(120)				Xe–F	
509(90,b)		515(off scale)		Xe–F	
		496(off scale)		$XeF_{2(c)}$	
467(90)	452(50)			Xe–F	
449(70)				Xe–F	
	423(30)		ν_8 or	Xe–F	
395(15)					
385(3)					ν_4
374(3)	369(3,b)	372(15)			ν_5
300(10)		310(7)			
293(10)	297(7,b)	295(7)	ν_3		
		236(5)	ν_5		

(a) The 3:2 would have two distinct XeF_5^+ ions and could thereby show two distinct ν_1 at 673 and 662.

Table 9-2. "M:1" Summary of XeF_2:$XeF_5^+AsF_6^-$ Composition Phase Study in Raman[a]

Mole % XeF_2	35.8	50	54.5	57.4		60	65		65.5	66	74.2	75	80.3
M	0.56	1.00	1.23	1.35		1.50	1.87		1.9	2.00[b]	2.89	3.04	4.08
Initial Mixture					1:2 + 2:1	1:2 + 2:1							
Mixtures Slow Quench			3:2 + 1:1	3:2 + 1:1	3:2 + 1:1	3:2	3:2 + XeF_2			(2:1)	2:1M + XeF_2	2:1M + XeF_2	
Mixtures LN_2 Quench	1:2	1:1		2:1 + 3:2	2:1 + 1:1	2:1 + 1:1	2:1 + 1:1		2:1M		2:1 + XeF_2	3:1 + XeF_2	3:1 + XeF_2
Final[c] Melting Point°C	65	57-8	62	(58)	53	49	56	58	59		(70)	(80)	103
Initial[d] Melt°C	42		58	51		40-2	52	43	55		39	44	

(a) These mixtures are visible in one or more regions of the solid. The solid may not be a homogeneous mixture. In some slow precipitations, one phase was primarily at the bottom while another was near the top.

(b) A 2:1 was not prepared, but is put on the summary for completeness.

(c) Visually determining the point at which the final melt occurs can be difficult. The values in parenthesis are approximate.

(d) The point of first melt is difficult to determine visually with any accuracy. At times there is a subtle color change or darkening in a local region which has been noted. In all cases, there was a substantial liquid/solid regime between the initial and final melting point.

Figure 9-1
Raman Spectra of XeF_2 : $XeF_5^+AsF_6^-$ Adducts

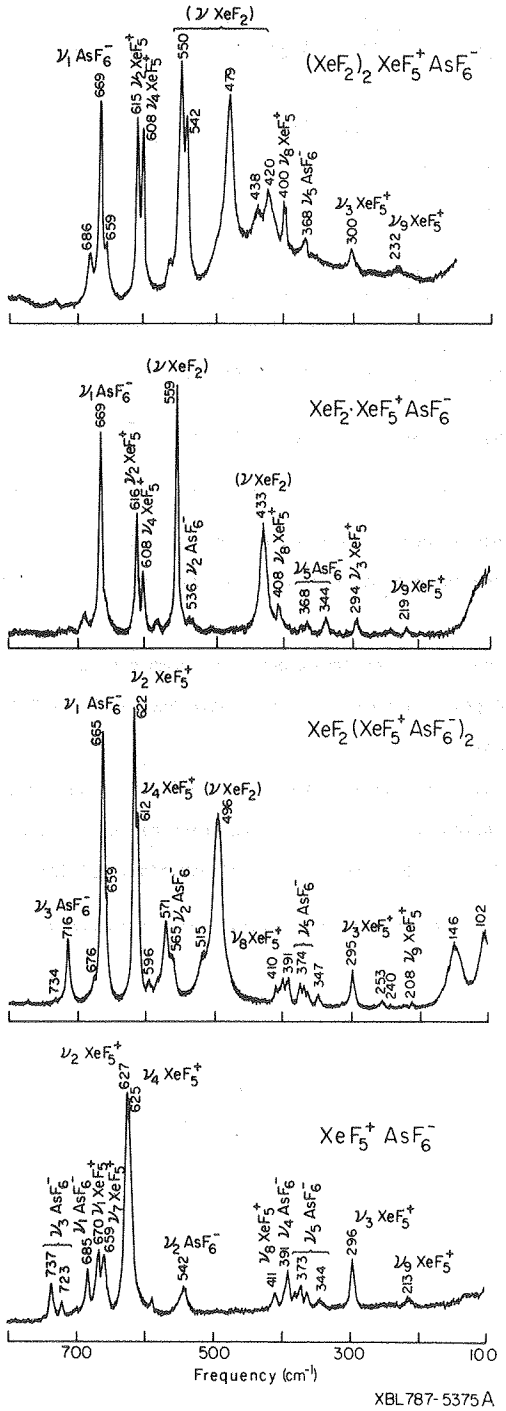

XBL787-5375A

Figure 9-2
Raman Spectra of New XeF_2 : $XeF_5^+AsF_6^-$ Adducts

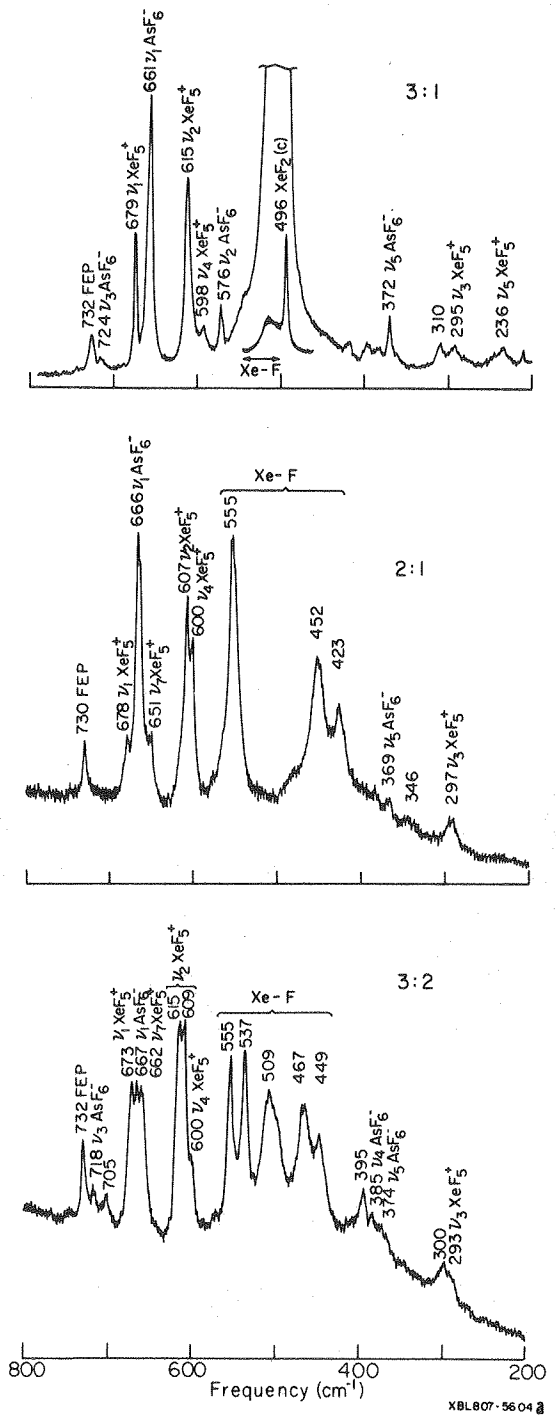

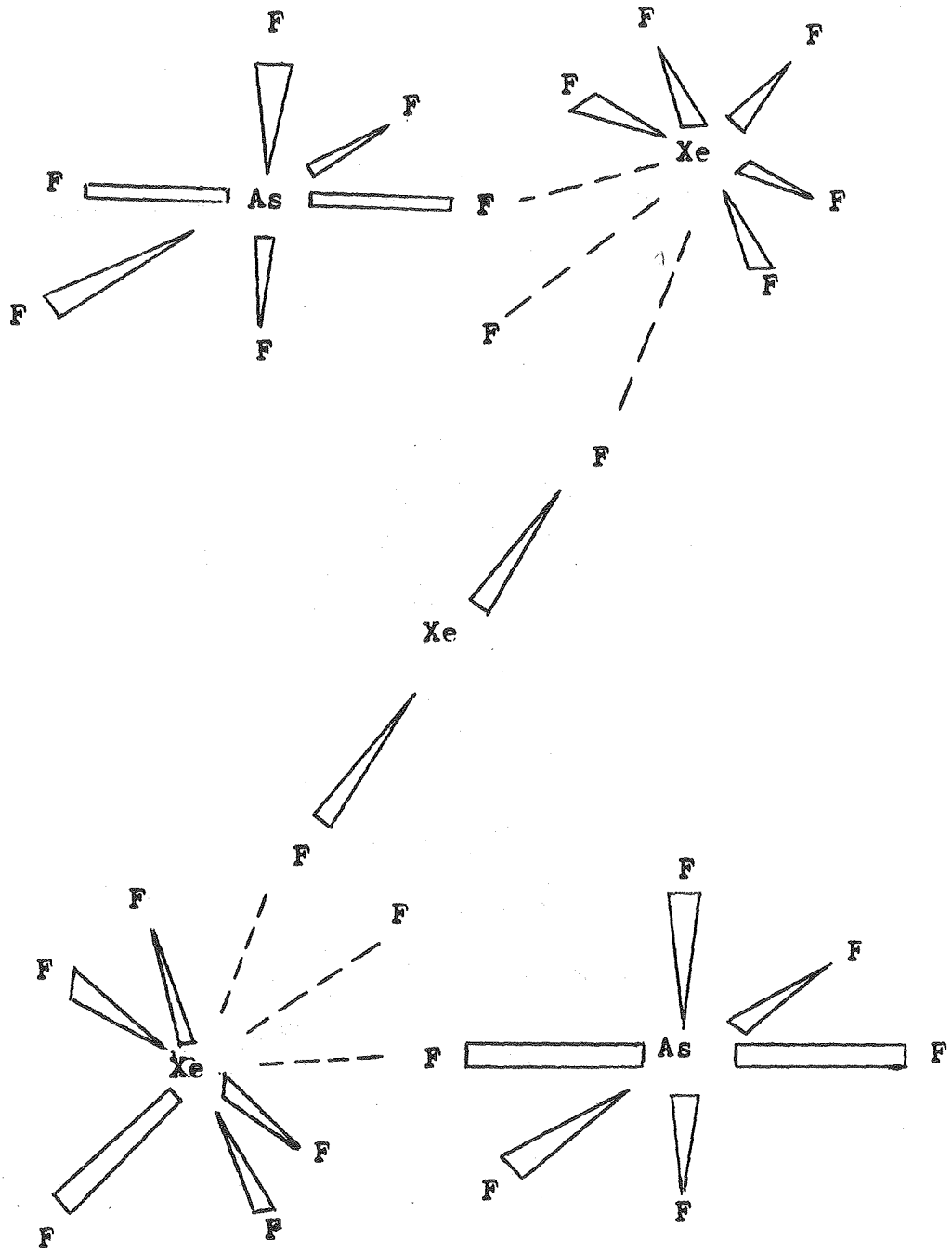

Figure 9-3

Local Structure of XeF_2 : $2XeF_5^+AsF_6^-$

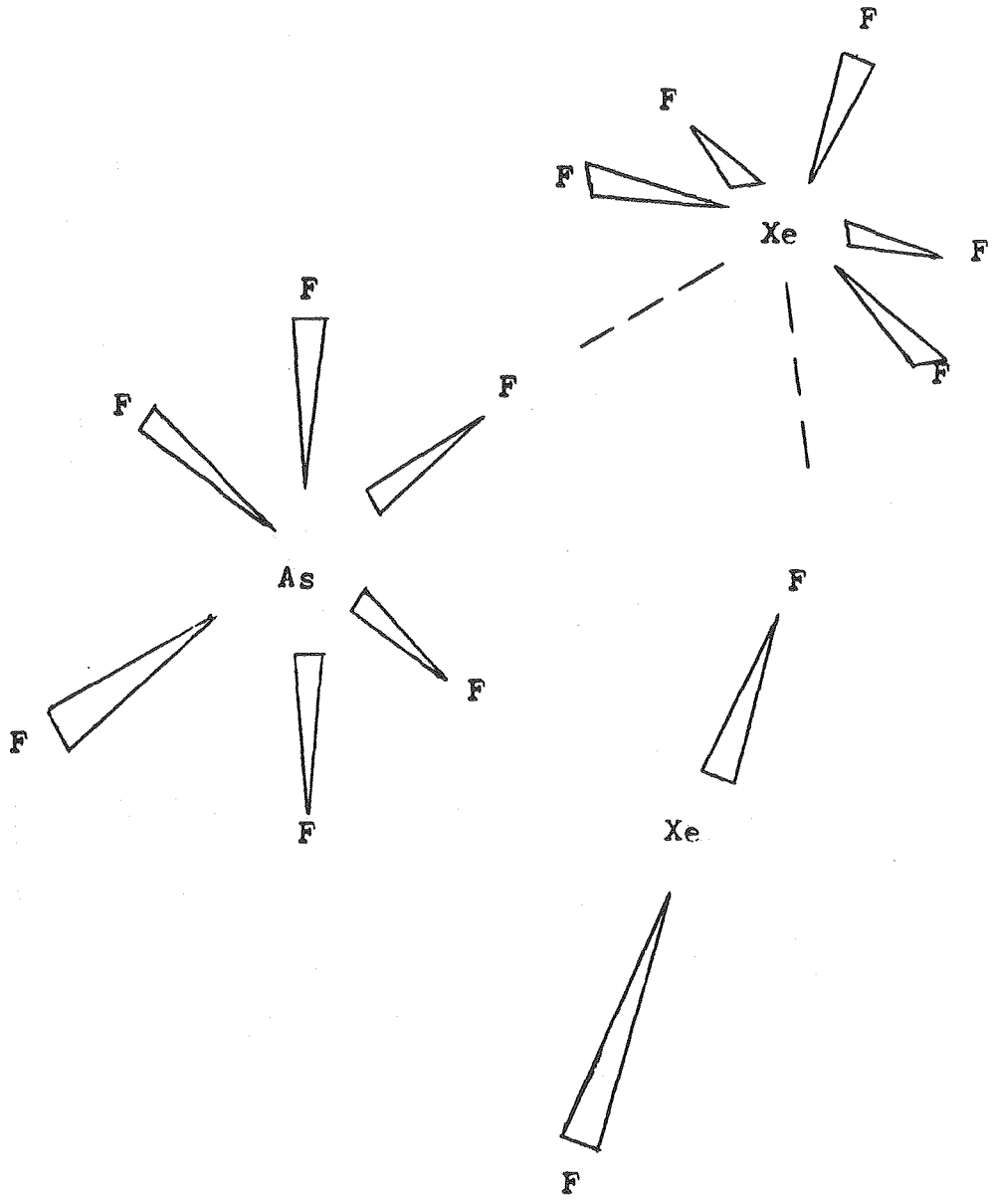

Figure 9-4

Local Structure of XeF_2 : $XeF_5^+AsF_6^-$

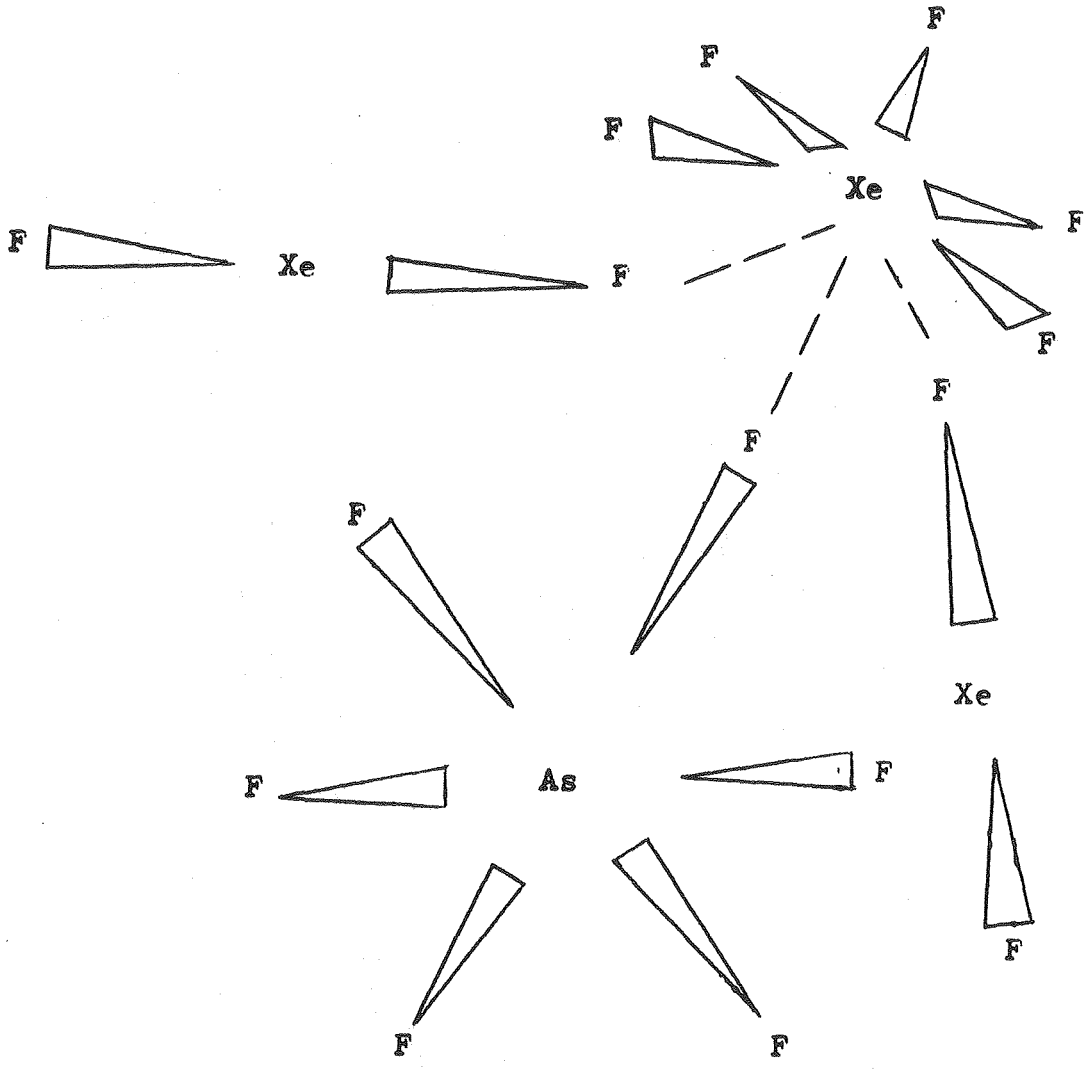

Figure 9-5

Local Structure of $2XeF_2$: $XeF_5^+AsF_6^-$

Figure 9-6

Proposed Local Structure of $3XeF_2 : 2XeF_5^+AsF_6^-$

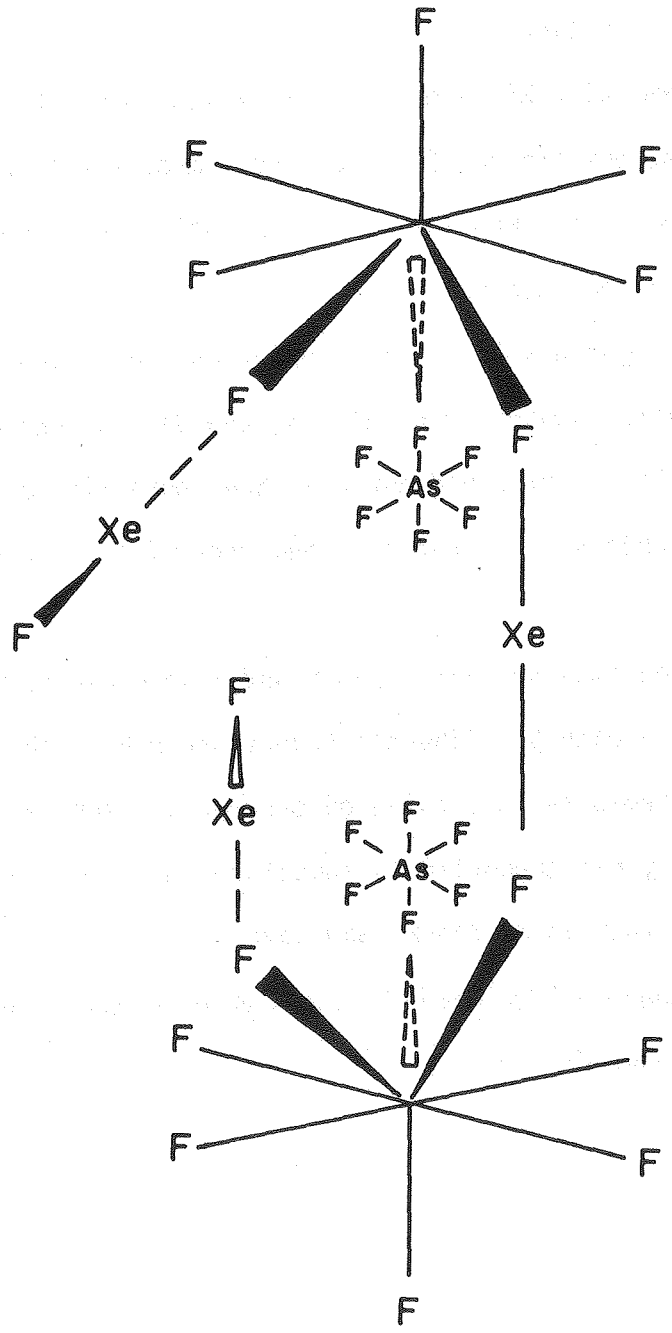

XBL 807-5605A

ACKNOWLEDGEMENTS

To Neil Bartlett goes my most sincere thanks and admiration. His insight, enthusiasm, and ability to simplify complex issues, was a steady source of inspiration.

To Lionel Graham, Rich Biagioni, Fran Tanzella, Sam Yeh, Gene McCarron and Tom Mallouk, thanks for the good times, sweat and song. To Sandy Jennings and Lydia Frucine go my admiration for keeping the office madness under some control.

Special acknowledgements go to Alan Robertson, John Kirby, and Mel Klein for many fruitful labors, long nights, and discussions over X-ray absorption. This work could not have been done without the labors of untold machinists, librarians, and other fifth floor inhabitants.

I must acknowledge the special support and friendship of my fellow Dominicans associated with St. Albert's Priory and DSPT. Those associations kept chemistry in a balanced perspective for me.

Lastly, my family has supported my education, my goals, and me. All I can return to them is my thanks and love.

This work was supported by the U.S. Department of Energy under Contract No. W-7405-ENG-48.